5-1-1998

Williamsburg Bridge Replacement Orthotropic Deck As-Built Fatigue Test

William J. Bocchieri

John W. Fisher

LEHIGH
University

WILLIAMSBURG BRIDGE REPLACEMENT ORTHOTROPIC DECK AS-BUILT FATIGUE TEST

by

William J. Bocchieri
Research Assistant, ATLSS Center

John W. Fisher
Director, ATLSS Center

ATLSS Report No. 98-04
Interim Report on Phase II for Federal Highway Administration
U.S. Dept. of Transportation, New York Dept. of Transportation
and New York City Dept. of Transportation

May 1998

ATLSS is a National Center for Engineering Research on Advanced Technology for Large Structural Systems

117 ATLSS Drive
Bethlehem, PA 18015-4729

Phone: (610)758-3525
Fax: (610)758-5553

www.lehigh.edu/~inatl/inatl.html
Email: inatl@lehigh.edu

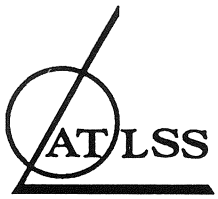

LEHIGH
University

WILLIAMSBURG BRIDGE REPLACEMENT ORTHOTROPIC DECK AS-BUILT FATIGUE TEST

by

William J. Bocchieri

John W. Fisher

ATLSS Report No. 98-04
Interim Report on Phase II

May 1998

ATLSS is a National Center for Engineering Research on Advanced Technology for Large Structural Systems

117 ATLSS Drive
Bethlehem, PA 18015-4729

Phone: (610)758-3535
Fax: (610)758-5553

www.lehigh.edu/~inatl/inatl.html
Email: inatl@lehigh.edu

TABLE OF CONTENTS

LIST OF TABLES

LIST OF FIGURES

ABSTRACT

As part of the ongoing Williamsburg Bridge Reconstruction Project, the original deck on the south, inner and outer roadway has been replaced by a closed rib, steel, orthotropic deck. Several key elements in the design of this deck were based on the conclusions of an extensive laboratory test, now referred to as Phase I, of a full-scale, prototype segment of this deck. These include using a combination full penetration groove - fillet weld rib to diaphragm connection; increasing the thickness of the diaphragm plate, as well as making it continuous with constant depth; increasing the thickness and depth of the bulkhead plate, and using larger fillet welds for the bulkhead to rib connection.

A second full-scale laboratory investigation involving static and fatigue testing, Phase II, was performed to study the effectiveness of these changes implemented in the design of the actual replacement deck, as well as develop additional experimental data on the fatigue strength of the welded details. During the first 5 million cycles of the fatigue test (Phase IIA), no fatigue cracks were expected to develop. The objective of the remaining 2 million cycles of the fatigue test (Phase IIB) is to produce as much cracking as possible in the rib to diaphragm welds in order to acquire fatigue test data and properly classify the fatigue resistance.

Both the static and fatigue test results demonstrated that the design changes were effective in making the deck resistant to fatigue cracking under the estimated AASHTO LRFD extreme live load conditions. A comparison of static test data showed there was a significant reduction in the peak diaphragm stresses from Phase I to Phase

II. After 5 million cycles of loading corresponding to two fatigue trucks traveling adjacent to each other in the inner and outer lanes, no cracks developed at any of the rib to diaphragm welds. One crack was detected in a diaphragm cutout half-way through the fatigue test; this crack, however, grew from an initial defect in the diaphragm plate cutout edge where the flame cut edge was not completely removed and surface nicks existed. The 5 million cycle fatigue test approximated 64 years of service for the cantilevered roadway.

1.0 INTRODUCTION

1.1 Background

An orthotropic steel deck primarily consists of a continuous, flat, steel plate, with closely spaced open or closed stiffeners (ribs) welded to its underside in a parallel pattern. Figure 1.1[1] displays a typical layout of such a deck with closed ribs. These ribs run perpendicular to the floorbeams supporting the deck plate and make the deck much more rigid in its longitudinal direction than its transverse direction. Because their structural properties vary in orthogonal directions, such decks are *orthogonally anisotropic* and are thus called *orthotropic* for short[2].

These decks consist of a series of prefabricated panels, the size of which depends on the fabrication, transportation and erection facilities available, which are field-spliced together using both welded and bolted connections. Diaphragm plates welded to their underside improve the rigidity in the transverse direction and the composite action of these panels. They also provide a means for attaching them to their supporting floorbeams also using either welded or bolted connections. The ribs stiffening the deck plate may be either open or closed, as shown in Figure 1.2[3]. Open ribs are often made from flat bars, bulb shapes, inverted T-sections, angles, or channels. Closed ribs often have either a semicircular, triangular, boxed, or trapezoidal shape. Closed ribs have much greater torsional stiffness than open ribs; however, they can only be welded to the deck plate from one side, and they are closed to visual inspection.

Initial designs of orthotropic steel decks for bridges were based on battledeck floors of Navy warships. These floors allowed for a forty percent increase in permissible stresses in the steel plating due to composite action between the deck plate and longitudinal stringers. In the 1930's, such decks were adapted and used on the Triborough Bridge in New York City and other structures in the U.S. The Triborough Bridge Deck consisted of a steel plate stiffened by welded open ribs made from rolled sections.

Modern orthotropic steel decks were developed in Europe over four decades ago, spurred on by material shortages in the years following World War II. Despite their light weight and otherwise excellent structural characteristics, their performance has often been beset by a variety of fatigue problems. Fatigue cracks in structures are usually the result of high cyclic stresses in combination with poor welding details. Both large live loads and distortion commonly cause such high cyclic stresses. When such stresses exceed certain limits over a given period of time, cracking will occur.

Since the time of their development, the use of orthotropic decks has been much more prevalent in Europe than in the United States. Many of their common fatigue problems, which are thoroughly discussed by Lugger, have been solved by researchers and practicing engineers on a trial-and-error basis. However, significant problems still remain.

In the United States, orthotropic decks have primarily been used as replacement decks on older, deteriorating bridges, such as the George Washington Bridge, the Golden Gate Bridge, the Ben Franklin Bridge, and the Throgs Neck Bridge. The most recent of

such major refurbishing projects was on the Williamsburg Bridge. Orthotropic decks were also placed on new structures such as the Luling Cable Stayed Bridge and the Poplar St. Bridge in St. Louis.

1.2 Williamsburg Bridge Background

The Williamsburg Bridge opened in 1903, and at the time it had the longest span, 488 m (1600 ft), of any suspension bridge in the world. Located in New York City, it crosses the East River, connecting Manhattan with the town of Williamsburg in Brooklyn. Figure 1.3[4] shows a cross-sectional view of the bridge deck and the horse and buggy traffic it was originally designed to carry. The bridge has been modified and expanded over the years to its present capacity of eight vehicular lanes of traffic, two train tracks, and a pedestrian walkway. Both high traffic volumes and corrosion have caused it extensive deterioration, and in 1989 it was decided to refurbish this vital artery. Figure 1.4a[5] shows a current photograph of the bridge, and Figure 1.4b[6] displays a cross section of the deck upon completion of the entire ongoing rehabilitation project. Only the south, outer roadway is completed and carrying traffic in 1998.

Several different deck types were considered for replacing the existing deck system, but ultimately it was decided to use a steel orthotropic deck with closed, trapezoidal ribs. It was selected to provide long term, uninterrupted use with minimal maintenance requirements, to reduce the dead load carried by the aging suspension cables (which were not to be replaced), and to decrease the live load deflections of the 7.6 m (25 ft) long cantilevered floorbeams supporting the outer roadways. A closed rib orthotropic

deck was chosen over an open deck in order to achieve a torsionally stiff deck and to further reduce the live load deflections of the cantilevered floorbeams.

The bridge carries four lanes of traffic on simply supported inner roadways, and also has two outer roadways with two lanes each which are cantilevered off both sides of the bottom chord of the main bridge truss. The original design of the planned retrofit scheme of the outer roadways incorporated 12.19 m (40 ft) long by 6.10 m (20 ft) wide prefabricated orthotropic deck panels which are bolted to floorbeams through 8mm (0.313 in.) thick diaphragm plates which were not continuous between all adjacent ribs. Other elements of the proposed design consisted of a 16 mm (0.625 in.) deck plate, 9.5 mm (0.375 in.) thick closed rib sections, and 8 mm (0.313 in.) thick bulkhead plates. Figure 1.5[3] displays a dimensioned cross-sectional view of the deck's original design. Panels of the continuous deck system were to be joined in the field with a bolted splice on each of the ten longitudinal ribs and a full penetration weld between adjacent deck plates. The outer roadways were to be connected to the bottom chord of the main bridge truss by a series of 3.75 m (12.3 ft) long shear connectors. These carry the horizontal shear in the longitudinal direction of the bridge providing compatibility of the truss, thereby reducing out-of-plane bending in the floorbeams and diaphragm plates.

The New York City firm Steinman Boynton Gronquist & Birdsall designed the orthotropic deck system for the Williamsburg Bridge after performing a comprehensive review of these systems around the world. During this process, they resolved all design issues except the weld connection detail between the diaphragm plate and closed rib.

This detail is critical to the fatigue strength of the deck system because it is subject to a complex combination of in-plane and out-of-plane stresses.

Because of the concern for the fatigue strength of this critical connection, two possible weld details were developed in the design process. The AASHTO LRFD Bridge Specification recommends Option "B", a fillet-welded connection which terminates short of the cutout, shown in Figure 1.6. Steinman used an improved connection, Option "A", which includes a combination of fillet welds and full penetration groove welds, shown in Figure 1.7. This detail requires that 102 mm (4 in.) adjacent to the termination of the diaphragm cut-out be fabricated with a full penetration weld reinforced by a fillet weld. This combination weld continues beyond the edge of the diaphragm plate and is ground into a smooth radius to remove any weld discontinuities at its termination. The remainder of the connection consists of double sided fillet welds, similar to the Option "B" detail. At the time, no research or actual records gave any quantitative comparison of the fatigue strengths of these two details. Therefore, New York City DOT (NYCDOT), New York State DOT (NYSDOT), and the FHWA decided to prepare contract documents showing both weld details, and to perform a full-scale fatigue test of both details to provide a basis for a final selection.

Until then, no full-scale, complete panel fatigue tests of orthotropic decks had ever been conducted in the laboratory. In addition to studying the two proposed weld details, such a test program offered the advantage of more accurately duplicating the complex distribution of stresses in the deck system, thereby "proof" testing all details on the deck system. Hence, a full-scale fatigue test of the Williamsburg Bridge orthotropic

deck system was conducted at Lehigh University's ATLSS Engineering Research Center[3]. This first test is now referred to as Phase I in a series of three tests studying the behavior of the deck system.

1.3 Previous Research - Overview of Phase I

1.3.1 Test Panel Fabrication

A full-scale, prototype deck system 18.3 m (60 ft) long and 6.1 m (20 ft) wide modeling a segment of the Williamsburg Bridge's outer cantilevered roadways was fabricated by Leonard Kunkin Associates, the same fabricator selected to manufacture the deck system for the actual bridge. Figure 1.8[3] shows a plan view of the test setup. The test deck modeled a cantilevered section of the roadway rather than a simply supported section because the cantilevered section experiences larger stresses in the transverse direction. Thus, a design which is adequate for the cantilevered roadway also accommodates a simply supported roadway. The test panel was supported by four equally spaced floorbeams, each 6.9 m (22.5 ft) long, as a three span continuous unit with transverse field splices made in the deck adjacent to the two interior floorbeams. Each of the two rib/diaphragm weld connections were used in the test panel and were symmetrically detailed to provide a fair comparison of their fatigue endurance. A single 3.75 m (12.3 ft) long shear connector and various attachments for the bridge railing system were also fabricated with the test panel.

The deck panels were fabricated to meet all applicable NYSDOT specifications and inspection requirements. Weld procedures were reviewed and shop inspection was performed by NYSDOT. These requirements were similar to those specified for the deck system on the actual bridge reconstruction project. Particular emphasis was placed on the fit-up of the deck system. To ensure proper tolerances, the entire deck panel was preassembled, including floorbeams, at the fabricator's shop prior to delivery to the laboratory.

1.3.2 Specifics of the Test Setup

To simulate the roadway conditions of the actual bridge deck, the 18.3 m x 6.1 m (20 ft x 60 ft) deck panel spanned continuously over the four cantilevered floorbeams at a three percent longitudinal grade and a two percent transverse slope. Even though the floorbeam spacing on the bridge is 6.07 m (19.92 ft), the span length in the test setup was increased by 25 mm (1 in.) to match the reaction wall attachment spacing. The ends of the cantilevered floorbeams attached to specially designed W14x398 columns bolted directly to the reaction wall. Each wall column was designed to carry the maximum applied moment with a minimal amount of distortion at the beam to column connection, thereby preventing excessive deflections due to a rigid body rotation of the deck system. The only component of the cantilevered roadway which was omitted from the test panel was the asphalt concrete overlay. However, sand bags placed on the steel deck plate simulated this load condition.

An inner and outer lane of wheel loads were applied to the deck panel with

530 kN (120 kip) hydraulic actuators at five locations along its length. Through a spreader beam arrangement, the load from each of the five actuators was distributed to four patch loads which simulate AASHTO recommended 305 mm x 711 mm (12 in. x 28 in.) wheel footprints. A 3 mm (0.125 in.) thick neoprene pad was placed under each footprint to ensure that the load was evenly distributed under the loading plate. Loads from the five actuators were applied in a unique, five-step sequence which was conceived and analytically developed by the NYCDOT to produce effects at the two interior diaphragms equivalent to two AASHTO fatigue trucks traveling adjacent to each other across the actual bridge. By correctly sequencing applications of the loads, the dynamic effects of vehicles moving on the bridge deck were accurately produced at these two groups of interior rib/diaphragm connections. All of such connections over one of the interior floorbeams used the Option "B" weld detail, and the Option "A" weld detail was used in all connections over the other interior floorbeam. Thus, the test provided an accurate means of comparing the fatigue resistance of these two critical weld details.

1.3.3 Phase I Test Procedure

Both static calibration and dynamic fatigue tests were performed on the test panel. The static load tests were conducted to determine the three-dimensional stress distribution in the deck system under the equivalent fatigue truck wheel loads. Analyses revealed locations of high stress and identified stress gradients around the rib/diaphragm connections. After completion of the static calibration load tests, it was decided to conduct the dynamic test so that the cumulative effect of the two simulated vehicles was

equal to twice the AASHTO LRFD fatigue vehicle, corresponding to the AASHTO LRFD extreme life check[7]. This was accomplished by applying the fatigue vehicle (i.e., 75 percent of an HS20 truck) without impact in the inside lane and with 30 percent impact in the outside lane.

1.3.4 Phase I Conclusions

After the application of two million load cycles, the decision was made to proceed with the fabrication of the replacement orthotropic deck using the Option "A" weld detail. At this point in the test, only one crack had developed in all the Option "A" details at the lower end of this rib/diaphragm connection, whereas three of the Option "B" details had cracked in this same location. When the test had finished at ten million cycles, only one more crack had developed in all of the Option "A" details, whereas four more had developed in the Option "B" details. Furthermore, the crack in the Option "A" detail was successfully arrested and retrofitted by peening and drilling.

In addition, no fatigue damage was observed in any of the other weld details, including the transverse deck splice, longitudinal rib to deck welds, and miscellaneous attachments for the bridge railing system. Since the loading scheme did not subject the rib to diaphragm connections over either of the outer floorbeams to a complete stress cycle, none of these connections showed any sign of fatigue damage.

Several important design changes were also made as a result of this test. Figure 1.9 displays a cross-sectional view of the deck which includes all of these modifications. Since it was observed that in-plane stresses controlled the stress cycle of the diaphragm, it

could be made thicker without causing an increase in its stress cycle component due to out-of-plane bending. A thicker plate would reduce these dominant in-plane stresses, and, thus, reduce the stress cycle subjected to the diaphragm. Also, making the diaphragm plate with uniform depth and continuity would help distribute the load between the ribs, thereby improving the composite action of the deck. These results, coupled with data from finite element analyses, showed that a continuous diaphragm with an increased thickness of 13 mm (0.5 in.) should reduce the highest stresses at the rib to diaphragm connection below the CAFL. Furthermore, design engineers decided to replace the existing floorbeams supporting the cantileverd portion of the deck with new ones inclined at two percent, thereby permitting the diaphragm in the replacement deck to have a constant depth while retaining the proper transverse slope of the roadway. Thus, the final design incorporates a continuous, constant depth diaphragm with a thickness of 13 mm (0.5 in.).

Increasing the thickness of the diaphragm also meant increasing the thickness of the bulkhead to 13 mm (0.5 in.) because it provides continuity of the diaphragm through the ribs. In addition, whereas the bottom of the bulkhead was at the same rib depth as the exterior diaphragm connection in the original design, the bulkheads were also extended 18.75 mm (0.75 in.) deeper into the rib below the exterior diaphragm connection to avoid having the diaphragm and bulkhead intersecting the rib at the same location. The bulkhead to rib welds were also increased to satisfy the AASHTO specifications for load carrying fillet welds.

1.4 Purpose of Phase II Testing

The replacement orthotropic deck for the Williamsburg Bridge was fabricated and erected incorporating the Phase I design changes, and thus is expected to be resistant to fatigue cracking under normal loading conditions. However, in order to verify the efficacy of these design changes and to determine the deck's fatigue strength, a second test, Phase II, is being conducted at the ATLSS Center on the final design of the cantilevered section of the Williamsburg Bridge's replacement orthotropic deck.

As in Phase I, Phase II involves static calibration and dynamic fatigue tests of the orthotropic deck using hydraulic jacks to simulate the effects of two vehicles traveling across the roadway. The static load tests were conducted with actuators to determine the three-dimensional stress distribution in the deck system. In addition, for comparison purposes quasi-static tests were also performed with a pair of rolling axles similar to an HS20 truck.

During the first five million cycles of the fatigue test, actuators will apply a carefully timed sequence of loads to produce dynamic effects equivalent to those applied in Phase I. No fatigue cracks are expected to develop under this loading condition. However, the magnitude of the loads will be increased during the final three million cycles of the fatigue test in such a manner that they correspond to roughly twice the AASHTO LRFD extreme life check. By doing so, the actual fatigue resistance of the Option "A" rib/diaphragm weld detail will be quantified.

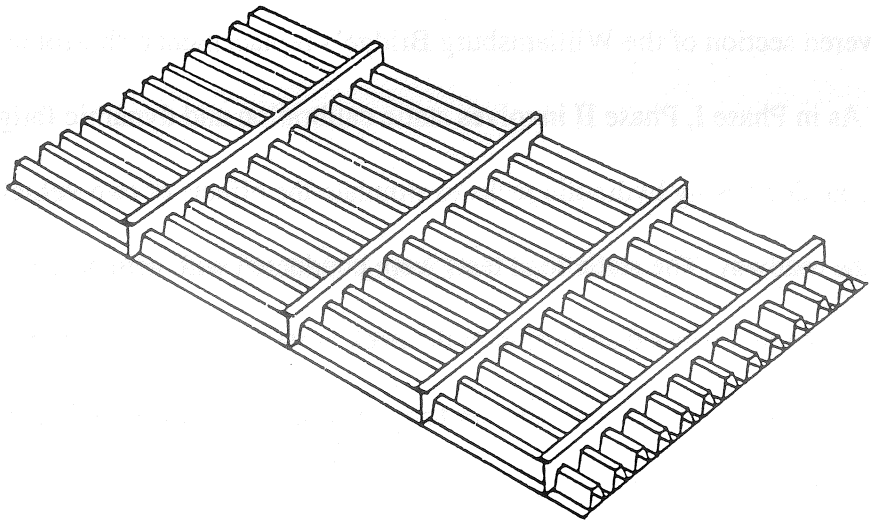

Figure 1.1 Typical Closed Rib Orthotropic Deck Viewed from Bottom

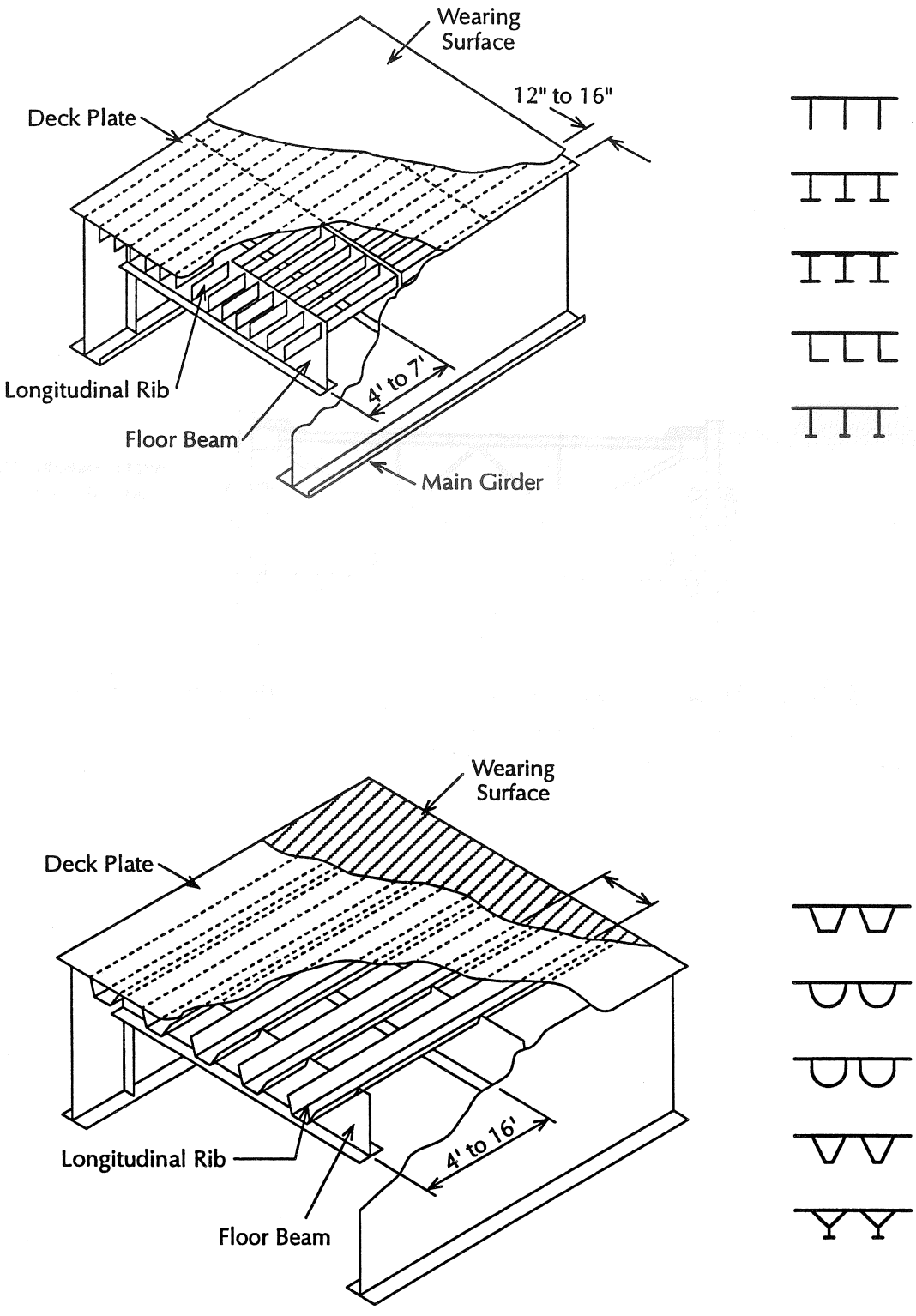

Figure 1.2 Example of an Open and Closed Rib Deck

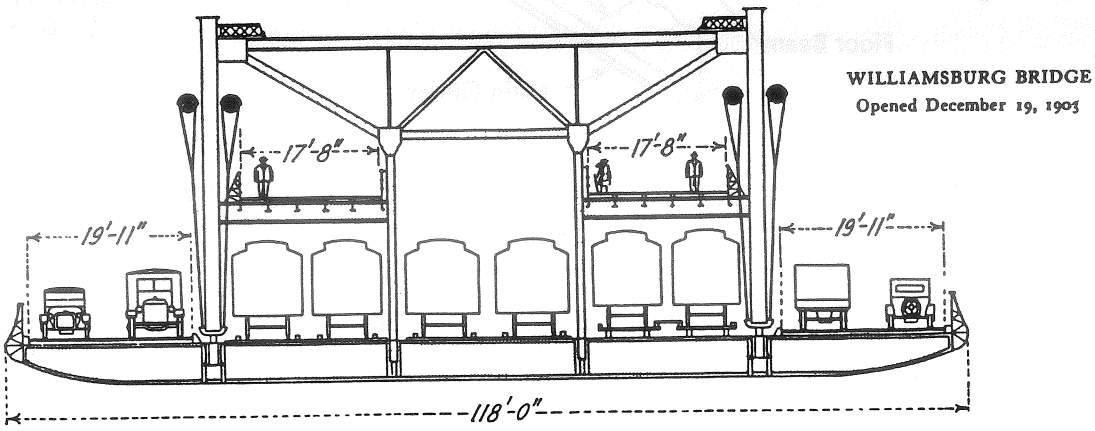

Figure 1.3 Cross-Section of Original Deck

Figure 1.4a Williamsburg Bridge

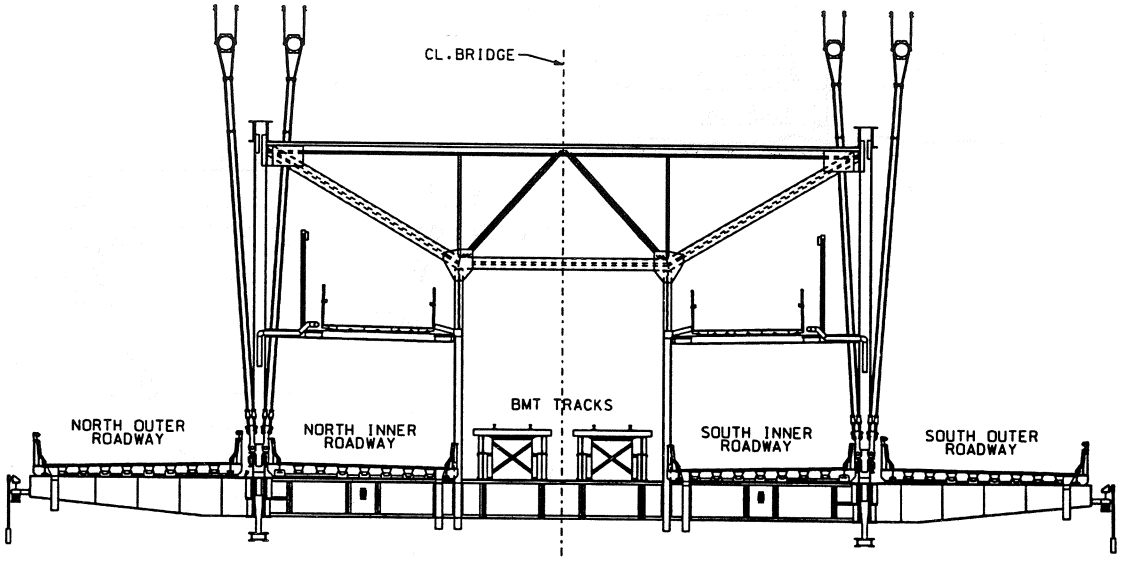

Figure 1.4b Cross Section of Deck Upon Completion of Rehabilitation Project

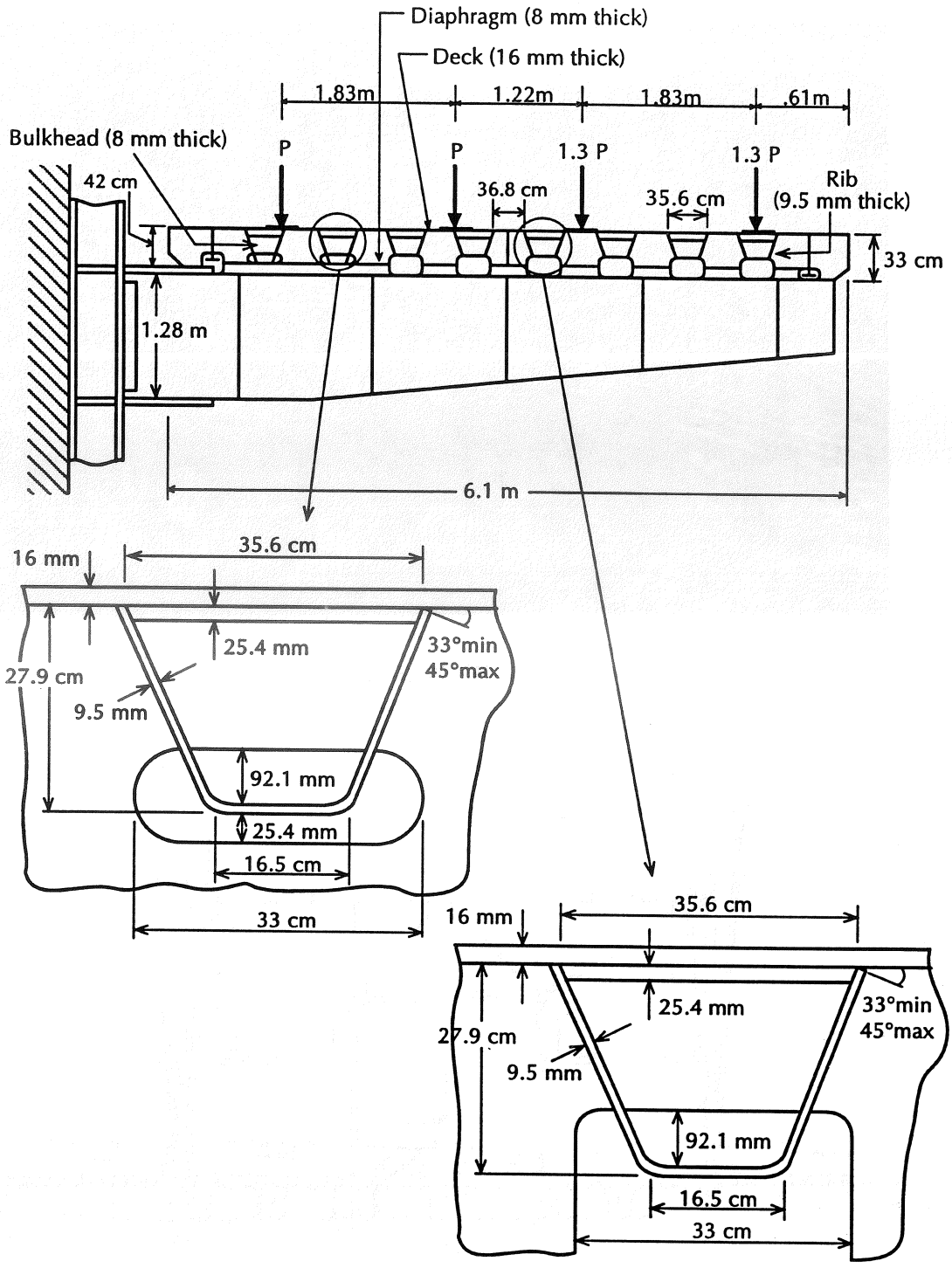

Figure 1.5 Dimensioned Cross-Section for Phase I

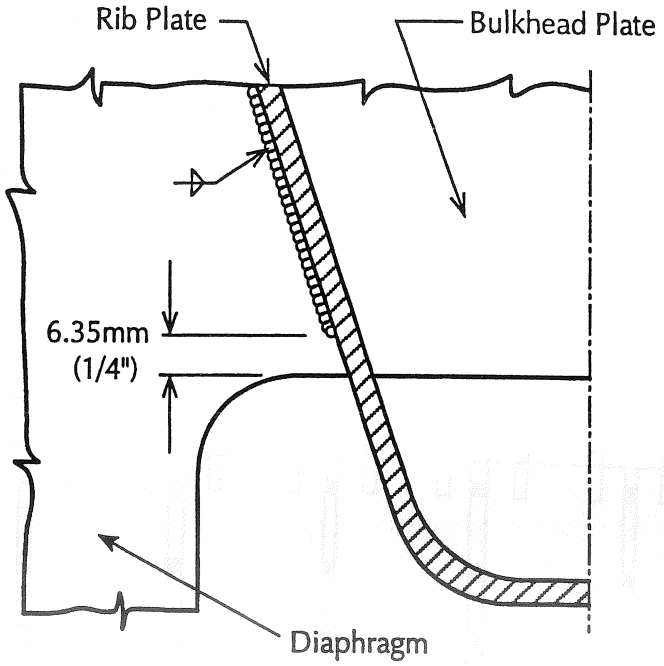

Figure 1.6 Weld Option B for Rib to Diaphragm Connection

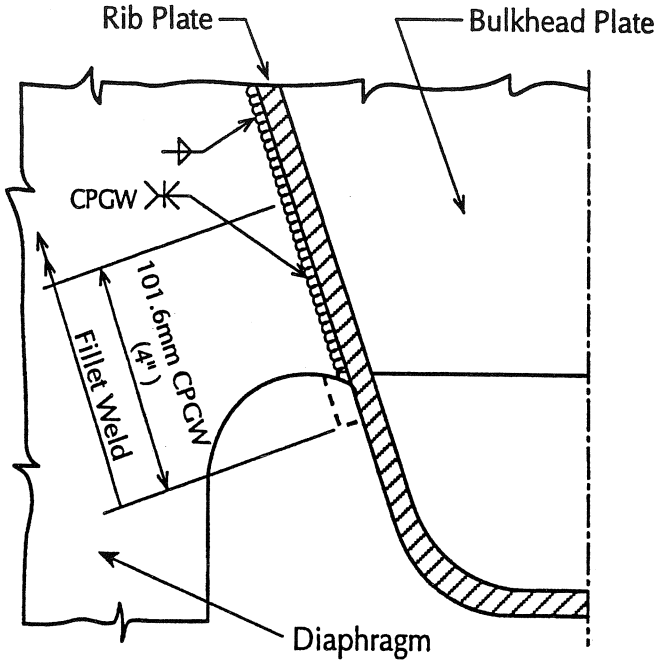

Figure 1.7 Weld Option A for Rib to Diaphragm Connection

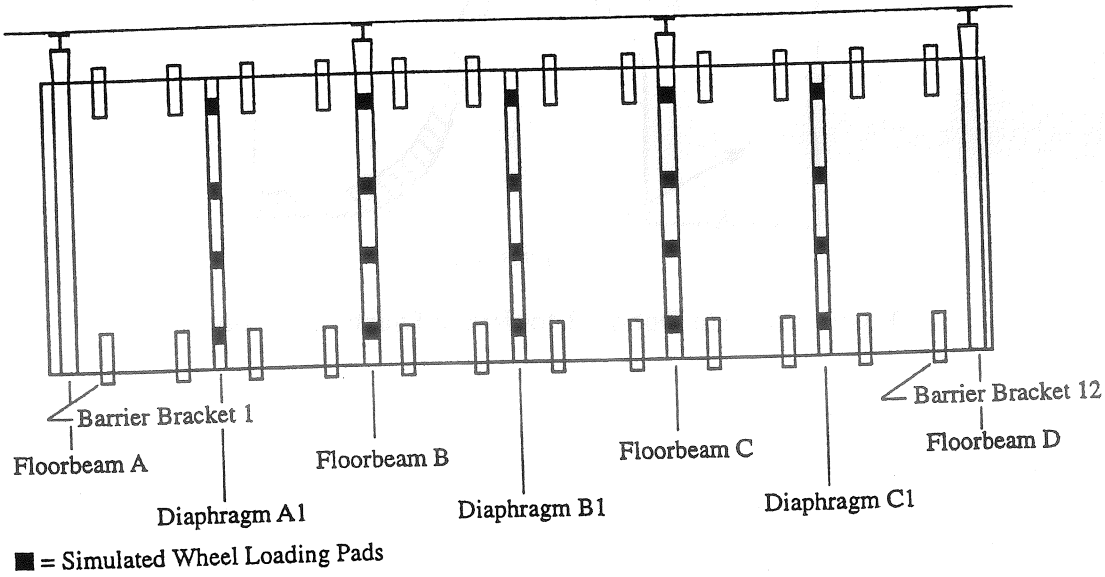

Figure 1.8 Plan View of Phase I Deck Panel

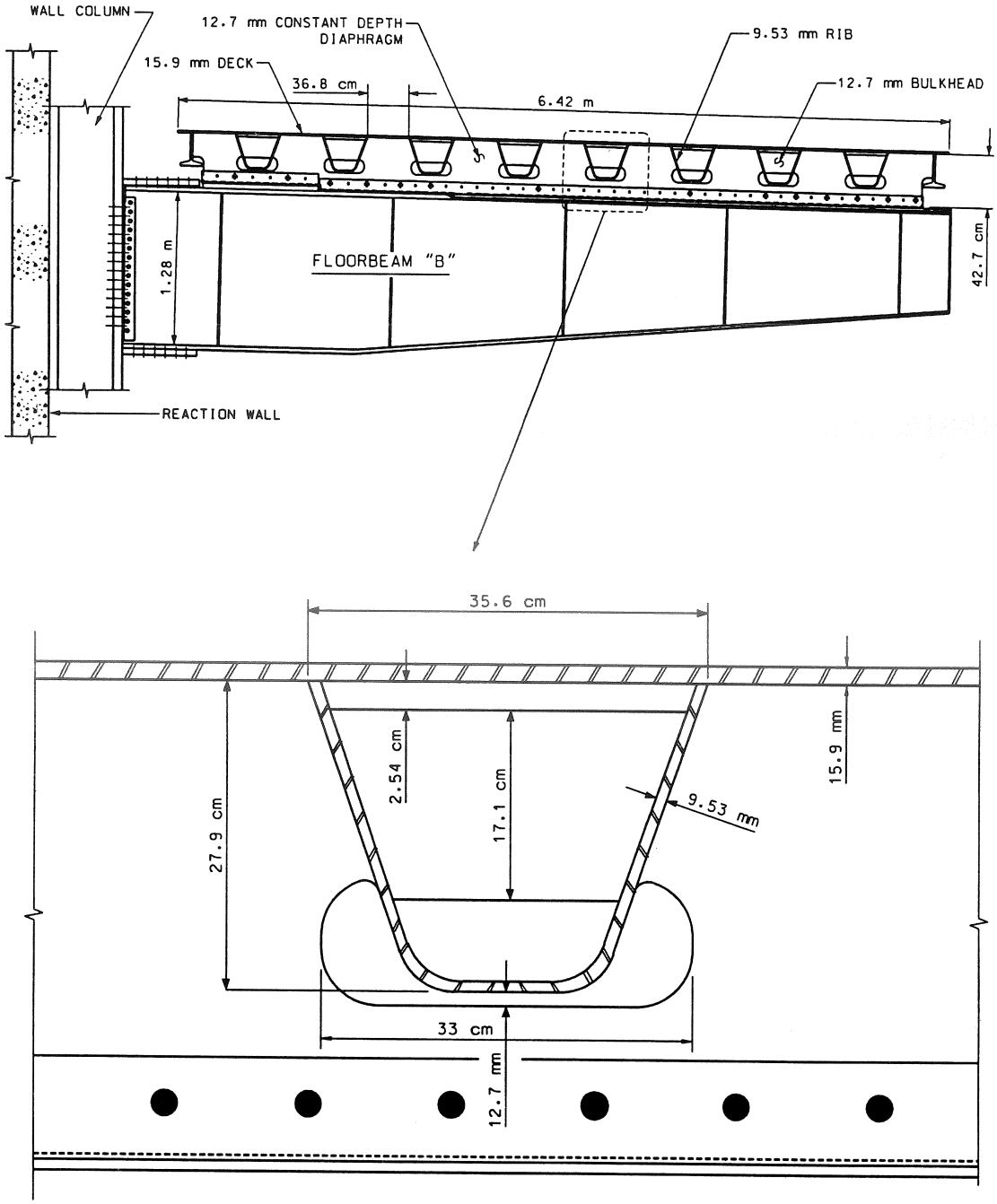

Figure 1.9 Cross-Section of Final Design of Actual Replacement Deck

2.0 TEST SETUP

2.1 Test Deck Preparation

2.1.1 Reconfiguration of Existing Test Panel

In order to conduct the Phase II test, the prototype deck panel from Phase I was modified to incorporate the design changes implemented into the final design of the bridge's actual replacement deck in 1995. The main purpose of the Phase II test is to examine the behavior of the combination full penetration - fillet weld rib to diaphragm connection (Option "A"), with associated changes in the diaphragm and bulkhead plate thicknesses and the diaphragm depth, under normal and extreme loading conditions. The modified test deck only needed to evaluate the actual fabricated connection. Whereas the test deck in Phase I was a three-span continuous system supported by four floorbeams with two internal diaphragms, the modified Phase II test deck is a two-span continuous system supported by three floorbeams with one internal diaphragm. Several steps were taken in order to incorporate all of these changes in the test deck.

The prototype deck in Phase I was comprised of three test panels which were joined by two transverse full penetration deck welds and bolted rib connections, as shown in Figure 2.1a. The middle test panel, being slightly longer than the two identical end panels, contained the two interior floorbeam diaphragms which were the focus of the Phase I test (as the end floorbeams were not significantly loaded). All fatigue cracks from the previous test occurred at the two interior floorbeam diaphragms

on the middle panel since they were loaded to simulate trucks crossing the span. The two end panels could be reused for the Phase II test as they were not subjected to significant loads.

ATLSS lab technicians removed the middle test panel by flame cutting through the center of the two transverse deck welds and by unbolting the rib connections and the internal diaphragm connections to Floorbeams B and C. An overhead crane was then used to remove the middle test panel, as shown in Figure 2.1b. During this time, the free ends of the two end test panels were supported by temporary shoring.

Next, the bolted connections between the end diaphragm on the northern test panel and floorbeam D were removed. Using the overhead crane, the northern test panel was moved south and its diaphragm was reattached to floorbeam C, as shown in Figure 2.1c. Temporary shoring supported its free end. Floorbeam D was removed and scrapped.

2.1.2 Design and Fabrication of New Test Panel

A new, short section of deck, approximately 0.79 m (2.6 ft) in length, was designed to fill in the gap between the original two end panels. Figure 2.1d shows this final configuration of the Phase II test setup. ATLSS researchers designed this new deck segment to match the existing test panels. NYCDOT, NYSDOT, and Steinman approved the fabrication drawings before the test segment was fabricated. The new deck section incorporated all of the final design changes implemented into the actual replacement deck. It had a continuous, constant depth, 13 mm (0.5 in.) thick diaphragm

which attached to the interior floorbeam with bolted connections, as illustrated in Figure 1.9. Continuity of the diaphragm was accomplished by making smaller rib cutouts which did not extend to the bottom edge of the diaphragm plate, as shown in Figure 1.5. All rib to diaphragm connections were made with the Option A combination full penetration - fillet weld and were ground smooth at the end to avoid any discontinuities. The bulkhead plates were 13 mm (0.5 in.) thick and extended 18.75 mm (0.75 in.) below the ends of the exterior diaphragm to rib connection so that both of these plates did not intersect the rib wall at the same depth.

Leonard Kunkin Associates manufactured the new deck section using the same processes, weld designs, and tolerances they had used in fabricating the actual replacement deck. Assembly began with laying out the deck plate. After bending the longitudinal ribs into trapezoidal cross sections and welding the bulkheads in place, the ribs were attached to the deck plate with partial penetration welds. Finally, the diaphragm plate was fitted and welded to the ribs and deck plate. NYCDOT inspected the entire fabrication process to ensure it met all applicable specifications.

2.1.3 Interior Floorbeam Modifications

Before erecting the new deck section, ATLSS technicians had to reposition the existing interior floorbeam to accommodate the new section's constant depth diaphragm such that the roadway maintain the proper longitudinal and transverse gradients. In the Phase I test, which utilized the original design of the replacement deck, the floorbeams were approximately level. The diaphragm plate was tapered to produce the two percent

transverse slope of the roadway. However, after the changes of Phase I were adopted, it was found necessary to replace the existing floorbeams as field surveys by the contractor demonstrated that large variations in the floorbeams' alignments existed. It was more cost effective to fabricate new floorbeams that could be installed with the proper inclination to accommodate a constant depth diaphragm and provide the required two percent slope. In order to adapt the existing floorbeam in the laboratory, its fixed end had to be lowered slightly before the beam could be tilted due to the physical constraints of its connection to the wall column. However, lowering the entire floorbeam meant that fill plates needed to be placed on top of the floorbeam's top flange so that the new deck section would be at the same elevation as the existing sections supported by the end floorbeams.

2.1.4 Installation of New Test Panel

Upon completion of the floorbeam alterations, erection of the new deck section took place. Because of the short length of this section, it could not be installed using the Phase I procedure. ATLSS lab technicians followed a similar procedure which was approved by NYCDOT engineers and monitored by a NYCDOT inspector. As in the field, the new section connected the existing sections using bolted rib splice plate connections and complete penetration transverse deck welds. The transverse deck splices used a submerged arc welding process which left the backing bars in place. The transverse groove welds were ultrasonically tested to ensure they had no rejectable discontinuities. In order to study the effect of the transverse deck weld's root opening

length on the unsupported deck section over the rib cutouts for the backing bar, different root openings were used in the two splices between the new deck section and the existing deck sections. As shown in Figure 2.2, these two welds had root openings of 9.5 mm (0.375 in.) and 28.5 mm (1.125 in.), which were the minimum and maximum root openings allowed in the actual replacement deck.

2.2 Specifics of the Test Setup

2.2.1 Physical Parameters of Test Deck

Simulating the conditions of the actual roadway on the replacement deck, the 12.2 m (40 ft) long by 6.1 m (20 ft) wide test deck spanned continuously over three cantilevered floorbeams at a three percent longitudinal grade and a two percent transverse slope. As in the Phase I test, the 6.9 m (22.5 ft) long floorbeams were spaced at 6.1 m (20 ft). Figure 2.3 shows a photograph of the fully assembled test deck and actuator layout. The exterior floorbeam diaphragms were from the Phase I test and did not incorporate the design changes implemented in the actual replacement deck. However, the loading scheme subjected only the interior diaphragm to a complete stress cycle, so fatigue cracking should be minimized at the exterior diaphragms. All floorbeams and wall columns were used in the Phase I test. Only the interior floorbeam had been modified as described in the preceding section. The 3.75 m (12.3 ft) long shear plate connector used in the center panel of Phase I was reattached to the northern test panel to prevent longitudinal motion and twisting of the roadway. As in the Phase I

test, the asphalt concrete overlay was also omitted from the test deck. During the dynamic fatigue test, the actuators were used to provide a minimum load which accounted for the dead weight of the overlay in lieu of the sand bags that were placed on the deck during Phase I.

2.2.2 Loading Methods

Static loads were applied to the test deck in two ways: by moving a single test vehicle slowly across the deck in several transverse locations, and by employing an actuator setup similar to that used in Phase I. Phase II utilized both these test methods in order to examine the actuator loading distribution through the distribution pads that simulated the tire prints and the adequacy of discrete load points. Furthermore, test results will also be compared with results from field tests on the actual roadway.

2.2.2.1 Rolling Truck Test

As shown in Figure 2.4, the test vehicle consisted of a simple steel frame connecting a pair of truck axles. Using a cable and pulley system, the overhead crane was used to slowly pull the vehicle across the test structure at an approximate speed of 0.2 m/s (0.5 miles/hr). The frame was loaded with five steel blocks to give it a weight of 235 kN (53 kips). The four tires on each of the 1.8 m (6 ft) long axles were inflated to 620 KPa (90 psi). Tests were performed with the experimental vehicle positioned in both the inner and outer lanes, and axle spacings of 1.22 m (4 ft) and 3.05 m (10 ft) were used in both these locations. These tests are not discussed in this report.

2.2.2.2 Actuator Tests

The actuator loading scheme, used in both the static and dynamic tests, applied an inner and outer lane of wheel loads to the test deck with 530 kN (120 kip) actuators at three transverse locations along the length of the deck. Figure 2.5 shows the locations of the wheel load patches, two groups of which were applied at the midsection of the two spans, and the other of which was applied directly over the interior floorbeam. As in Phase I, spreader beams distributed the load from each actuator to four patch loads which simulated AASHTO recommended 305 mm (12 in.) x 711 mm (28 in.) wheel footprints. Neoprene pads 3 mm (0.125 in.) thick were again placed under each footprint to ensure uniform loading distribution under the loading plates. The outermost wheel load was centered 610 mm (2 ft) from the edge of the roadway, and the centers of the three remaining wheel loads are spaced at 1830 mm (6 ft), 1220 mm (4 ft), and 1830 mm (6 ft) intervals as detailed in the AASHTO specification. Figure 2.6 shows the transverse locations of these wheel loads on the test deck at the interior floorbeam. To simulate the extreme loads corresponding to the AASHTO extreme life check, loads were applied without impact in the inside lane and with 30 percent impact in the outside lane. Loads from the three actuators were applied in a sequence similar to that used during Phase I and subjected the diaphragm and interior floorbeam to the same stress cycle caused by two vehicles traveling adjacent to each other over the actual bridge deck.

2.3 Simulated Truck Loading Method

Phase II employed an actuator loading scheme similar to that used in Phase I to conduct static calibration and dynamic fatigue tests. However, due to the reduced size of the test specimen from three spans supported on four floorbeams to two spans supported on three floorbeams, the loading method had to be altered. These modifications included a reduction in the number of actuators used in the test, a decrease in the number of steps required for one complete loading cycle, and changes in the load magnitudes in each step of the sequence. A description of the loading method used in Phase I is reviewed before explaining the loading method developed for Phase II.

2.3.1 Phase I Loading Method

NYCDOT devised the loading method used in Phase I on the basis that the most important objective of the fatigue test was to evaluate the performance of the rib to diaphragm connection details[8]. It therefore aimed to accurately represent the maximum in-plane and out-of-plane effects in the diaphragms at each interior floorbeam. To accomplish this, simple beam models were used. As shown in Figure 2.7a, a design truck was moved along a continuous beam model of the bridge deck to produce the maximum applicable response. A three span beam model of the actual test specimen was then created with loads applied at stationary locations, shown in Figure 2.7b, which corresponded to the actual actuator locations. The stationary loading sequence produced reactions, deflections, and rotations of the two interior floorbeams

similar to those of the moving loads.

The five-step loading cycle in Phase I produced sequential peak out-of-plane and in-plane effects at the inner floorbeams caused by traffic moving along the test specimen. At Step 0 there was no load on the deck. Step 1 produced maximum counterclockwise rotation (out-of-plane effects) at floorbeam B and maximum clockwise rotation at floorbeam C. Steps 2 and 3 produced maximum in-plane effects at floorbeams B and C, respectively. Step 4 produced maximum clockwise rotation at floorbeam B and maximum counterclockwise rotation at floorbeam C.

2.3.2 Derivation of Phase II Load Cycle

As in Phase I, a five-span continuous beam model of the orthotropic deck was created to help derive the loading sequence for Phase II. This continuous beam model rested on six spring supports which provided resistance to vertical deflections. Simulating the constraints of the actual floorbeams, the supports were fixed in the horizontal direction and were free to rotate. The value of the spring constant was estimated by applying a load on a finite element model of a floorbeam and setting the stiffness equal to the load magnitude divided by the deflection of the beam at the location of the load. The geometrical properties used in the beam model were the cross-sectional area and moment of inertia of the actual deck. Wheel loads of an HS20 design truck with various axle spacings were moved across this beam model to determine the maximum out-of-plane rotations and in-plane displacements at the interior supports. The stiffness of the supports depended on the location of the load

used in the floorbeam finite element model. However, three different spring constants were used in this analysis, and the locations of the wheel loads which produced the desired maximum effects were the same in each case.

The derivation of the Phase II loading cycle proceeded by creating a two-span continuous beam model of the test specimen which rested on three spring supports. The cross-sectional properties of the beams used in this model were identical to those used in the five-span model. Three complete analyses, identical in all respects except for the stiffnesses of the supports, were performed using the same spring constants from the five-span beam model. In each analysis, loads were applied at the locations of the three actuators to be used in the Phase II test.

The Phase II loading cycle was divided into four steps: at Step 0 no load was on the deck; Step 1 produced the maximum counterclockwise rotation of the interior support; Step 2 produced the maximum in-plane displacement of the interior support; Step 3 produced maximum clockwise rotation of the interior support. Figure 2.8 displays the beam models in each of these steps. These maximum rotations and displacements of the interior support were the same as those determined using the five-span continuous beam models. The load values which produce these maximum rotations and displacements were determined on a trial-and-error basis.

The loads determined in each step of the loading sequence for the three cases of different spring constants were quite similar. An average value of the load in each step was therefore used to create the final sequence. In the analyses performed, the loads of the HS20 design truck applied to the five-span beam models were due to one wheel

load at each axle location. Because the Phase II test aimed to simulate the effects of the passage of two HS20 trucks traveling side-by-side over the bridge deck, the averaged actuator loads should be multiplied by four. However, to produce a dynamic impact factor of 1.3 on the outside wheel loads as was done in the Phase I test, the averaged wheel loads were multiplied by 4.6. Figure 2.9 displays the equivalent HS20 wheel loads at each footprint, without impact factors, used in the static tests.

The loads applied during the dynamic test were lower than the equivalent HS20 loads applied in the static calibration tests because AASHTO prescribes HS15 trucks for fatigue design. Under sufficiently slow load applications, the dynamic loads would therefore be 75% of the static loads. However, due to inertial effects caused by the loading rate used in the fatigue test, the loads had to be further decreased such that strain ranges of the gages monitored in the dynamic test were about 75% of their static ranges.

2.4 Instrumentation Plan

The instrumentation plan developed for Phase II aimed at studying the global behavior of the entire deck system and the local behavior at fatigue critical connection details identified in Phase I. Over 200 strain gages and twelve displacement transducers measured strains and deflections at numerous locations on the test specimen during the static calibration tests with the actuators. Locations of high strain were identified, and 26 of the gages in these locations were monitored at regular intervals throughout the fatigue test.

2.4.1 Global Behavior

Studying the global behavior of the deck panel during the static tests focused on measuring the midspan strains of the ribs and deck plate, strains at the fixed end of the interior floorbeam, midspan displacements, and deflections at the free ends of the floorbeams. This information will be most useful for comparison purposes with a finite element model which will be created of the test deck. Also for this purpose, displacements of the wall columns immediately above the top flange and below the bottom flange of the fixed end of the floorbeam were measured with respect to the reaction wall to determine if there was any relative rotation of these supports. This information will determine the support conditions of the floorbeams used in the finite element model.

Locations of gages measuring the deck and midspan strains are shown in Figure 2.10 and 2.12. Figure 2.11 displays the locations of gages at the fixed end of the interior floorbeam, as well as positions of the linear variable displacement transducers (LVDTs) used to measure displacements at each of the three floorbeams. Locations of LVDTs measuring displacements along the span of the deck are also shown in Figure 2.12.

As a general note to these and all other figures displaying instrumentation locations, not every section of the deck has all or any of the instrumentation shown at that section in the figure. For example, only Ribs 5 and 9 have the gages shown in Figure 2.10. Detailed drawings showing precise locations of all instrumentation are

provided in Appendix A.

2.4.2 Local Behavior

2.4.2.1 Diaphragm Gages

As shown in Figure 2.13, strain gages were installed at numerous locations on the interior diaphragm plate around the ribs to study local behavior and monitor stress ranges acting on fatigue critical connections of the orthotropic deck system. In the Phase I test, fatigue cracks occurred in the diaphragm plate near Ribs 3, 5, 6, 7 and 9 at the termination of the Option B rib to diaphragm connections, but only at Rib 5 for the Option A detail. Since the Phase I peak diaphragm stresses were found near the termination of the rib to diaphragm welds at Ribs 5 and 7, most of the strain gages in Phase II cluster around these locations at these ribs. Both Ribs 5 and 7 have back-to-back rosettes installed on the diaphragm plate directly above the cutout about a 1/4" from the rib to diaphragm weld toe to determine the maximum stress ranges acting at this fatigue critical location. These rosettes were positioned on both sides of these ribs and were installed back-to-back to determine what proportions of the diaphragm stress are due to in-plane and out-of-plane bending. Data from these gages should confirm the conclusion from Phase I that in-plane stresses dominate bending of the diaphragm plate. Furthermore, during the Phase I test, gages were installed in the same location and orientation as these rosettes, so a direct comparison can be made between the maximum

stress ranges in the two tests.

Gages were installed at two other locations along the rib to diaphragm weld toe on the diaphragm on both sides of Ribs 5 and 7 to measure the strain gradient along the weld toe. Either rosettes or biaxial gages were positioned one inch above the rosettes immediately above the cutout, and they were also installed slightly below the bottom of the deck plate. All of these gages are located about 1/4" from the rib to diaphragm weld toe.

Numerous gages were installed around the diaphragm cutouts of Ribs 5 and 7 to study the stress distribution throughout the continuous diaphragm. Because the diaphragm was not continuous in the Phase I test and the shape of the cutout was different, it is not known if there are any areas of high stress concentration around the cutout. Gages were positioned as shown in Figure 2.13 as the Phase I studies verified hot-spot locations exist.

While most gages on the diaphragm were positioned around Ribs 5 and 7, numerous gages were installed around the other ribs to measure strains throughout the entire diaphragm plate, as can be seen in Figure 2.14. This will allow for a comparison of diaphragm strains among most of the ribs. Of the trapezoidal ribs, only Rib 2 had no gages installed because no cracking occurred at this rib in Phase I. Nor were gages positioned adjacent to Ribs 1 or 10 because T-shaped ribs have not exhibited susceptibility to fatigue cracking in the past. The layouts of the gages installed around the other ribs (Ribs 3, 4, 6, 8, and 9) are subsets of the gages around Ribs 5 and 7.

Thus, these ribs have some of the gages that are installed around 5 and 7, but not all of them. No rosettes were installed around any of these other ribs, and, except for Rib 6, they only have gages on one side. Gages were placed adjacent to the rib to diaphragm weld immediately above the cutout and slightly below the bottom of the deck plate. During the initial static calibration test, there were no back-to-back gages installed around any of these ribs. However, after studying data from this test, it was decided that back-to-back gages would be needed on Ribs 8 and 9 along the rib to diaphragm weld toe immediately above the cutout, as bending gradients through the web thickness were apparent at all ribs. They were installed and used during all subsequent static calibration tests, which were conducted at one million and 2.5 million cycles into the fatigue test. No gages were positioned around the diaphragm cutouts of any of these ribs.

Biaxial gages were positioned on the diaphragm between two pairs of ribs (4&5 and 6&7). Figure 2.15 displays the locations of these gages. Since it is difficult to predict strains at locations of high stress concentration using finite element models, it was decided to install some diaphragm gages at locations where comparisons between computer analyses and experimental results could be made.

2.4.2.2 Bulkhead gages

Several cracks occurred at the terminations of the bulkhead to rib weld connections in the Phase I test. Thus, for the actuator test, uniaxial strain gages were

installed at the top and bottom corners on the south sides of the bulkhead plates in Ribs 5 and 7 to monitor the stress ranges acting on these welds. Locations of these gages are shown in Figure 2.13. For the rolling truck test, rosettes were installed at these same locations on the north sides of these bulkheads. Rosettes were also positioned at mid-depth on the east and west sides of the north bulkhead faces for the truck tests.

All these gages had to be installed before the ribs were welded to the deck plate because the bulkheads were inaccessible after welding. Furthermore, these gages could not be positioned too close to the edges of the bulkhead due to danger of excessive heat exposure when welding the diaphragm to the ribs. Despite these precautions, several of the gages were destroyed during the welding process. As a result, strains were not monitored at all four corners of the bulkheads during the initial static calibration tests with the actuators. However, during all subsequent static calibration tests, several of the rosettes originally installed for the truck tests were also monitored and strains at all corners of the bulkheads were recorded.

2.4.2.3 Rib Gages

As shown in Figure 2.16, gages were also mounted on the exterior rib walls adjacent to the interior diaphragm to measure strains in the longitudinal and transverse directions. No cracks occurred at the locations of these gages during the Phase I test. Many of them were installed primarily for comparison purposes with gages in the same

locations in this previous test.

Most of the exterior rib wall gages were installed on Ribs 5, 6, and 7. Other ribs have gages on just one side, but these three ribs had similar gage layouts on both their east and west sides. For comparison purposes with identical gages in Phase I, gages were positioned two inches north of the diaphragm near the top and bottom of the rib walls oriented in the longitudinal direction of the ribs. On Rib 6, one of these lower gages was actually located on the bottom along the centerline of the rib. Either rosettes or biaxial gages were used near the top of the rib to measure transverse strains transmitted directly by overhead wheel loads (rosettes were used on Rib 5 to obtain principal strains at this location). Uniaxial gages were positioned in the transverse direction near the top of the rib two inches south of the diaphragm for this same purpose. Rib 5 also has gages located directly beneath the bottom of the rib to diaphragm weld to measure strains transmitted from the diaphragm into the rib wall.

To measure strains transmitted from overhead wheel loads into the rib wall above the bulkhead weld, uniaxial gages were installed on the interior rib walls of both sides of Ribs 5 and 7 in the gap between the top of the bulkhead and the bottom of the deck plate. These gages, designated number eight as shown in Figure 2.16, had to be installed before the ribs were welded to the deck plate and, unfortunately, only one survived the welding process.

Numerous gages were installed on the exterior rib walls of Ribs 3, 4, 6, 8, and 9 so that strains can be compared among most of the ribs. The layouts of the gages on

these ribs are shown in Figure 2.16, but they only have gages on one side. As with the diaphragm, Ribs 1, 2, and 10 do not have any gages on their rib walls.

2.4.2.4 Transverse Deck Weld Gages

Due to concerns that large root openings in transverse deck welds may cause high local bending stresses in the unsupported region of the deck plate over the rib cope when wheel loads pass directly overhead, the root opening between the new test panel and the existing southern test panel was purposely made as large as permitted by actual construction tolerances, 1 1/8" (see Figure 2.2). The root opening between the new panel and the existing northern panel was made as small as allowable, 3/8". Two uniaxial gages were installed on the bottom of the deck plate along the centerline of the eastern wall of Rib 5 as close as possible to the supports of this longer unsupported span of deck, as shown in Figure 2.17. These gages were installed to assess local effects, primarily for the rolling truck test, and are to be compared with strains recorded by gages in similar locations during field tests of the actual roadway. It was not expected that the actuator loading scheme would develop a peak response in these gages since load is not introduced directly over the transverse deck weld; nonetheless, these and an additional gage on top of the deck plate directly above the southern aforementioned gage were monitored during the actuator test.

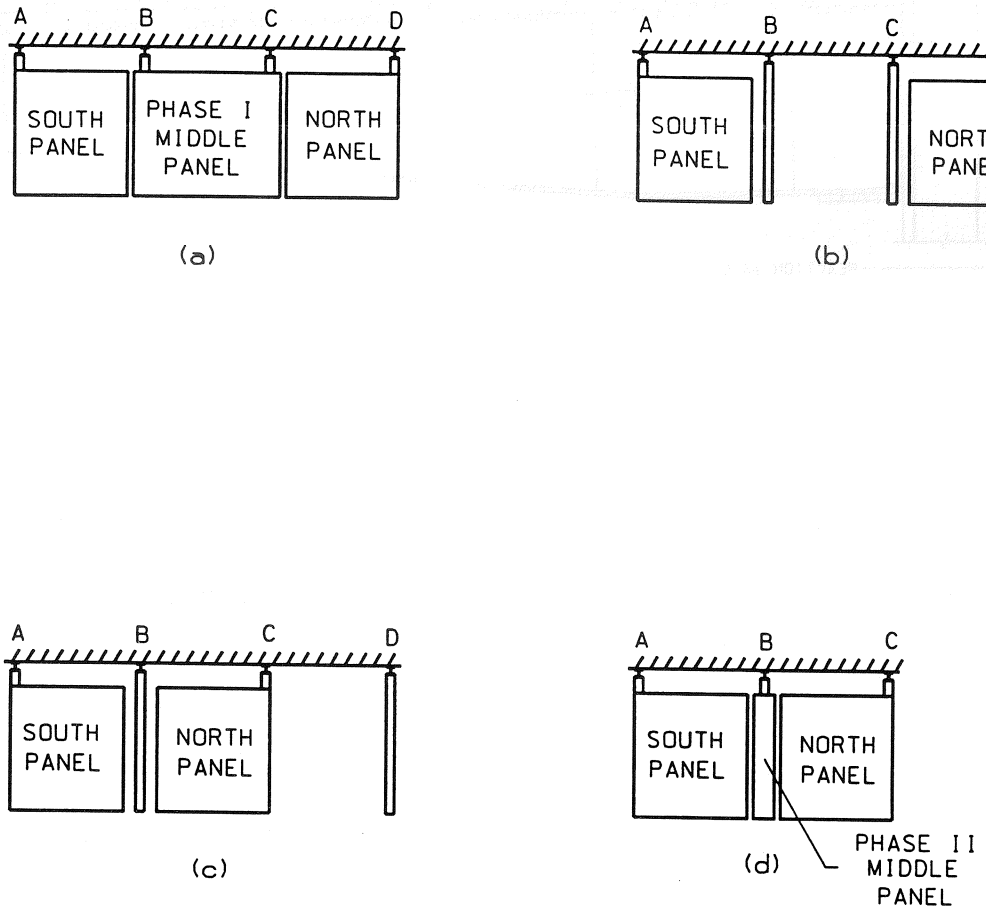

Figure 2.1 Test Panel Reconfiguration

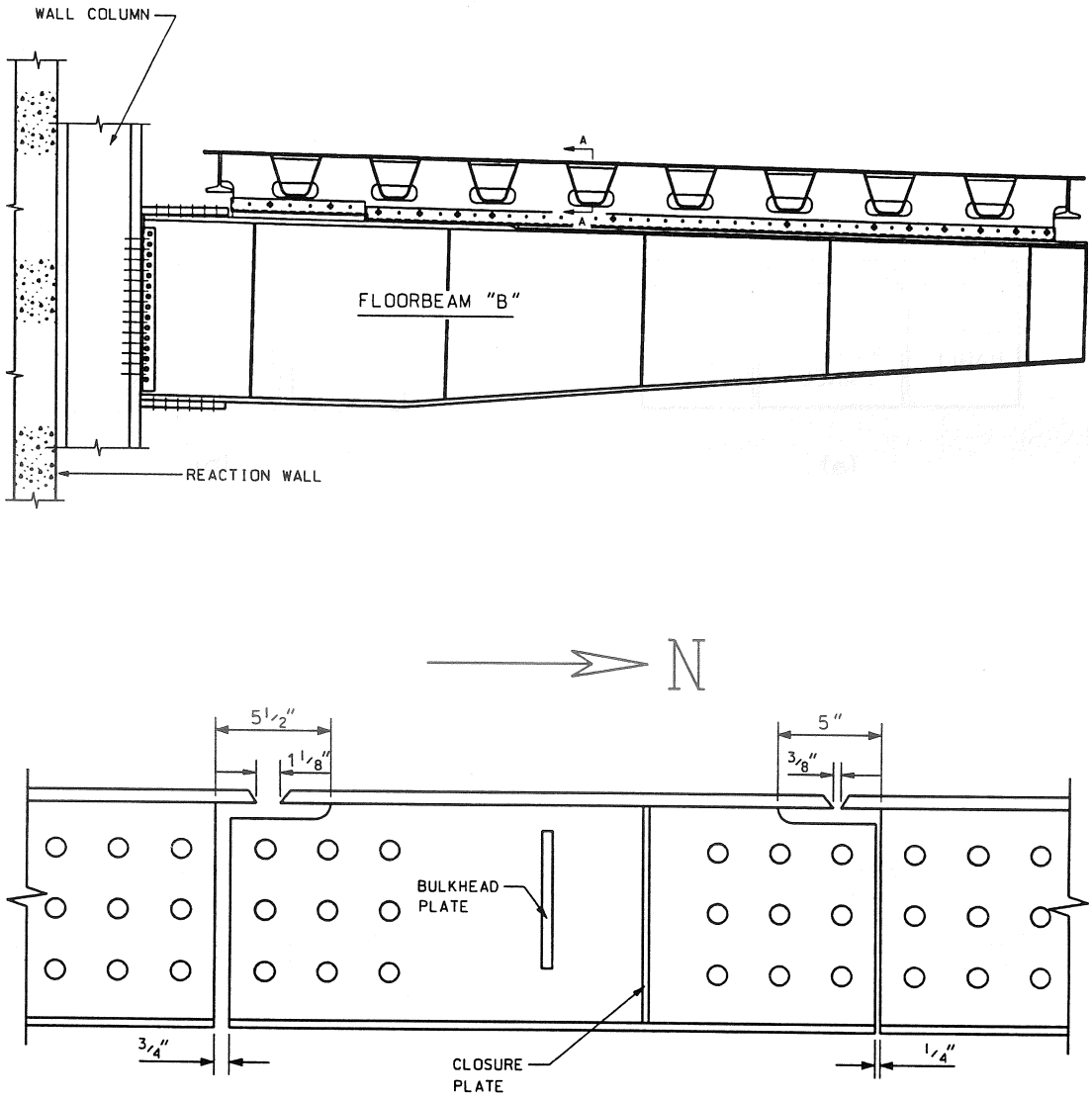

Figure 2.2 View of Trapezoidal Rib Wall Showing Deck Root Openings

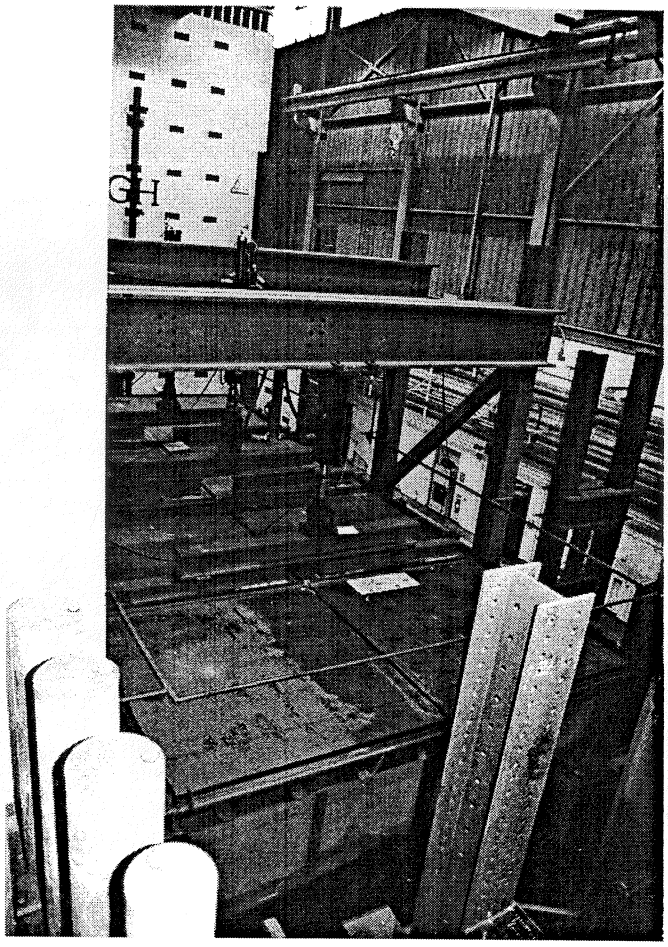

Figure 2.3 Assembled Test Deck and Actuator Layout

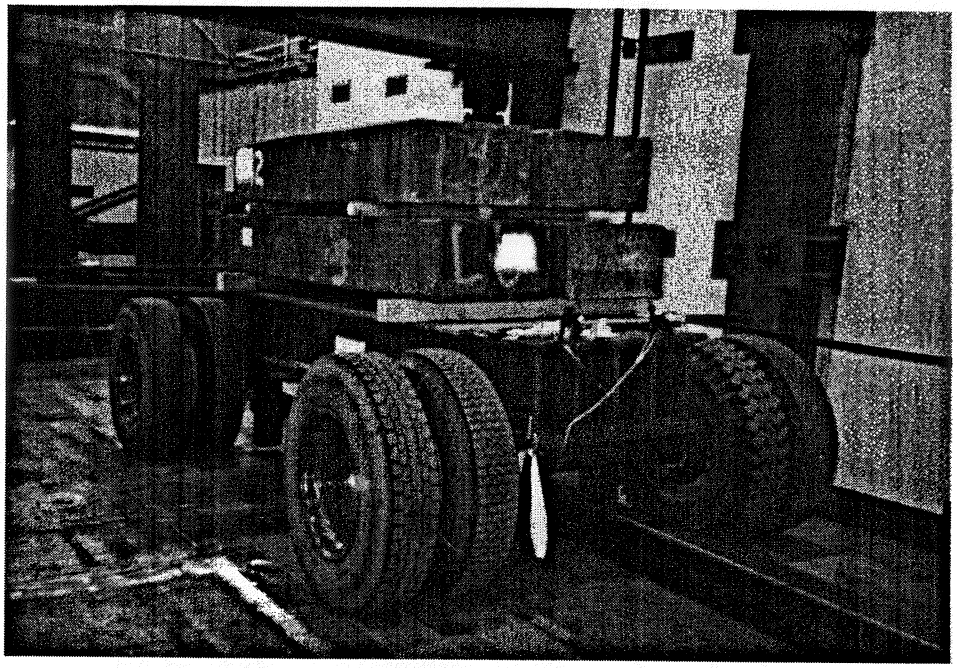

Figure 2.4 Test Vehicle

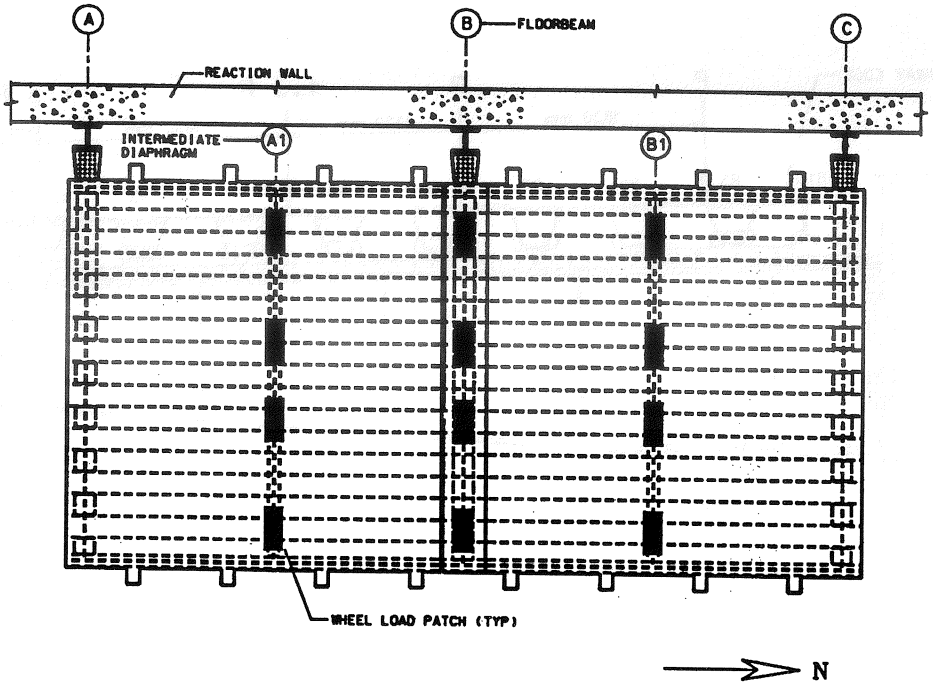

Figure 2.5 Plan View of Test Deck Showing Wheel Load Patch Locations

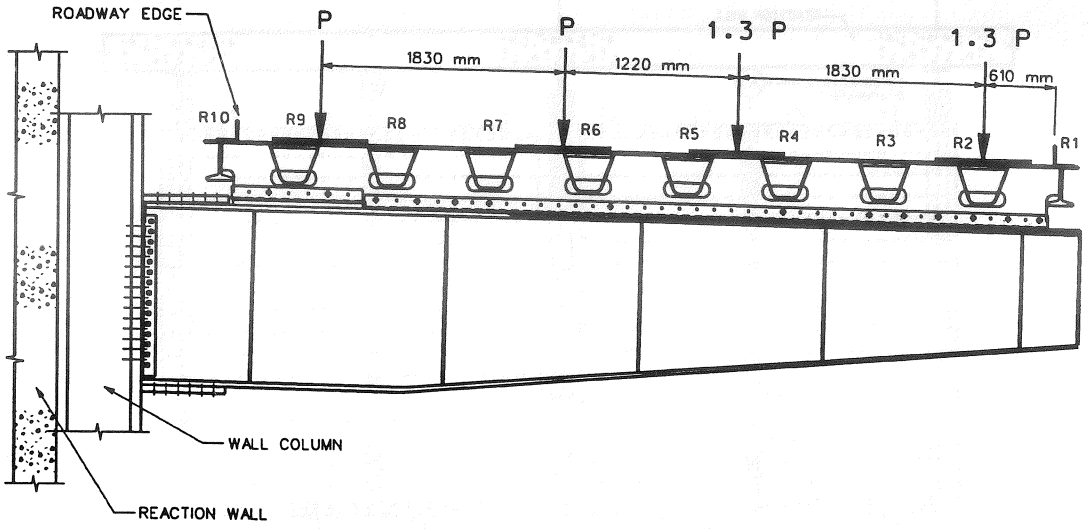

Figure 2.6 Wheel Load Patch Locations

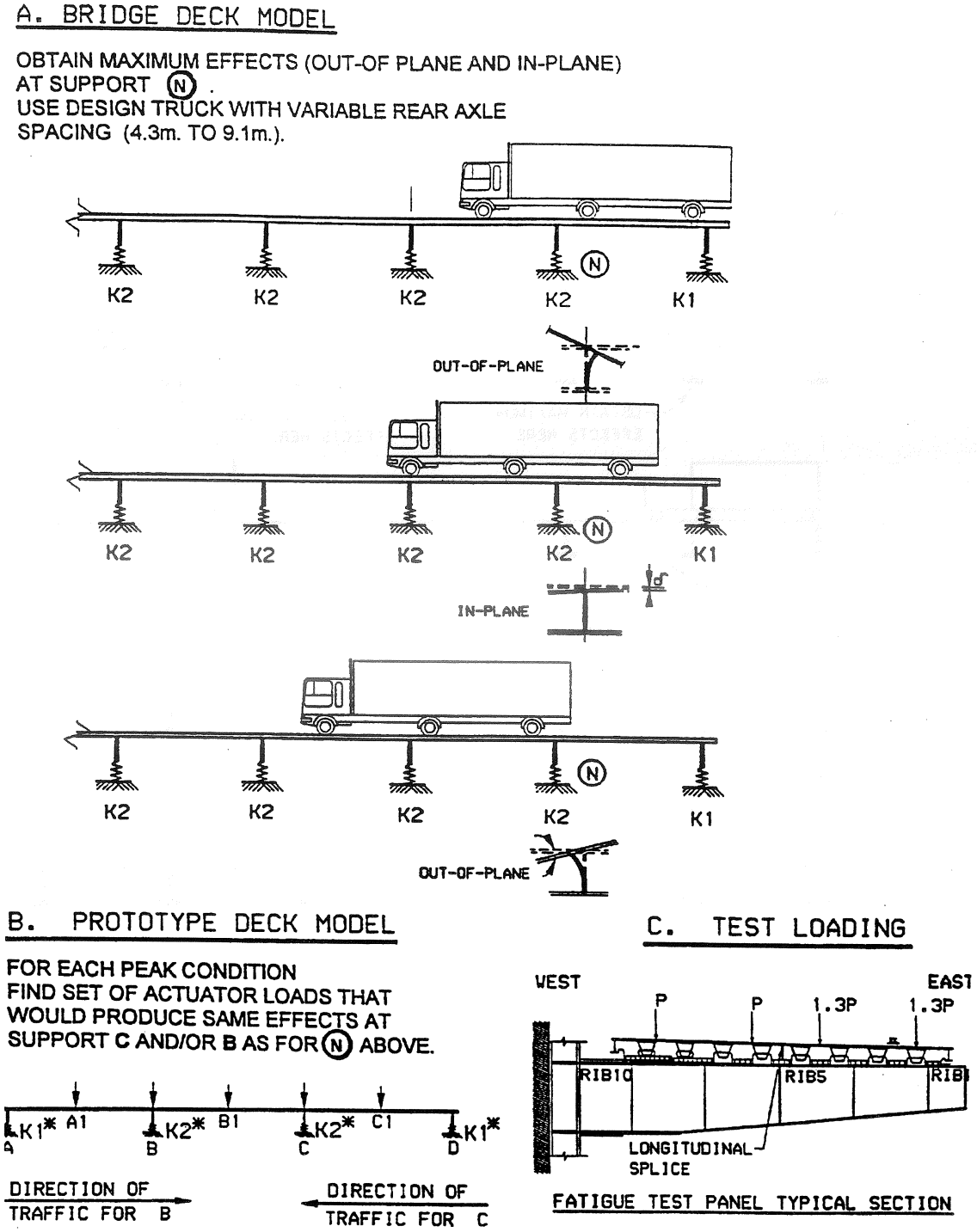

Figure 2.7 NYCDOT Procedure to Obtain Equivalent Truck Loads During Phase I

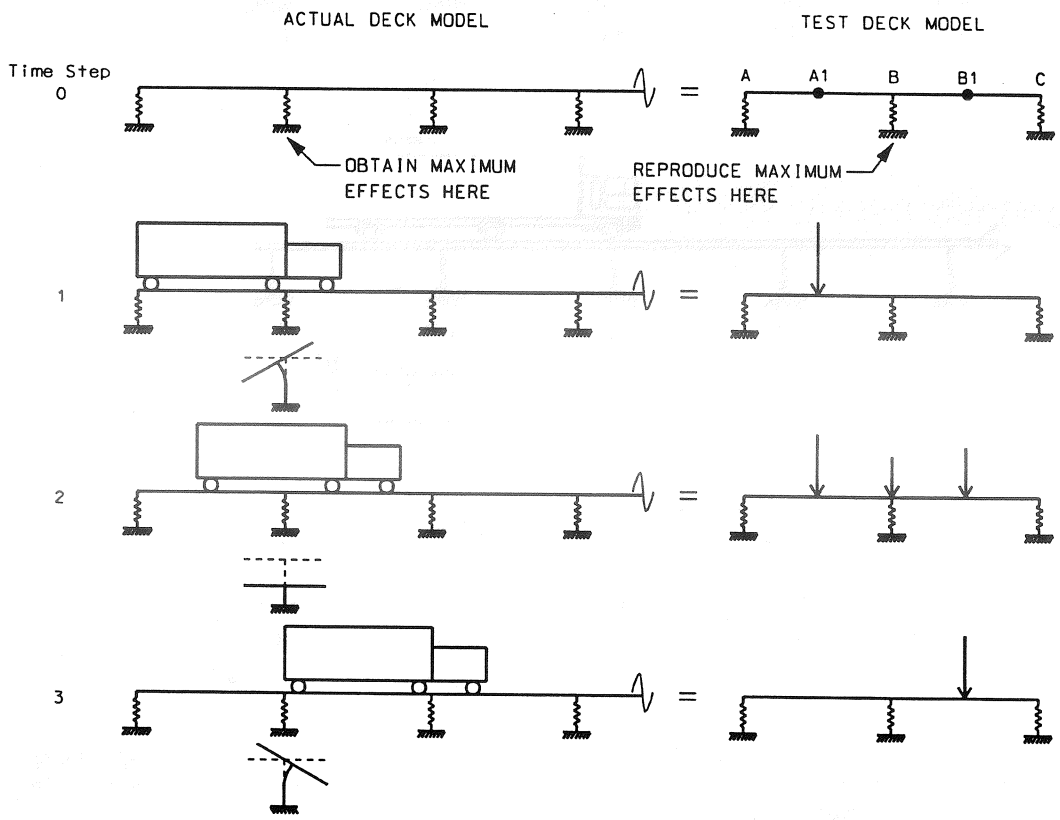

Figure 2.8 Phase II Beam Models

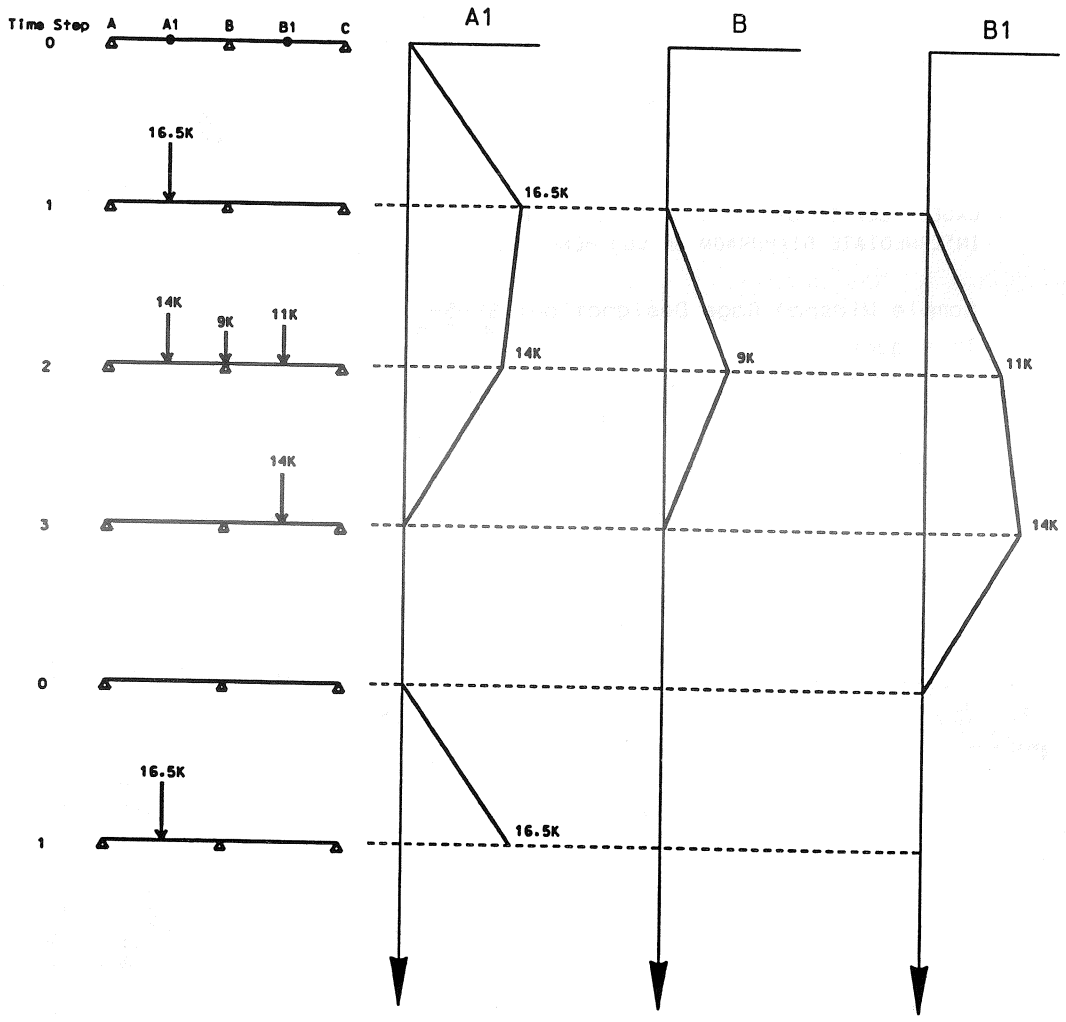

Figure 2.9 Phase II Equivalent HS20 Wheel Loading Scheme

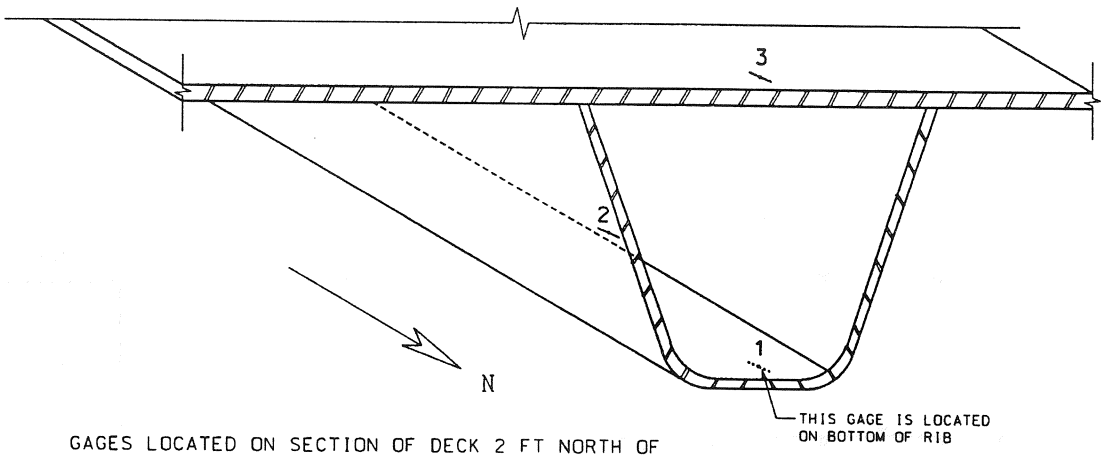

GAGES LOCATED ON SECTION OF DECK 2 FT NORTH OF INTERMEDIATE DIAPHRAGM ON SOUTHERN TEST PANEL

Sample Midspan Gage Designation: SP-5-1
△ ○ □

This gage is:

△ located near midspan of southern deck panel

○ on Rib 5 or on deck immediately above Rib 5

□ in position 1 shown in above figure

Figure 2.10 Gages Measuring Midspan Strains

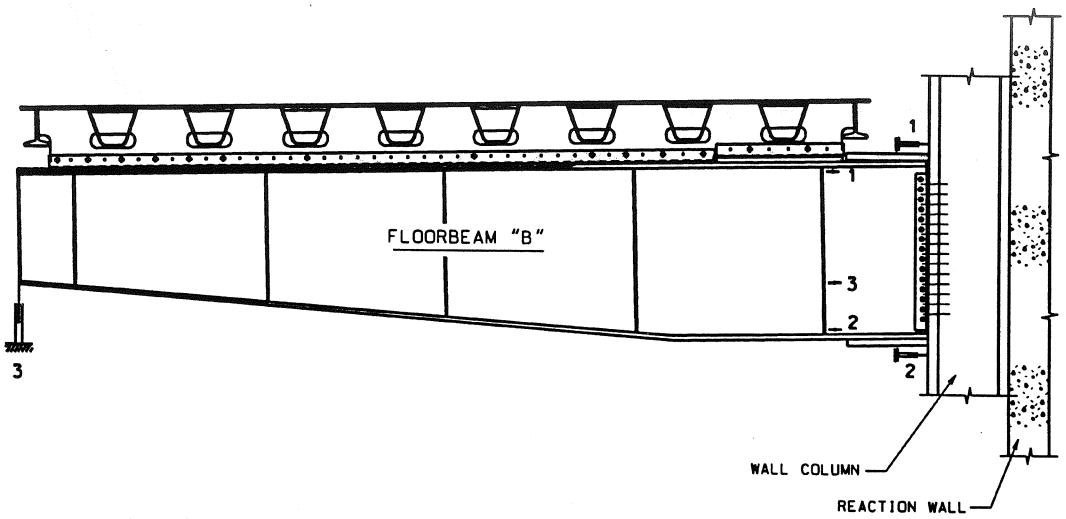

Sample Floorbeam LVDT Designation: DT-B-3
△ ○ □

This instrument is:

△ a displacement transducer

○ on floorbeam B

□ in position 3 shown in figure above

Sample Floorbeam Gage Designation: FB-B-3
△ ○ □

This gage is:

△ on floorbeam

○ on floorbeam B
(A and C do not have any gages)

□ in position 3 shown in figure above

Figure 2.11 Floorbeam Strain Gages and LVDTs

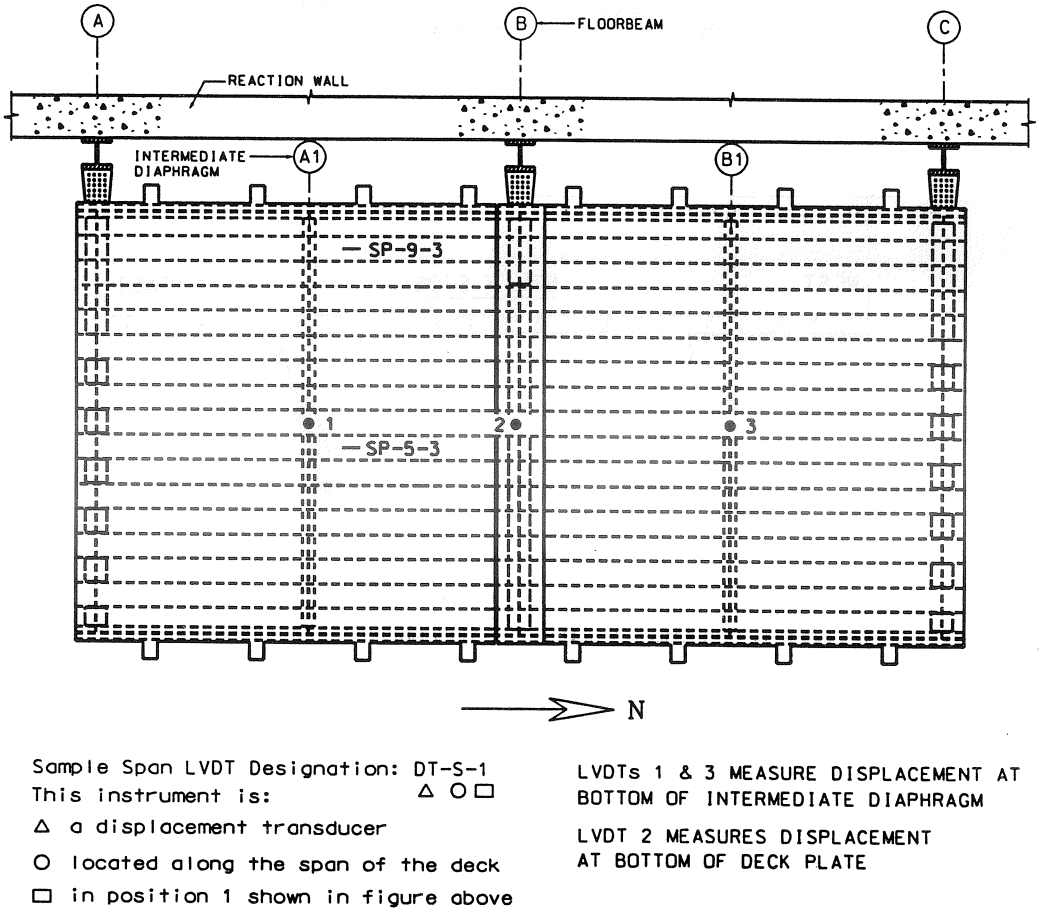

Figure 2.12 Locations of LVDTs Measuring Deck Displacements Under Actuators

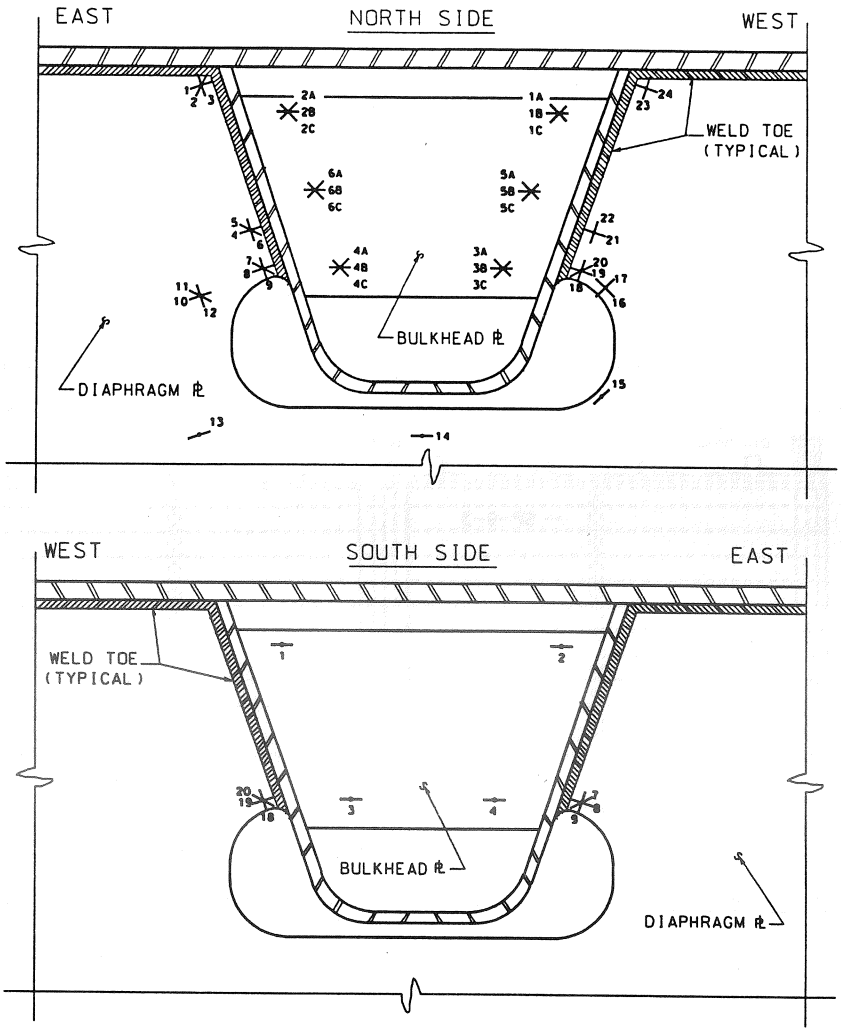

Sample Diaphragm Gage Designation: D5-N-13
△○ □ ◇

This gage is:

△ on diaphragm plate

○ on section of diaphragm around Rib 5

□ on north side of diaphragm

◇ in position 13 shown in above figure

Sample Bulkhead Gage Designation: B5-N-1A
△○ □ ◇

This gage is:

△ on bulkhead plate

○ on bulkhead inside Rib 5

□ on north side of bulkhead

◇ in position 1A shown in above figure

Figure 2.13 Diaphragm and Bulkhead Gages Around Ribs

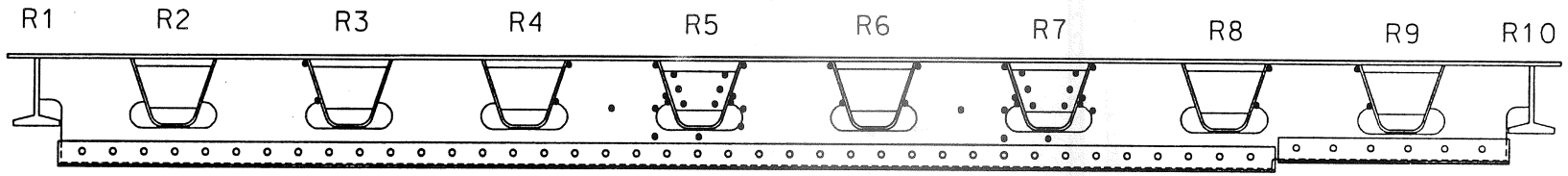

Figure 2.14 Gage Locations on Northern Face of Diaphragm and Bulkheads

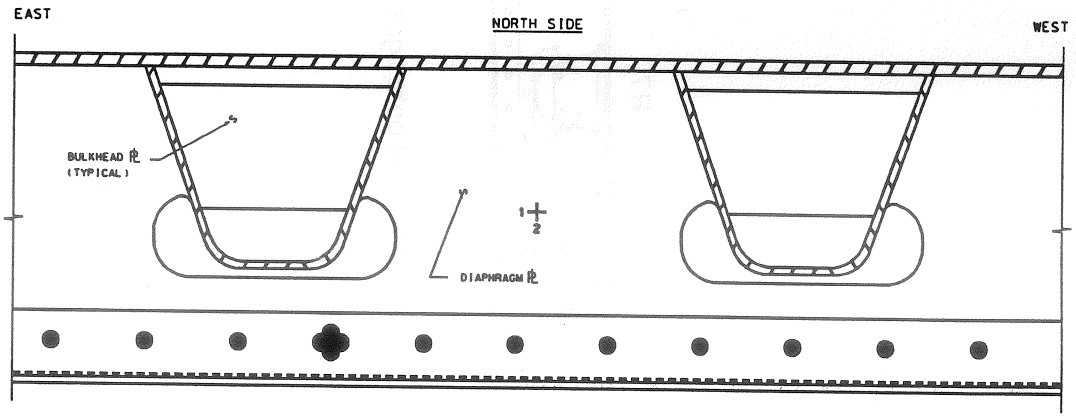

Sample Diaphragm Gage Designation: D45-N-1
This gage is: △ ○ □ ◇

△ on diaphragm plate
○ between Ribs 4 and 5
□ on north side of diaphragm
◇ in position 1 shown in above figure

Figure 2.15 Locations of Biaxial Gages Between Ribs

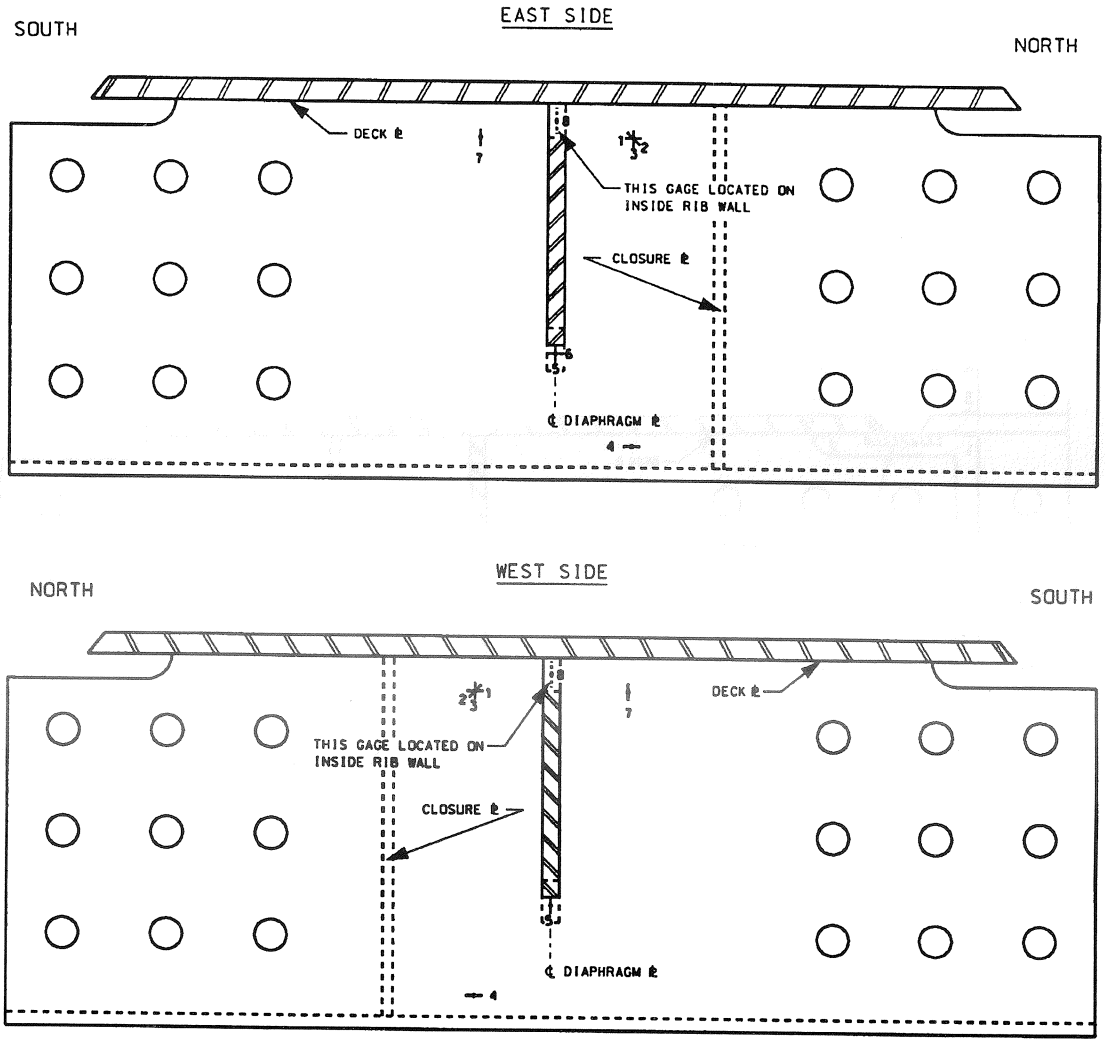

Sample Rib Wall Gage Designation: R5-E-4
▵o ▭ ◇

This gage is:

▵ on rib wall

o on Rib 5

▭ on eastern side of rib

◇ in position 4 shown in figure above

Figure 2.16 Locations of Gages on Rib Walls

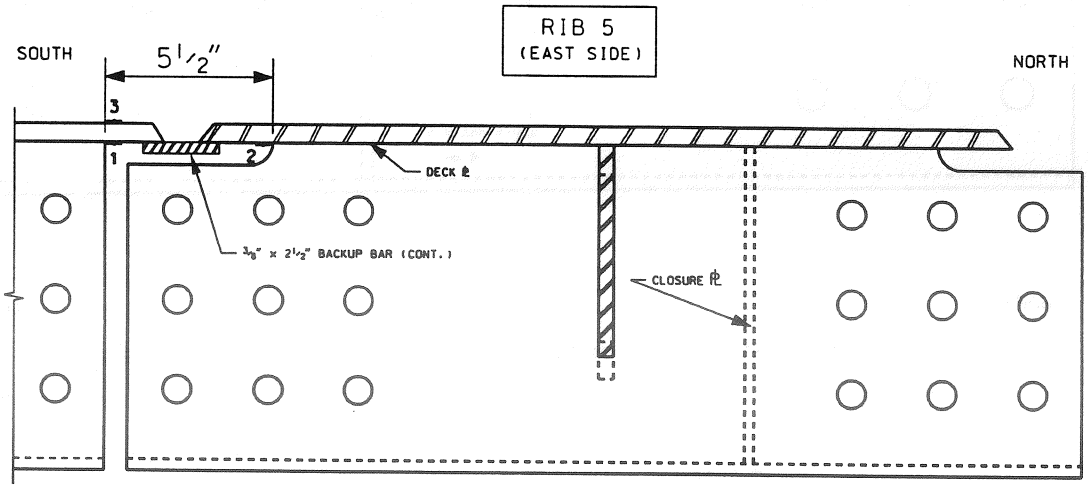

Sample Transverse Weld Gage Designation: TW-1
This gage is: △ ○

△ near transverse deck weld between southern and middle panels

○ in position 1 shown in above figure

Figure 2.17 Locations of Gages Near Transverse Deck Weld

3.0 STATIC TEST RESULTS

3.1 Descriptions of the Four Static Tests

A total of four individual static calibration tests were performed at intervals throughout the entire testing program to study the global behavior of the deck system and the local behavior of the fatigue critical connection details. In each of these tests, data were recorded from over 200 strain gages and LVDTs at each of the four time steps of the equivalent HS20 loading cycle. After achieving the desired loads at each time step, data were taken at a sampling rate of 2 Hz for five second periods using a Keithley Metrabyte DAS 1802 ST/DA conversion board and recorded using the VIEWDAC software package. The data from all channels were then averaged to reduce the effects of random noise as much as possible. All the results from each of these tests are presented in tabular form in Appendix B.

It should be noted that whereas the data in Appendix B correspond to the equivalent HS20 static load cycle including 30% impact in the outside lane, all the static test data presented in the text, tables, and figures of Chapter 3 correspond to the equivalent HS15 dynamic load cycle used for the fatigue test. This facilitates comparisons between this static and the dynamic test data presented in Chapter 4. As in the Phase I test, the equivalent HS15 loads were used during the dynamic tests because the higher HS20 loads exceeded the anticipated maximum stress range in service. Furthermore, the equivalent HS15 loads on two lanes correspond to the AASHTO extreme life check.

3.1.1 Static Test 1

Static Test 1 was performed before the start of the dynamic test. Based on these results, the strain gages recording the highest stress ranges in fatigue critical locations were identified and selected to be monitored periodically throughout the dynamic test. Each of the static tests required three instrumentation hookups due to limitations on the number of channels capable of being monitored by the data acquisition system; thus, it was desirable to limit the number of channels in the dynamic test to one hookup and record data from only the key gages. It is important to note that the shear plate connector was not used during this first static test. Not until after the start of the dynamic test was it deemed necessary to install the shear plate connector to prevent longitudinal motion of the deck. The absence of this component may contribute to some discrepancies, which will be discussed later, between this first and the remaining static tests.

3.1.2 Static Test 2

Static Test 2 was performed at 1.09 million cycles into the dynamic test. Another static test monitoring only those channels selected for the dynamic test was performed earlier at 100,000 cycles immediately after installation of the shear plate connector. This earlier test was performed for the sole purpose of recalibrating the dynamic load values to account for any changes caused by the addition of the shear plate connector. The results of this test were identical with those in Static Test 2 and are therefore not presented in this report. Because all components of the deck were in place and it had adequate time to shake down by this point, the data from Static Test 2 are most representative of the deck

system's true behavior when it had no indications of fatigue damage. Thus, unless specifically noted otherwise, all the data discussed in this chapter are from Static Test 2.

3.1.3 Static Test 3

Static Test 3 was conducted at 2.485 million cycles into the dynamic test immediately after a crack was found in the diaphragm on the east side of Rib 7. This test was conducted to determine if the formation of this crack caused any redistribution of stress in the diaphragm. Other than in the gages immediately next to the crack, there were no significant changes between Static Test 2 and 3.

3.1.4 Static Test 4

The final static test, Static Test 4, was conducted at the end of the 5 million cycle "proof test" portion of Phase II (referred to as Phase IIA). This test was conducted to document the stress distribution throughout the entire deck system before the application of the extreme loading conditions in the second part of Phase II (Phase IIB).

3.1.5 Comparison of Static Tests

Table 3.1 compares the stress induced during the in-plane load step (step 2) at several key gages during the four static tests. These key gages are located on the diaphragm directly adjacent and perpendicular to the rib to diaphragm weld toe immediately above the diaphragm cutout (gages 8 and 19 as shown in Figure 2.13). As in Phase I, the in-plane load step produced the maximum stresses in the diaphragm, and they

are summarized in the table. Most of the significant stresses did not change much between Static Tests 1 and 2. However, the stress at D7-S-19 did increase by over 400% from -9.4 MPa to a relatively high value of -50 MPa. This and all other changes can be attributed to the addition of the shear plate connector and shakedown of the structure during the 1 million cycles between these two tests. The data from Static Tests 2, 3, and 4 are virtually identical except for the gages located nearest the crack. Gages D7-N-8 and D7-S-8 (back-to-back gages on the east side of Rib 7) were located just above the crack at the time of Static Test 3. The stresses at these gages increased by 36% and 30%, respectively, between Static Tests 2 and 3, indicating that the region of the diaphragm above the crack had to pick up the stress which could no longer be carried by the cracked region. By the end of the test, the cracked section had grown closer to these gages and the measured stresses had dropped significantly due to stress redistribution. It should also be noted that although there were large percentage changes at D8-S-19 and D9-N-8 between Static Tests 2 and 3, the actual stress magnitudes at these locations were so small that these variations were insignificant.

3.2 Global Behavior

Several LVDTs and strain gages were installed at various locations on the test deck to measure its overall global behavior. This information will ultimately be used for verification of a finite element model of the entire test setup (although creation of the finite element model is beyond the scope of the work presented in this paper) and for comparison purposes with the Phase I test.

3.2.1 Floorbeam and Deck Displacements

The maximum displacements measured at the tips of each floorbeam during the load cycle are summarized in Figure 3.1. As expected, the overall maximum deflection of 6.4 mm (0.25 in.) was recorded at the center floorbeam during load step 2, the time step during which the maximum load was applied. The same maximum displacement was measured at the tips of both interior floorbeams in the Phase I test, indicating that the stiffnesses of the two test setups are identical. No comparison can be made between the deflections of the exterior floorbeams in the two tests because the loading cycles were created to simulate truck loads at the interior floorbeams only. The fact that the southern floorbeam experienced a greater deflection than the northern floorbeam is due to the asymmetrical load cycle.

LVDTs 1 and 2, as shown in Figure 3.1, were attached with brackets to the reaction wall at the fixed end of each floorbeam to measure the displacements of the wall columns with respect to the reaction wall. These instruments showed no deflections during any of the load steps, indicating that the floorbeams' connections to the reaction wall were rigid. The data in Appendix B show that the maximum displacement recorded by any of these deflection instruments is less than their margin of error. Furthermore, dial gages set up in a similar fashion during Static Test 1 indicated no movement of the wall columns. Consequently, several of these instruments were not monitored during the remaining static tests.

The deflections of the deck plate were measured under each of the actuators and are summarized in Figure 3.2. The greatest displacement, 4.5 mm (0.18 in.) was

measured at time step 2 under the southern actuator, which is the actuator that applies the highest load.

3.2.2 Midspan and Floorbeam Stresses

Midspan stresses were recorded for Ribs 5 and 9 at a section of the deck 609 mm (24 in.) north of the southern actuator. Figure 3.3 displays the maximum stresses at these locations and the time steps at which they occurred. The maximum stresses were all produced during step 1, the time step in which the southern actuator reached its maximum load. Compared to stresses measured at fatigue critical locations on the diaphragm, the midspan stresses on the ribs and deck plate were relatively low. None of the stress ranges are nearly high enough to warrant any concern for fatigue damage. The stresses at each of the gages on Rib 5 were greater than their counterparts on Rib 9, probably due to Rib 5's proximity to two wheel load patches.

Figure 3.1 also displays the maximum stresses at the fixed end of the web of the interior floorbeam. As expected, all of these stresses were produced during the in-plane load step, which produced the highest load.

3.3 Diaphragm and Bulkhead Behavior

As in Phase I, the Phase II in-plane load step (step 2) produced the maximum stresses in the diaphragm over the internal floorbeam. Most of the diaphragm gages did not experience any stress reversal (changes in sign) during the loading cycle, as examination of the data in Appendix B reveals. Hence, maximum diaphragm stresses are

in effect the stress ranges at these locations. This is true for all the key gages whose peak stresses exceeded 70 MPa (10 ksi). Thus, unless indicated otherwise, the stresses given in the text, figures, and charts in this chapter were all produced during the in-plane load step.

3.3.1 Diaphragm Stress Distribution Near Ribs 5 and 7

Figures 3.4 and 3.5 show the in-plane load step stresses from Static Test 3 at all gages on the diaphragm and bulkheads at Ribs 5 and 7, respectively. Data from these ribs are shown because they were the most heavily instrumented, and the highest diaphragm stresses were measured at these locations. Furthermore, the trends in the data observed at these ribs were found at most other ribs as well. As in Phase I, the highest stresses were recorded at gage locations 8 and 19 on both diaphragm faces on both sides of both ribs (see Table 3.1). These gages are located directly adjacent and perpendicular to the rib to diaphragm weld toe immediately above its termination at the diaphragm cutout. These regions experience such high stresses because of the geometrical conditions at the diaphragm and rib to diaphragm weld at these locations. The diaphragm cut out below each rib causes stress concentrations at both rib connection points. The peak stress of 125 MPa (18.1 ksi) was measured at gage location D7-S-8 during Static Test 3. As explained in the previous section, this stress was higher in this test than the previous static tests due to the formation of a crack directly below the gage. In Static Test 2, before the crack was detected, the highest tensile stress, 96.3 MPa (14.0 ksi), was recorded at this same location. Crack growth resulted in higher stresses. However, the greatest stress measured

without influence of the crack was in compression equal to -106.5 MPa (-15.4 ksi) at gage D7-N-19. These peak stresses likely include some degree of stress concentration because of the proximity of the gage to the weld toe. No crack growth was detected along the weld toe. The crack at Rib 7 had developed from the edge of the cutout.

Other trends noticed in Phase I were also found here. The diaphragm stresses on the east side of any particular rib (facing the free end of the floorbeam) at gage location 8 were in tension, and those on the west side of the rib (facing the fixed end of the floorbeam) at gage location 19 were in compression. Twisting of the ribs along their longitudinal axes during the load cycle produces this behavior. The stresses dropped quickly 25.4 mm (1 in.) further along the rib to diaphragm weld toe, as measured by gages 21 and 22 on the west side of the rib, and 4, 5, and 6 on the east side. For example, on the west side of Rib 7 on the northern diaphragm face, the stress was observed to decrease from -106 MPa (-15.4 ksi) at gage 19 to -35 MPa (-5.1 ksi) at gage 21. Near the deck plate, the stress was at an even lower level of -15 MPa (-2.2 ksi) at gage 24. The stresses also decreased from the top of the cutout at the termination of the rib to diaphragm weld around and towards the bottom of the cutout. On the northern diaphragm face on the west side of Rib 5, the stress range decreased from -90 MPa (-13.1 ksi) at gage 19, to -77 MPa (-11.1 ksi) at gage 16, to 60 MPa (8.7 ksi) at gage 15, and to -0.3 MPa (-0.04 ksi) at gage 14.

3.3.2 Principal Diaphragm Stresses Near Ribs 5 and 7

Principal stresses produced during the in-plane load step were calculated using data from the rosettes located in these high stress concentration areas on both diaphragm faces on both sides of Ribs 5 and 7. These rosettes, shown in Figures 3.4 and 3.5, consisted of gages 7, 8, and 9 on the east side of the rib, and 18, 19, and 20 on the west side. Table 3.2 compares the maximum principal stresses with the stresses recorded by the gages oriented perpendicular to the rib wall and weld toe. The angle between these two planes of stress at each of the rosette locations is also tabulated. In all cases, the perpendicular stresses were nearly equal to the principal stresses, and they acted in nearby planes. The greatest difference was only 25% and occurred at gage D5-N-8, measuring 45.0 MPa (6.5 ksi). Its corresponding maximum principal stress was 60.4 MPa (8.8 ksi).

3.3.3 Bulkhead Stress Distribution Inside Ribs 5 and 7

As apparent from Figures 3.4 and 3.5, the peak stresses measured on the bulkhead plates were lower than those observed on the diaphragm. The highest bulkhead stresses were recorded on their top, eastern sides, and the stresses were generally higher on the east than the west. The overall maximum bulkhead stress of -42 MPa (-6.1 ksi) was found at gage location B7-N-2C.

3.3.4 Peak Diaphragm Stresses Near All Ribs

Figure 3.6 shows the in-plane load step stresses for Static Test 2 at all the key gages in the high stress concentration areas located adjacent and perpendicular to the rib

to diaphragm weld directly above the cutout. With the exception of Rib 8, these gages yielded the highest diaphragm stresses adjacent to each of the ribs. Because these gages were oriented along the longitudinal axis of the diaphragm, in-plane bending stresses were dominant in the diaphragm. Near Rib 8, the maximum diaphragm stress of -75.3 MPa (-10.9 ksi) was recorded at gage D8-N-18, located in the high stress concentration area but was parallel to the rib wall. Because this gage is oriented transversely to the longitudinal direction of the diaphragm, this abnormally high stress suggests that out-of-plane bending stresses dominated at this particular location. This anomaly may be due to the 3.8 cm (1.5 in.) transition in the depth of the diaphragm on the western side of Rib 8 or to the resulting discontinuity in the angle connecting the diaphragm to the floorbeam.

The highest diaphragm stresses were recorded along the sides of Ribs 5 and 7, which is where most of the cracks occurred during the Phase I test. The magnitudes were significantly reduced compared to their Phase I values, as shown in Table 3.6. As with Ribs 5 and 7, stresses on the eastern side of the ribs, facing the free end of the floorbeam, were tensile, and those on the western side of the ribs, facing the fixed end of the floorbeam, were compressive. The one exception to this rule was on the northern face of the diaphragm near Ribs 8 and 9 as noted earlier. Significant out-of-plane stresses were a contributing factor to these discrepancies.

Figure 3.6 also shows that there were significant differences in the stresses recorded by the back-to-back gages on the diaphragm. These differences are evidence of a stress gradient through the thickness of the diaphragm due to out-of-plane bending. This gradient existed during in-plane loading because the loads at the southern and

northern jacks were not equal, thus causing rotations of the ribs over the interior floorbeam and out-of-plane bending of the diaphragm. Significant out-of-plane stresses were also observed at back-to-back diaphragm gages during the in-plane load step in Phase I. It was suggested that initial imperfections in the diaphragm could also be their cause[3].

3.3.5 In-Plane and Out-of-Plane Stress Components in Diaphragm

The stresses at these back-to-back gages can be broken into their in-plane and out-of-plane components. Averaging the measured stresses yields the mean in-plane stress, and the out-of-plane stress equals the difference between the measured and average stresses. Table 3.3 shows the mean in-plane and out-of-plane stresses during the in-plane load step at all the back-to-back gages in the high stress concentration areas on both sides of Ribs 5 and 7, the west side of Rib 8, and the east side of Rib 9. Both the in-plane and out-of-plane components of the stresses perpendicular to the weld exceeded the response at other gage orientations. As expected, the in-plane bending stresses at the key gages next to Ribs 5 and 7 oriented perpendicular to the weld were 2.8 to 5.6 times greater than the out-of-plane bending stresses in the diaphragm. For example, at gage location 19 on the west side of Rib 5, in-plane stresses measured –77.3 MPa (-11.2 ksi), while out-of-plane stresses measured only ±13.9 MPa (±2.0 ksi). In the anomalous region between Ribs 8 and 9, the in-plane stresses were slightly less than the out-of-plane stresses, probably due to the reasons already discussed. Significant stresses were recorded at the gages oriented 45° to the rib to diaphragm welds of Ribs 5 and 7, and in-plane stresses at

these gages dominated by ratios from 7.6:1 to 45 :1. As expected, out-of-plane stresses were more significant at gages located parallel to the rib to diaphragm weld since these gages were oriented to measure out-of-plane bending along the longitudinal axis. At gage location 18 on the west side of Rib 5, the in-plane stress of 1.9 MPa (0.28 ksi) was only 86 % of the out-of-plane stress of 2.2 MPa (0.32 ksi). However, the magnitudes of these stresses parallel to the weld were insignificant compared to those perpendicular to the weld.

Table 3.4 summarizes the same information at these gages that were produced during one of the out-of-plane load steps (step 3). The recorded stresses were all smaller than those in the previous table because the in-plane load step dominated bending in the diaphragm. However, at all the key gages next to Ribs 5 and 7 that were oriented perpendicular to the rib to diaphragm weld, the out-of-plane stresses were larger in comparison to the in-plane stresses than they were during the in-plane load step. The in-plane stresses only dominated by ratios from 1.5:1 to 2.1:1. At gage location 19 on the west side of Rib 5, in-plane stresses measured -38.6 MPa (-5.6 ksi), while out-of-plane stresses were ±18.6 MPa (±2.7 ksi). Hence, as in Phase I, in-plane stresses dominated during out-of-plane loading. This was also true at the gages oriented 45° to the weld, where in-plane stresses were 5.5 to 62 times greater than out-of-plane stresses. As during the in-plane load step, out-of-plane stresses were more significant at gages parallel to the weld toe, but their magnitudes were very small compared with stresses in gages perpendicular to the weld toe.

3.3.6 In-Plane and Out-of-Plane Stress Components in Bulkheads

Using data from Static Test 3, measured stresses at back-to-back gages on the bulkheads in Ribs 5 and 7 were broken into their in-plane and out-of-plane components wherever possible. Table 3.5 summarizes these data along with the same information at nearby back-to-back gages on the diaphragm. As with the diaphragm, in-plane stresses dominated out-of-plane bending of the bulkheads. For example, at gage location 4 on Bulkhead 7, in-plane stresses measured 21.3 MPa (3.1 ksi), while out-of-plane stresses were only ±2.0 MPa (±0.29 ksi). In every case, the diaphragm stress and both its components exceeded the stress levels in the bulkhead. At gage location 4 on Bulkheads 5 and 7, the direction of the stress gradient was the same as on the diaphragm (compression on north face, tension on south face). However, at gage location 3 on the bulkhead in Rib 5, the stress gradient was opposite that of the diaphragm.

3.3.7 Comparison of Diaphragm Stresses Between Phase I and II

The Phase I test also showed that in-plane stresses dominated bending of the diaphragm. Thus, the diaphragm was made thicker in the final design of the actual replacement deck (and in the Phase II test) to provide greater resistance to in-plane stresses. Even though this might cause an increase in out-of-plane stresses from rotation, this design change would decrease the overall stress range as the dominant in-plane stress was reduced at the fatigue critical connection details, in particular the region near the termination of the rib to diaphragm weld.

Table 3.6 compares the in-plane load step stresses recorded at the key gages located perpendicular to the rib to diaphragm weld directly above the diaphragm cutout and in identical locations in both the Phase I and II tests. In Phase I, gages were installed on the 7.94 mm (0.313 in.) diaphragms connected to both interior floorbeams; rib to diaphragm connections over Floorbeam B were made using the Option A detail (combined full penetration and fillet weld), and those over Floorbeam C were made using the Option B detail (fillet weld only). Theoretically, the symmetrical loading cycle should have produced identical diaphragm stresses at both floorbeams. However, significant variations occurred, probably due to out-of-plane effects noted in the Phase II tests. Table 3.6 compares stresses at both Phase I diaphragms with their Phase II counterpart. These key gages in Phase I were located only on the south side of the diaphragm, so no comparison can be made between Phase I and II in-plane and out-of-plane component stresses. Phase II stresses on the north side of the diaphragm are included in the table to show that significant variations exist between back-to-back diaphragm stresses and between different floorbeams, both of which are likely due to out-of-plane effects.

In ten of the twelve cases where direct comparisons are possible, there were significant decreases, ranging from 15% to 99%, from Phase I to II. For example, at Phase II gage location D5-S-19, the stress range dropped from -161 MPa (-23.4ksi) at Floorbeam B and -223 MPa (-32.3 ksi) at Floorbeam C to -63.4 MPa (-9.2 ksi). However, in two cases the stress ranges actually increased. At Phase I gage location B-D7-E1 (the "B" refers to the diaphragm over Floorbeam B), the stress rose from 54.2

MPa (7.9 ksi) to 96.3 MPa (13.9 ksi). But at the same location over Floorbeam C, the Phase I stress measured 181.4 MPa (26.3 ksi); thus, when compared with this gage, the Phase II stress decreased at this location as well. This same type of discrepancy occurred at the other location of increased stress. At Phase I gage location B-D9-E1, the stress rose from 29.4 MPa (4.3 ksi) to 57.9 MPa (8.4 ksi). However, at gage location C-D9-E1, the Phase I stress measured 96.7 MPa (14.0 ksi). Thus, with the exception of a few locations, the peak stresses decreased from Phase I to II.

3.4 Stress Distribution in Ribs Near Diaphragm

The stresses measured on the rib walls near the diaphragm were low compared to those measured on the diaphragm itself. In orthotropic decks, bending stresses in the diaphragm can result in distortion of the rib walls, particularly when bulkhead plates are not used, thereby producing high stresses in the rib. However, as the Phase I test also showed, the addition of the bulkhead plate has eliminated this problem by forcing the ribs to maintain their shape.

The stress distribution was uniform among all the ribs, and Figure 3.7 displays such a typical distribution at Rib 5 produced during in-plane loading. As in the diaphragm, the in-plane load step produced the highest stresses at these rib gages near the diaphragm, and since they generally did not experience stress reversals, these in-plane load step stresses are, in effect, stress ranges. The highest stresses were measured at gage 4, located near the bottom of the rib wall along the longitudinal axis of the rib; since this section of the rib is in a negative moment region, these stresses were compressive and

ranged from -15.3 MPa (-2.2 ksi) to -25.8 MPa (-3.7 ksi). Longitudinal stresses measured near the top of the rib were tensile and ranged from 1.0 MPa (0.15 ksi) to 7.3 MPa (1.1 ksi).

The highest stress found among all the ribs, 26 MPa (3.8 ksi), was at gage 5 on the eastern wall of Rib 5 (which was the only rib to have gages in this location). This gage measured vertical stress in the rib wall directly beneath the termination of the rib to diaphragm weld. The fact that gage 5 was in tension on the eastern rib wall and in compression on the west is evidence of the rib's twisting along its longitudinal axis. This phenomenon was noted earlier in that the key diaphragm gages followed this same pattern (tension on the east side of the rib and compression on the west).

Vertical stresses measured at gages 3 and 7 at the top of the rib wall near the deck plate were low, ranging from 1.3 MPa (0.19 ksi) to 13.4 MPa (1.9 ksi). Contrary to the twisting near the termination of the rib to diaphragm weld, these gages were generally in compression on the east side and in tension on the west. At ribs directly under load plates, these vertical stresses were somewhat similar to those transmitted into the diaphragm. The stress measured at gage 3 on the eastern side of Rib 5, -3.8 MPa (-0.55 ksi), is comparable to the diaphragm stress of –5.2 MPa (-0.75 ksi) measured parallel to the eastern wall of Rib 5 directly beneath the deck plate (as measured by gage D5-N-3, shown in Figure 3.4). Similarly, the gages on the western wall and diaphragm of Rib 6 (Static Test 3 values at R6-W-3 and D6-N-23) measured 5.6 MPa (0.81 ksi) and 12.8 MPa (1.9 ksi), respectively. These stress magnitudes differ, but, as in the previous case, their signs are the same.

Only one gage positioned on the inside rib wall between the bulkhead and deck plate survived the fabrication process. This gage, on the eastern wall of Rib 7 (R7-E-8), measured very low stresses. Its peak stress of 2.0 MPa (0.29 ksi) was produced during load step 1. This vertical stress transmitted directly into the rib to bulkhead weld may be higher at ribs located directly beneath wheel load patches.

These measurements suggest that there is not likely to be any crack growth at the termination of the rib to bulkhead weld toe as occurred in the Phase I study.

3.5 Deck Plate Stresses Near Transverse Deck Weld

The stresses measured in the deck plate near the transverse deck weld were low. The maximum stress of 9.7 MPa (1.4 ksi) was measured at gage location TW-1 on the bottom of the deck plate (see Figure 2.17). The actuator loading scheme was not expected to produce high stresses at these gages because it was designed to yield maximum effects only in the diaphragm. A load passing directly over the weld, such as actual wheel loads, would produce higher stresses near the ends of this unsupported region of deck.

Table 3.1 Comparison of Static Equivalent HS15 In-Plane Load Step Stresses (MPa)

Gage	Static Test 1 0 cycles	Static Test 2 1090000 cycles	Static Test 3 2485000 cycles	Static Test 4 5000000 cycles	Change (%) Test 2 & 3
D3-N-8	27.3	36.2	34.9	35.0	-3.5
D4-N-19	-69.6	-68.1	-67.8	-68.9	-0.4
D5-N-8	32.8	45.0	43.5	46.6	-3.4
D5-S-8	82.8	86.4	84.9	89.2	-1.7
D5-N-19	-87.6	-91.2	-89.6	-93.3	-1.7
D5-S-19	-45.8	-63.4	-64.8	-67.6	2.3
D6-N-8	22.6	39.4	39.6	38.5	0.4
D6-N-19	-69.2	-75.5	-74.2	-73.4	-1.7
D7-N-8	26.3	52.4	71.3	16.7	36.2
D7-S-8	90.7	96.3	125.5	91.5	30.4
D7-N-19	-97.4	-106.5	-106.1	-108.6	-0.4
D7-S-19	-9.4	-50.4	-52.5	-55.7	4.2
D8-N-19	8.7	4.0	4.2	4.0	5.5
D8-S-19	-	-1.3	-2.8	-4.2	109.7
D9-N-8	-71.0	-4.6	-3.4	-2.5	-26.0
D9-S-8	-	57.9	56.3	56.6	-2.8

Note: Gages located adjacent and perpendicular to rib to diaphragm weld toe directly above diaphragm cutout.

Table 3.2 Maximum Principal Stresses at Rosettes Near Termination of Rib to Diaphragm Weld - Static Test 2

Gage Perpendicular to Rib Wall	Gage Stress (MPa)	Principal Stress (MPa)	Inclination of Principal Stress Plane from Gage (°)
D5-N-8	45.0	60.4	-27.5
D5-S-8	86.4	?	?
D5-N-19	-91.2	-91.2	-1.4
D5-S-19	-63.4	-63.9	-5.3
D7-N-8	52.4	68.0	-25.6
D7-S-8	96.3	97.2	5.4
D7-N-19	-106.5	-108.6	-7.6
D7-S-19	-50.4	-56.2	-18.0

? Indicates one of the rosette gages was not working
Positive angle is CCW

Table 3.3 Static Test 2 Equivalent HS15 In-Plane Load Step (Step 2) Stresses (MPa) at Back-to-Back Gages Broken Into In-Plane and Out-of-Plane Components

Gage	Position	Stress (Mpa)	In-Plane Component	Out-of-Plane Component	Ratio IN/OUT
D5-N-7	East Side of Rib 5	53.9	58.9	-4.9	11.9
D5-S-7	45° to weld	63.8	58.9	4.9	
D5-N-8	East Side of Rib 5	45.0	65.7	-20.7	3.2
D5-S-8	Perpendicular to weld	86.4	65.7	20.7	
D5-N-9	East Side of Rib 5	3.8	-	-	-
D5-S-9	Parallel to weld	?	-	-	
D5-N-20	West Side of Rib 5	-41.2	-39.5	-1.7	23.2
D5-S-20	45° to weld	-37.8	-39.5	1.7	
D5-N-19	West Side of Rib 5	-91.2	-77.3	-13.9	5.6
D5-S-19	Perpendicular to weld	-63.4	-77.3	13.9	
D5-N-18	West Side of Rib 5	4.0	1.9	2.2	0.9
D5-S-18	Parallel to weld	-0.3	1.9	-2.2	
D7-N-7	East Side of Rib 7	58.8	57.5	1.3	45.1
D7-S-7	45° to weld	56.2	57.5	-1.3	
D7-N-8	East Side of Rib 7	52.4	74.3	-22.0	3.4
D7-S-8	Perpendicular to weld	96.3	74.3	22.0	
D7-N-9	East Side of Rib 7	-0.3	-1.5	1.2	1.3
D7-S-9	Parallel to weld	-2.6	-1.5	-1.2	
D7-N-20	West Side of Rib 7	-33.5	-38.5	5.1	7.6
D7-S-20	45° to weld	-43.6	-38.5	-5.1	
D7-N-19	West Side of Rib 7	-106.5	-78.5	-28.0	2.8
D7-S-19	Perpendicular to weld	-50.4	-78.5	28.0	
D7-N-18	West Side of Rib 7	8.3	3.7	4.6	0.8
D7-S-18	Parallel to weld	-0.9	3.7	-4.6	
D8-N-19	West Side of Rib 8	4.0	1.3	2.7	0.5
D8-S-19	Perpendicular to weld	-1.3	1.3	-2.7	
D9-N-8	East Side of Rib 9	-4.6	26.6	-31.2	0.9
D9-S-8	Perpendicular to weld	57.9	26.6	31.2	

? gage not hooked up
- calculation not possible

Table 3.4 Static Test 2 Equivalent HS15 Out-of-Plane Load Step (Step 3) Stresses (MPa) at Back-to-Back Gages Broken Into In-Plane and Out-of-Plane Components

Gage	Position	Stress (MPa)	In-Plane Component	Out-of-Plane Component	Ratio IN/OUT
D5-N-7	East Side of Rib 5	27.2	28.8	-1.7	17.3
D5-S-7	45° to weld	30.5	28.8	1.7	
D5-N-8	East Side of Rib 5	10.4	32.8	-22.5	1.5
D5-S-8	Perpendicular to weld	55.3	32.8	22.5	
D5-N-9	East Side of Rib 5	3.9	-	-	-
D5-S-9	Parallel to weld	?	-	-	
D5-N-20	West Side of Rib 5	-20.2	-19.8	-0.3	61.5
D5-S-20	45° to weld	-19.5	-19.8	0.3	
D5-N-19	West Side of Rib 5	-57.1	-38.6	-18.6	2.1
D5-S-19	Perpendicular to weld	-20.0	-38.6	18.6	
D5-N-18	West Side of Rib 5	3.8	1.3	2.5	0.5
D5-S-18	Parallel to weld	-1.2	1.3	-2.5	
D7-N-7	East Side of Rib 7	36.3	34.3	2.0	17.0
D7-S-7	45° to weld	32.3	34.3	-2.0	
D7-N-8	East Side of Rib 7	18.3	40.5	-22.2	1.8
D7-S-8	Perpendicular to weld	62.6	40.5	22.2	
D7-N-9	East Side of Rib 7	0.0	-1.2	1.2	1.0
D7-S-9	Parallel to weld	-2.4	-1.2	-1.2	
D7-N-20	West Side of Rib 7	-17.3	-21.1	3.8	5.5
D7-S-20	45° to weld	-24.9	-21.1	-3.8	
D7-N-19	West Side of Rib 7	-68.1	-42.4	-25.7	1.7
D7-S-19	Perpendicular to weld	-16.7	-42.4	25.7	
D7-N-18	West Side of Rib 7	5.3	1.8	3.4	0.5
D7-S-18	Parallel to weld	-1.6	1.8	-3.4	
D8-N-19	West Side of Rib 8	3.5	6.1	-2.6	2.4
D8-S-19	Perpendicular to weld	8.7	6.1	2.6	
D9-N-8	East Side of Rib 9	-15.2	9.9	-25.2	0.4
D9-S-8	Perpendicular to weld	35.1	9.9	25.2	

? gage not hooked up
- calculation not possible

Table 3.5 Static Test 3 Equivalent HS15 In-Plane Load Step Stresses (MPa) at Back-to-Back Gages Broken Into In-Plane and Out-of-Plane Components at Adjacent Bulkhead and Diaphragm Gages

Bulkhead Gages, MPa				Diaphragm Gages, MPa			
Gage	Stress	In-Plane Component	Out-of-Plane Component	Gage	Stress	In-Plane Component	Out-of-Plane Component
B5-N-3B	-6.8	-11.6	4.8	D5-N-19	-89.6	-77.2	-12.4
B5-S-3	-16.3	-11.6	-4.8	D5-S-19	-64.8	-77.2	12.4
B5-N-4B	15.3	16.8	-1.4	D5-N-8	43.5	64.2	-20.7
B5-S-4	18.2	16.8	1.4	D5-S-8	84.9	64.2	20.7
B7-N-4B	19.3	21.3	-2.0	D7-N-8	71.3	98.4	-27.1
B7-S-4	23.3	21.3	2.0	D7-S-8	125.5	98.4	27.1

Table 3.6 Comparison of Static HS15 In-Plane Load Step Stresses Between Phase I Test 1 & Phase II Test 2

Phase I Gage	Phase II Gage	Phase I* Stress (MPa)	Phase II** Stress (MPa)	% Difference
B-D5-E1	D5-S-8	101.8	86.4	-15.1
C-D5-E1	D5-S-8	105.2	86.4	-17.9
-	D5-N-8	-	45.0	-
B-D5-W1	D5-S-19	-160.7	-63.4	-60.6
C-D5-W1	D5-S-19	-223.4	-63.4	-71.6
-	D5-N-19	-	-91.2	-
B-D7-E1	D7-S-8	54.2	96.3	77.5
C-D7-E1	D7-S-8	181.4	96.3	-46.9
-	D7-N-8	-	52.4	-
B-D7-W1	D7-S-19	-168.1	-50.4	-70.0
C-D7-W1	D7-S-19	-60.8	-50.4	-17.0
-	D7-N-19	-	-106.5	-
B-D8-W1	D8-S-19	-130.1	-1.3	-99.0
C-D8-W1	D8-S-19	9.9	-1.3	-86.6
-	D8-N-19	-	4.0	-
B-D9-E1	D9-S-8	29.4	57.9	96.9
C-D9-E1	D9-S-8	96.7	57.9	-40.1
-	D9-N-8	-	-4.6	-

Note: In Phase I there were no gages on north side of diaphragm
* 5/16 in. (7.94 mm) diaphragm
** 1/2 in. (12.7 mm) diaphragm

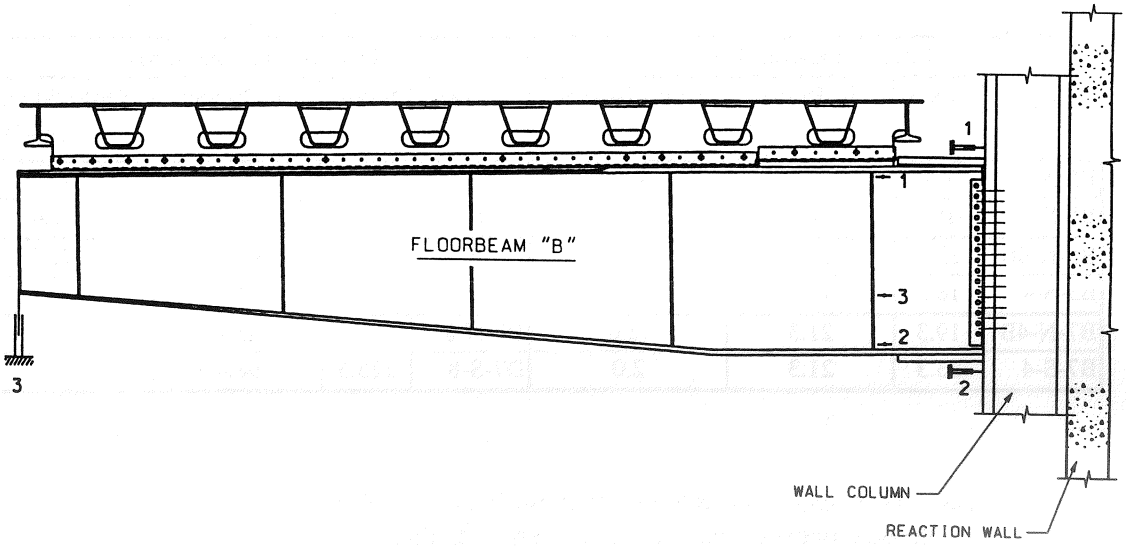

Maximum Displacements at Floorbeam Tips

LVDT	Displ. (mm)	
	Phase II	Phase I
DT-A3	-3.6	-
DT-B3	-6.4	-6.5
DT-C3	-2.2	-

Maximum Stress at Floorbeam Gages

Gage	Max Stress	
	Phase II	Phase I
FB1	10.8	9.8
FB2	-36.5	-32.0
FB3	-14.8	-10.4

Figure 3.1 Maximum Displacements at Floorbeam Tips and Maximum Stresses in Floorbeam Web

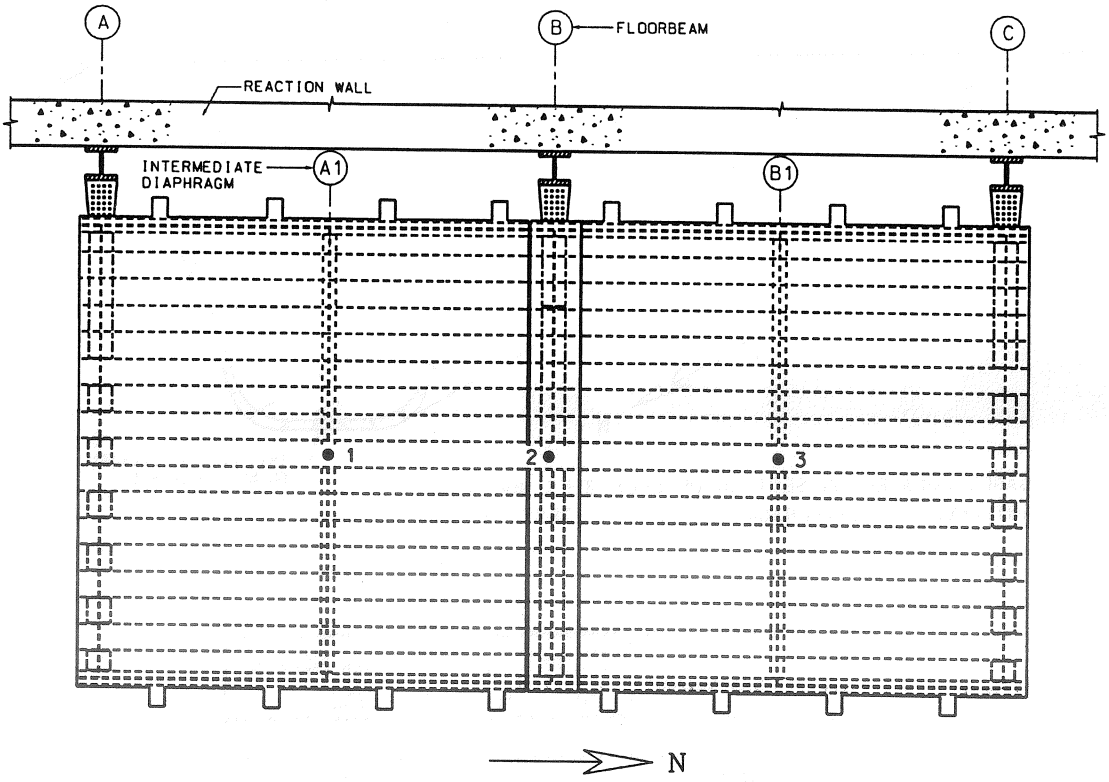

LVDT	Displacement (mm)
DT-S1	-4.5
DT-S2	-3.3
DT-S3	-3.6

Figure 3.2 Maximum Deck Displacements Under Actuators

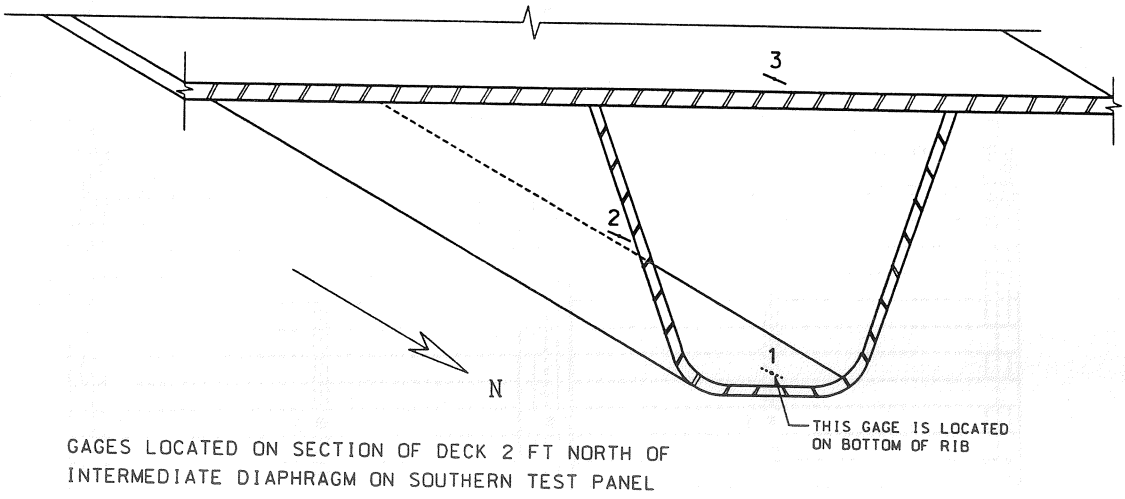

Strain Gage	Time Step of Max Stress	Max Stress (Mpa)
SP-5-1	1	32.7
SP-5-2	1	10.3
SP-5-3	1	-9.4
SP-9-1	1	18.6
SP-9-2	1	4.5
SP-9-3	1	-7.3

Figure 3.3 Maximum Stress in Midspan Gages

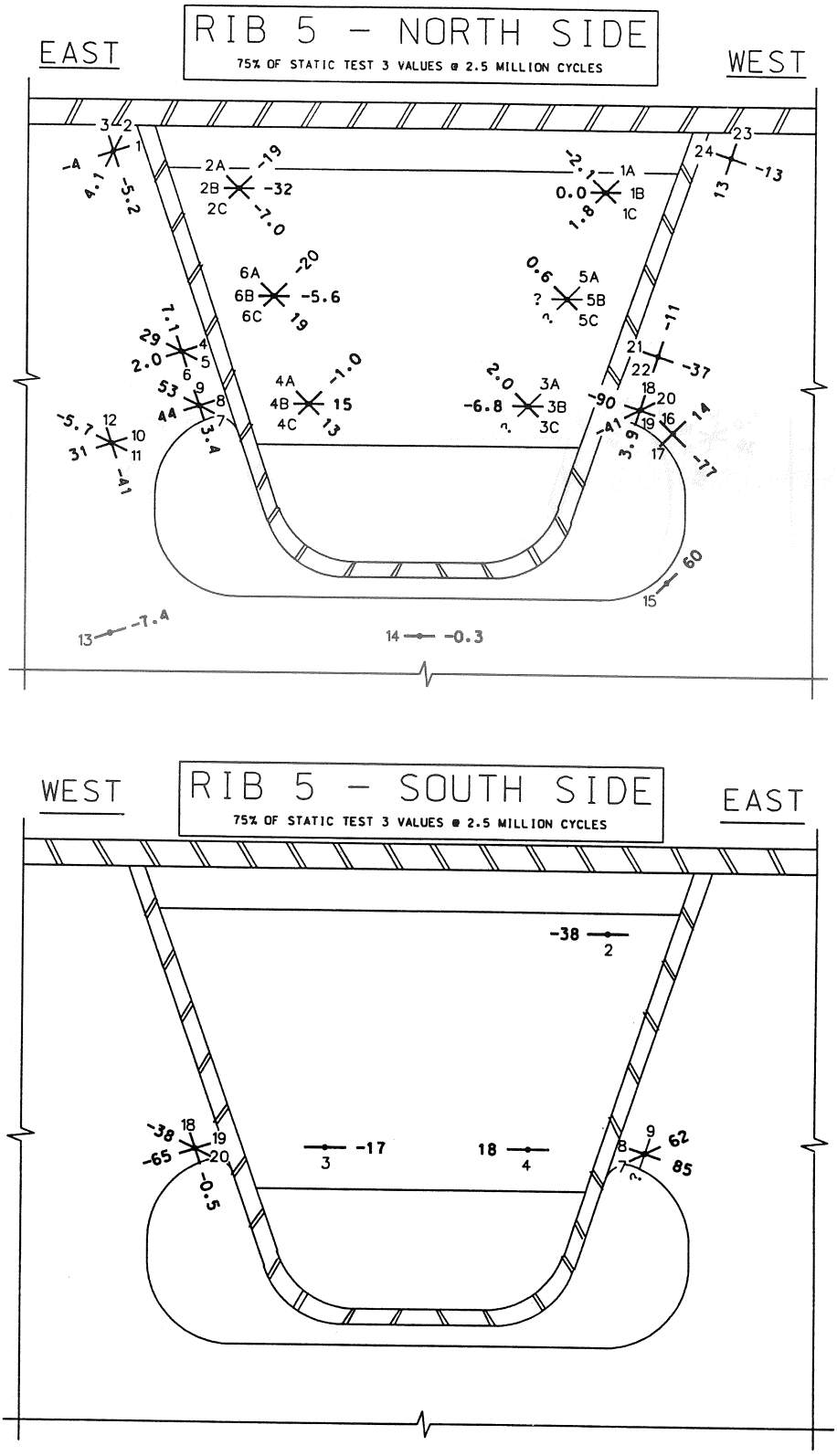

? gage not working

Figure 3.4 Diaphragm and Bulkhead Stresses (MPa) Near Rib 5

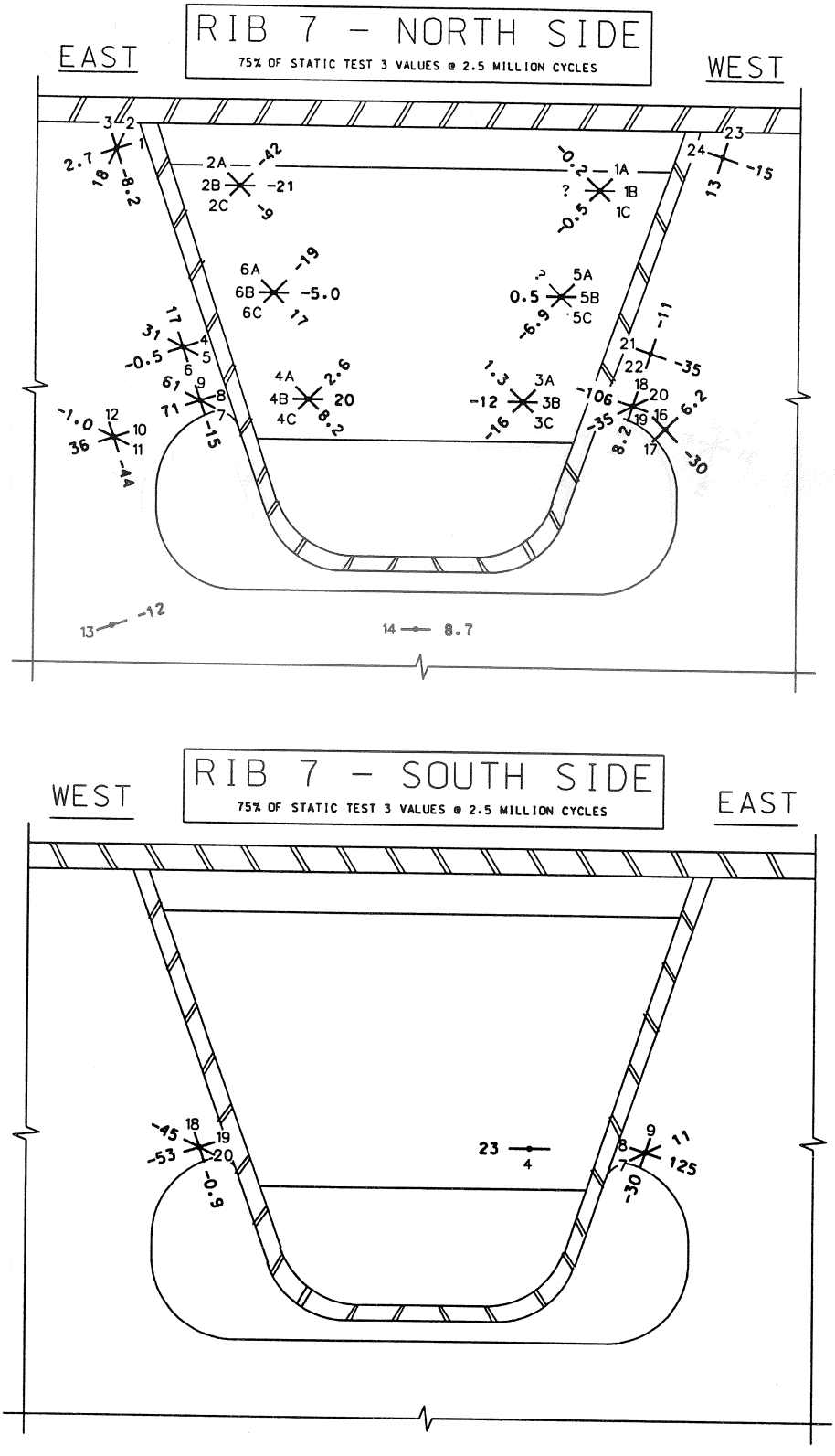

? gage not working

Figure 3.5 Diaphragm and Bulkhead Stresses (MPa) Near Rib 7

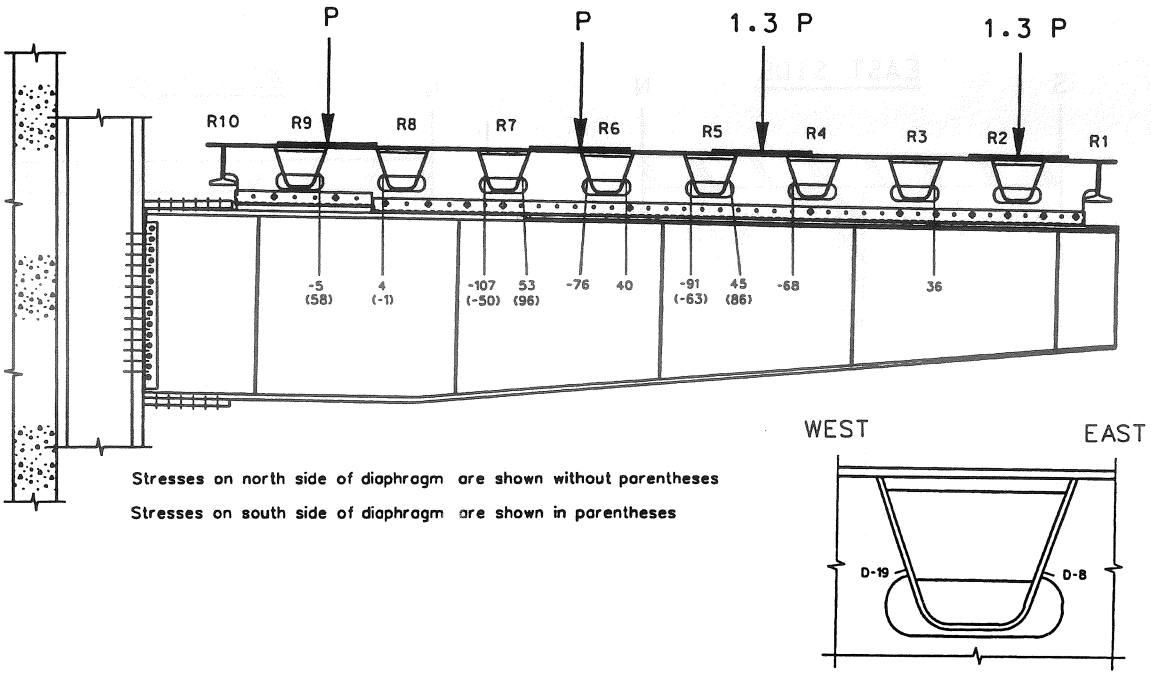

Figure 3.6 Peak Diaphragm Stresses - Static Test 2 @ 1.09×10^6 cycles

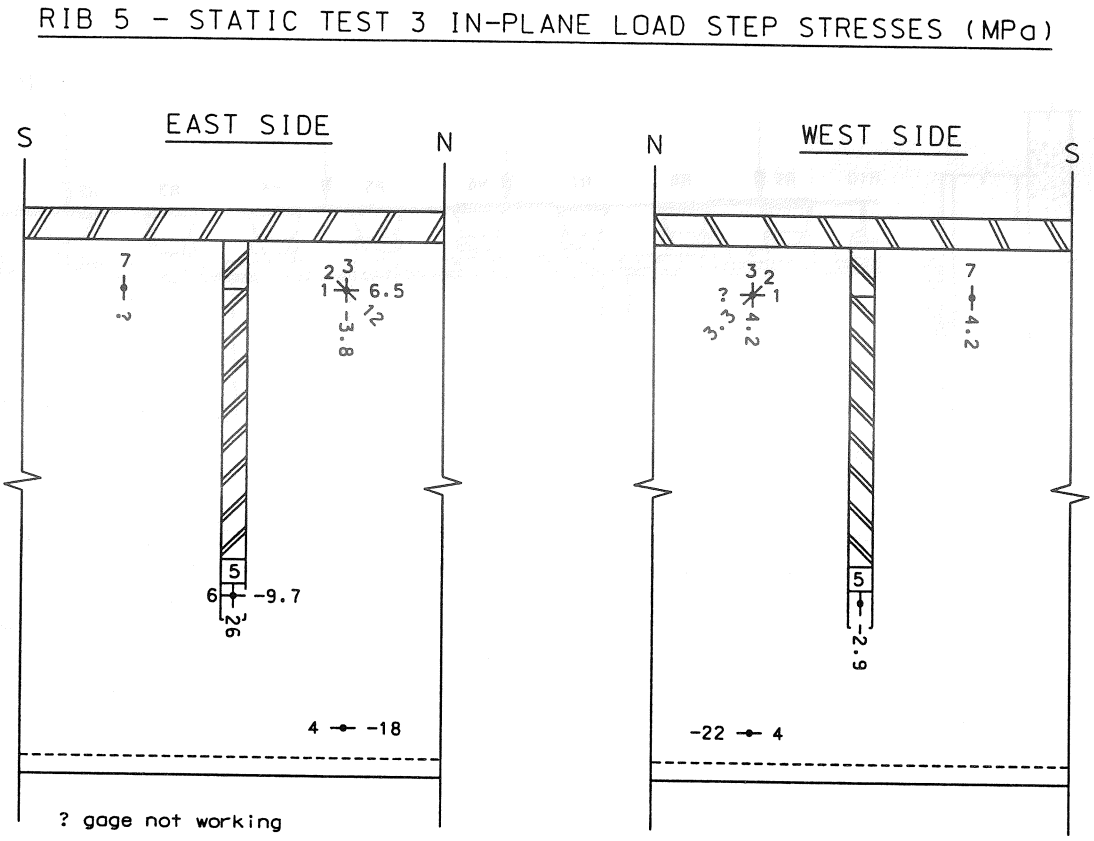

Figure 3.7 Peak Stresses in Rib Wall

4.0 DYNAMIC TEST

4.1 Purpose of the Dynamic Test

The dynamic fatigue test was run continuously for 5 million cycles, with periodic interruptions to carry out static control tests, by simulating AASHTO LRFD extreme live load conditions in order to study the effectiveness of the Phase I design recommendations incorporated into the actual replacement deck. The actuator loading scheme simulated the passage of two side-by-side HS15 fatigue trucks, without impact in the inner lane and 30% impact in the outer lane, corresponding to the expected maximum load in the random variable truck load spectra that will cross the bridge. Since the fatigue truck is representative of the Miner's equivalent effective load of this variable load distribution, and fatigue life is inversely proportional to the cube root of the applied stress range, the life corresponding to this extreme live load check is about one-eighth that of the normal random variable truck loading. Thus, the 5 million cycle fatigue test is equivalent to the passage of 40 million single fatigue trucks. Assuming the bridge East or West bound ADTT is 3450 (trucks and buses in excess of 10 tons in the inner and outer roadways)[9], the test approximates 64 years of service for the cantilever roadway.

After completing the 5 million cycles of Phase II loading, a second Phase IIB fatigue test will be carried out. The objective will be to create as much cracking as possible in the diaphragm plate at the various ribs within 2 million cycles of loading. This will be achieved by initially simulating loads corresponding to 2.3 times the fatigue truck in the outside lane. A complete set of static test loads will be applied (2.3 x HS20)

so that the rib to diaphragm connection stresses can be evaluated. The 1994 AASHTO LRFD Specification classifies the Option A and Option B rib to diaphragm welds and cutouts as Category D details. The Phase I and the current Phase II test data indicate that the Option A detail corresponds to a Category C resistance. Increasing the stresses acting on these welds in Phase IIB will promote fatigue cracking, producing a data base to aid in categorizing these details. This will be accomplished by applying the simulated truck loads in the outside lane only.

4.2 Dynamic Test Calibration

Due to the dynamic response of the prototype structure to the hydraulic and computer systems controlling the actuators, the maximum dynamic loading frequency was found to be 1.3 Hz. At this rate, the test deck was subjected to about 112,000 load cycles per day. The test was run continuously whenever possible. However, various hydraulic and computer communication errors often resulted in the system shutting down when no one was available to restart. This increased the test time to about three months.

Because the dynamic test simulated the passage of two HS15 fatigue trucks over the test deck, the dynamic jack load magnitudes were initially set equal to 75% of the static HS20 loads. Using the same data acquisition system as in the static tests, dynamic stresses were monitored at 25 gages which recorded stress ranges greater than 30 MPa (4.4 ksi) during the static tests. Data were sampled at a rate of 20 Hz to adequately capture the strain effects produced by the 1.3 Hz load cycle. However, because of inertial effects due to the loading rate, the dynamic stresses were greater than 75% of the static

stresses. The loads in the peak load step (Step 2) had to be further decreased by about 10% to ensure that the dynamic stress ranges were about 75% of the HS20 static load with impact stresses.

4.3 Dynamic Test Results

The 5 million cycle portion of the fatigue test (Phase IIA) focused on the performance of the rib to diaphragm weld connection. No cracking occurred at any of these critical weld details. One crack was found to develop in the diaphragm plate on the eastern side of Rib 7 adjacent to the rib to diaphragm weld. This crack initiated from an initial defect in the diaphragm plate edge, not at the rib to diaphragm weld toe. No cracks were found anywhere else in the diaphragm. Thus, the replacement deck has a significantly improved fatigue resistance compared to the original prototype Phase I system. Its corresponding service life should be at least 64 years without detectable damage. This will depend on the distribution of the average daily truck traffic and the paths used to cross the structure. Furthermore, data from this test and the Phase I test showed that the combination full penetration groove weld - fillet weld rib to diaphragm connection is a Category C detail which has a CAFL of 69 MPa (10 ksi). Many of the rib details had tensile stress ranges acting on these welds which were below the CAFL, as illustrated in Figure 3.6, indicating that they should never experience fatigue crack growth.

Dynamic stresses were recorded on a daily basis for 20 second periods to monitor the response and behavior of the test structure. Table 4.1 summarizes the stress ranges

measured at various intervals throughout the dynamic test. Since the dynamic test was calibrated with reference to 75% of Static Test 1 stresses, these data are also shown for comparison. Most of the stress ranges did not change throughout the dynamic test. Those at gage location D4-N-19, for example, fluctuated between 67.6 MPa (9.80 ksi) and 71.5 MPa (10.4 ksi), which are believed to be due to random variations in the actuator loads and noise in the data acquisition system. The only significant variations were recorded near the diaphragm crack at gage locations D7-7 and D7-8, on both the north and south faces of the diaphragm at Rib 7. These variations were in fact the first indications of the formation of a crack near these gages and led to its discovery at 2.46 million cycles. The stress ranges at the two gage 8 locations remained constant up to 2.15 million cycles, from which point they rose dramatically. The stress range at D7-N-8 increased from about 50 MPa (7.3 ksi) to 67 MPa (9.7 ksi), and that at D7-S-8 increased from 97 MPa (14 ksi) to 119 MPa (17.3 ksi). Details of the crack will be given later in the chapter, but from about 3 million cycles until the end of the test at 5 million cycles, the crack primarily grew on the northern face of the diaphragm. During this time, the stress range dropped significantly at D7-N-8 to 17 MPa (2.5 ksi), but only slightly at D7-S-8 to 112 MPa (16.2 ksi).

Figure 4.1 displays typical dynamic stress-time responses as recorded by back-to-back gages D7-N-8 and D7-S-8 at about 1.5 million cycles into the fatigue test (before the detection of the crack). These key gages are located adjacent and perpendicular to the rib to diaphragm weld toe on the east side of Rib 7 directly above the cutout. The load steps producing the stresses are also indicated as t_0, t_1, t_2, and t_3 along the time axis of the

graph. These diaphragm stress versus time plots are similar in shape to those produced during the Phase I test. As in Phase I, the in-plane load step, shown as t_2, dominated the stress cycle, thus controlling the fatigue behavior at the rib to diaphragm weld. Out-of-plane bending in the diaphragm plate caused by rotation of the ribs was a major concern in the design of this element. However, both tests have clearly shown that in-plane loading controls the fatigue resistance.

As evident in Figure 4.1, a strain gradient existed through the thickness of the diaphragm. At each of the load steps except Step 0 (in which only the minimum actuator loads were applied), the stress at D7-S-8 exceeded that at D7-N-8. Section 3.3.5 described how the diaphragm stress can be broken into its in-plane and out-of-plane components at back-to-back gages. This was done using the dynamic data displayed in Figure 4.1, and the resulting stress components are shown in Figure 4.2. As with the static test data discussed in Section 3.3.5, this graph clearly shows that the in-plane stress component exceeded the out-of-plane bending stress during each step of the load cycle. For example, during the in-plane load step, t_2, the in-plane stress was about 75 MPa (11 ksi), approximately three times greater than the out-of-plane bending stress of about ±25 MPa (±3.6 ksi). In-plane stresses equaled about 40 MPa (5.8 ksi) during each of the out-of-plane load steps, although the out-of-plane bending did not change significantly. Step 3 produced greater out-of-plane bending stresses than Step 1.

4.4 Diaphragm Crack Near East Side of Rib 7

Routine monitoring of dynamic stresses led to the discovery of a crack in the diaphragm near the rib to diaphragm weld toe on the eastern (tension) side of Rib 7. The crack grew out of a small defect hardly visible on the inside surface of the top of the cutout about 6.35 mm (0.25 in.) from the rib to diaphragm weld toe. It clearly did not originate from the weld toe. This defect, roughly 6.35 mm (0.25 in.) long and extending from the middle of the inside surface of the cutout to its southern edge at the time of detection, is shown in Figure 4.3 after 2.46 million cycles. This small notch is a residual flame cut edge and gouge produced during fabrication of the cutout that was not ground smooth. Upon completion of Phase IIA, a small section of the diaphragm containing the crack was removed for assessment.

The crack grew from this small defect on the inside surface of the top edge of the cutout towards both faces of the diaphragm. It first reached the southern face of the diaphragm, and upon its initial discovery at 2.46 million cycles, it was 1 mm (0.04 in.) long on the southern face and located approximately 6.4 mm (0.25 in.) east of the rib to diaphragm weld toe. It continued growing roughly parallel to the weld toe on the south face, and by 2.58 million cycles it had a surface length of 5.6 mm (0.22 in.). Figure 4.4 is a schematic that shows the position of the crack on the southern face of the diaphragm and its proximity to gages 7 and 8, which exhibited changes in measured stresses due to the crack growth. The largest changes were an increase in D7-S-8 and a decrease in D7-S-7 (see Table 4.1). At this same time, the crack had just reached the northern diaphragm face 3 mm (0.1 in.) east of the rib to diaphragm weld toe. By 2.72 million cycles, the

crack measured 6.1 mm (0.24 in.) on the southern face of the diaphragm and 2.5 mm (0.098 in.) on its northern face. At this point, the crack tip extended behind the backing of the rosette on the southern face and could no longer be monitored. However, the crack continued to grow straight up the northern face, and Figure 4.5 shows a photograph at 3.42 million cycles when it measured 3.8 mm (0.15 in.). At 4.44 million cycles it measured 5.1 mm (0.20 in.) and had begun to curve towards the weld. This change in direction is probably due to the 26° clockwise inclination of the principal stress plane with respect to gage D7-N-8. By the end of the test, it measured 18 mm (0.70 in.) and had grown into the weld. At this time the rosette on the southern diaphragm face was removed, revealing a crack length of 11 mm (0.45 in.). It had grown roughly parallel to the weld toe without any change in direction and perpendicular to the south face principal stress field which was inclined 5.4° counterclockwise with respect to gage D7-S-8.

Based on these observations, the hypothetical initial extension of the crack shown in Section A-A of Figure 4.4 was constructed. The initial defect was a semi-elliptical edge crack located close to the southern face of the diaphragm. It then grew into a corner crack and began propagating up the southern diaphragm face before the crack front reached the northern face. Soon thereafter it became an edge crack, visible on both faces of the diaphragm. By the end of the test, the crack extension was greater on the northern face than the southern face.

As mentioned earlier, the formation of the diaphragm crack led to a significant stress redistribution in its immediate vicinity. Gages D7-N-8 and D7-S-8 were positioned adjacent to and perpendicular to the rib to diaphragm weld toe, about 7.9 mm (0.31 in.)

above the cutout (gage position 8 is shown in Figure 4.4). Figure 4.6 summarizes the stress range history at each of these gages throughout the dynamic test. The elapsed number of cycles is plotted logarithmically on the x-axis to condense the graph. The stress ranges were fairly constant until about 1.5 million cycles when they both began to increase. The stress range at D7-S-8 rose from around 95 MPa (14 ksi) at the beginning of the test to 125 MPa (18 ksi) at 2.5 million cycles. Similarly, at D7-N-8 it rose from an initial value of 50 MPa (7 ksi) to a peak value around 65 MPa (9.4 ksi). Although the crack was not detected until 2.48 million cycles, it was clearly growing towards these gages after 2 million cycles, causing them to increase as the stress was redistributed as a result of the cracked section. From 3 million cycles until the end of the test, the stress range at D7-S-8 decreased slightly to 112 MPa (16.2 ksi), while it dropped significantly at D7-N-8 to 17 MPa (2.5 ksi). The crack direction differed on the two diaphragm faces and was consistent with the principal stresses on the surfaces.

Upon discovery of the diaphragm crack on the eastern side of Rib 7, all cutouts were carefully inspected. No other cracks were found, but a smaller defect, similar to the one leading to crack growth, was discovered on the inside top surface of the diaphragm cutout on the west (compression) side of Rib 5 near the rib to diaphragm weld toe. This defect did not result in detectable crack growth because it was in a compressive cyclic stress region. Since two such defects were found in this one test panel, it is possible that similar discontinuities may exist on the actual replacement deck. Any crack extension will depend on their size and the stress range at the defect.

After completion of the 5 million cycles of loading, the crack area was removed from the diaphragm so that crack growth could be arrested and the crack evaluated. This was accomplished by drilling a 1.27 cm (0.5 in.) hole above the crack tip, saw cutting between the hole and the edge of the cutout, and then flame cutting a segment from the diaphragm. This permitted the crack surface to be examined so that the initial defect could be determined.

Figure 4.7 shows the segments removed from the diaphragm. The crack surfaces are shown in Figure 4.8. A small, sharp notch was found at the ground plate edge. Figures 4.9 and 4.10 show a SEM view of the crack origin. They indicate that the initial defect is a combination of the residual flame cut surface and mechanical induced slivers on the plate edge. These provided an initial crack-like flaw. The depth of this defect was about 0.25 mm (0.01 in.).

The defect was evaluated to see if it would propagate. The crack shape was initially assumed to be an edge crack as the depth to width ratio was about 1/6. Hence, the stress intensity range would be:

$$\Delta K = 1.12 S_r \sqrt{\Pi a}$$

$$= 1.12(97\text{MPa})\sqrt{\Pi(2.5\text{x}10^{-4}\,\text{m})} = 3.04\text{MPa}\sqrt{\text{m}} > \Delta K_{th}$$

This indicated that the crack-like defect would exceed the crack growth threshold, ΔK_{th} = 3.02 MPa$\sqrt{\text{m}}$ (2.75 ksi$\sqrt{\text{in}}$).

For crack propagation, a corner crack was assumed applicable because of the observed crack growth and the stress gradient across the diaphragm plate thickness. The cycles to achieve through thickness was estimated from the relationship

$$N = \frac{1}{A}\int_{a_i}^{a_f} \frac{da}{\Delta K^3} = \frac{2}{A\left(Q\sqrt{\Pi}\right)^3 S_r^3}\left[\frac{1}{\sqrt{a_i}} - \frac{1}{\sqrt{a_f}}\right]$$

with $\Delta K = Q\, S_r \sqrt{\Pi a}$, $A = 2.18 \times 10^{-13}$, $S_r = 97$ MPa (14 ksi), $a_i = 0.25$ mm (0.01 in.), $a_f =$ 5.6 mm (0.22 in.), and $Q \sim 1.05$. The predicted life for the semi-elliptical corner crack to reach the north face is 2.47 million cycles. This compares well with the 2.58 million cycles observed during the test considering the crack shape effect, Q, is changing as the crack grows.

The assessment has verified the need to assure that crack-like defects be ground from the flame cut edge. Grinding nicks and tears must also be avoided.

4.5 Fatigue Strength of Rib to Diaphragm Weld

Figure 4.11 compares the S-N curve for Category C which is applicable to the combined full penetration - fillet weld rib to diaphragm connection with the test results obtained at Ribs 4, 5, 6, and 7. All tensile and compressive stress ranges (see Table 3.6) greater than 68 MPa (9.9 ksi) are plotted in Figure 4.11. The uncracked details plot at or above the S-N curve for Category C and the CAFL. The test results continue to verify that the rib to diaphragm connection is a Category C weld detail.

The plotted stresses may include some stress concentration effect. The stress field in the vicinity of the gage is complex. The nominal stress field normally associated with

the Category C fatigue resistance curve does not include the stress concentration associated with the "hot spot" region. With both in-plane and out-of-plane stresses occurring at the weld toe, the applicable damage conditions are more complex. Studies on out-of-plane distortion have also suggested that the combined stresses increase the fatigue resistance[10].

Table 4.1 Stress Ranges at Selected Intervals Throughout Dynamic Test

Gage	Stress, MPa						
	Static Test 1 x 75%	580,000 cycles	1,350,000 cycles	2,150,000 cycles	2,460,000 cycles	3,087,000 cycles	4,999,000 cycles
D4-N-19	68.1	68.5	70.3	71.5	67.6	68.3	68.5
D5-N-7	53.9	52.3	53.1	53.3	52.6	52.8	53.1
D5-S-7	63.8	73.9	63.3	63.5	62.0	61.5	62.3
D5-N-8	45.0	40.7	42.9	44.2	40.9	44.6	41.4
D5-S-8	86.4	87.6	86.8	87.6	84.6	86.1	85.6
D5-N-10	30.9	29.0	30.0	29.5	29.3	29.5	30.3
D5-N-12	41.4	42.7	41.9	42.9	40.9	41.7	41.7
D5-N-15	60.8	55.2	55.9	56.6	55.2	55.9	56.1
D5-N-16	78.3	77.6	77.9	77.4	75.4	75.4	76.2
D5-N-19	91.2	91.5	90.5	89.0	87.1	87.6	88.6
D5-S-19	63.4	67.5	61.3	62.8	59.3	63.7	59.3
D5-N-20	41.2	39.4	39.9	39.9	39.4	38.9	40.2
D5-S-20	37.8	49.4	36.5	37.0	36.0	36.7	36.5
D6-N-19	75.5	79.3	76.4	75.9	72.7	74.2	72.0
D7-N-7	59.1	58.0	57.3	64.2	61.3	37.7	11.9
D7-S-7	56.2	53.3	52.1	36.5	20.1	32.0	40.7
D7-N-8	52.4	47.6	50.8	56.3	62.5	67.2	16.9
D7-S-8	96.3	99.0	96.7	114.6	119.1	116.3	111.9
D7-N-10	38.4	37.7	36.0	34.7	35.0	33.5	29.3
D7-N-12	45.2	46.6	44.6	44.2	42.7	42.4	42.7
D7-N-19	106.5	108.6	102.7	102.4	99.2	101.5	102.2
D7-N-20	33.5	33.5	32.0	32.7	33.7	34.2	36.5
D7-N-21	36.0	39.1	34.1	34.6	33.4	32.9	31.9
D8-N-18	75.3	79.1	74.7	75.2	71.0	73.9	72.7
D9-S-8	57.9	-	-	-	-	55.4	54.2

- not hooked up

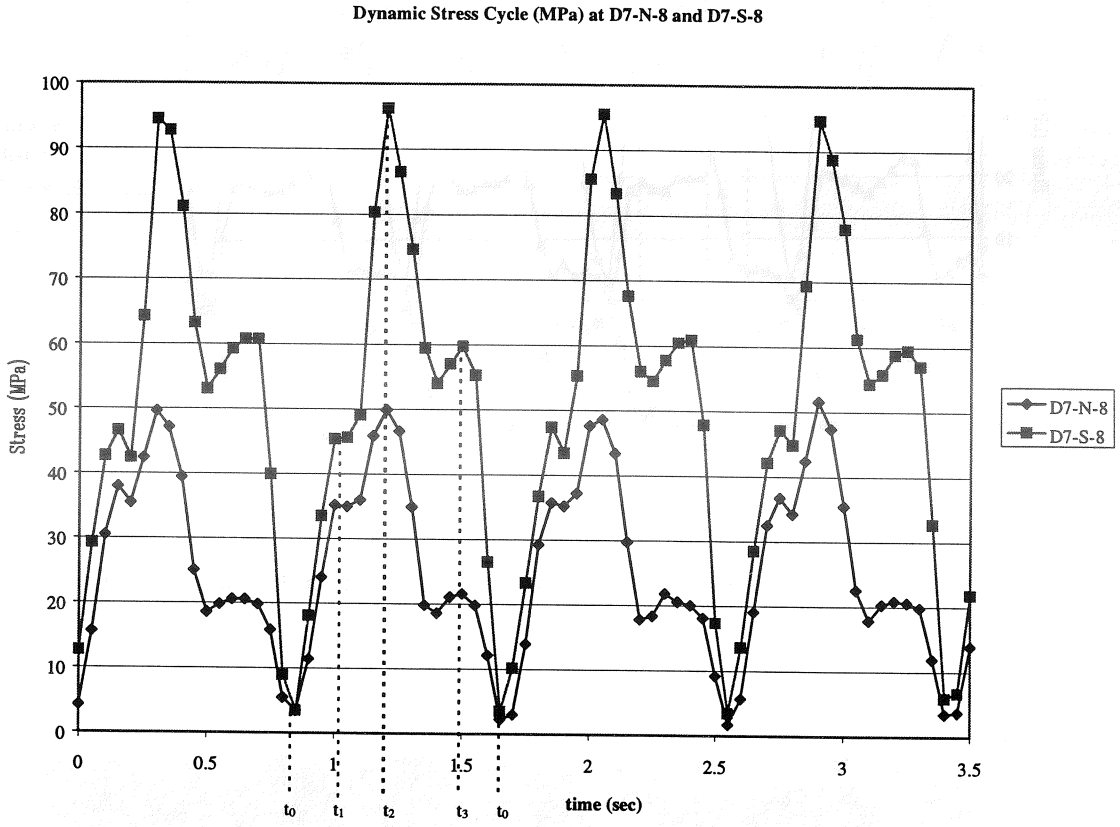

Figure 4.1 Tension Stress-Time History on Diaphragm Plate Adjacent to Rib 7

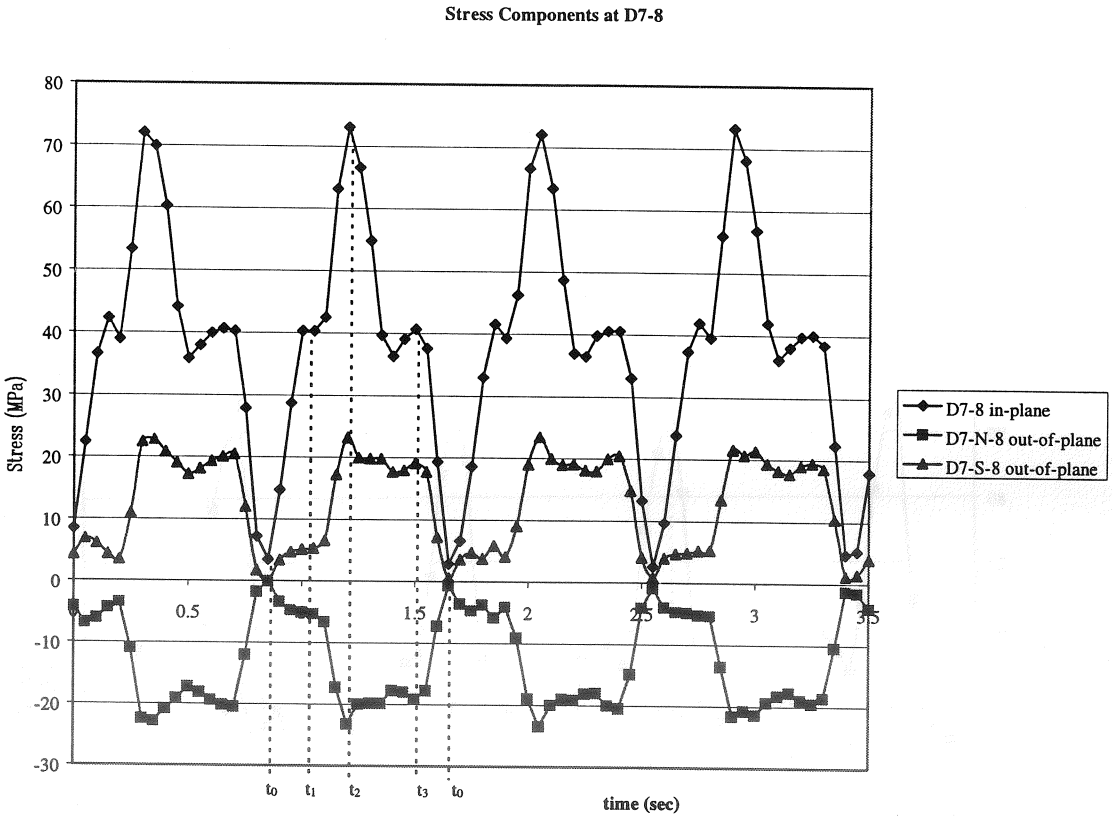

Figure 4.2 Dynamic Stress Components at Gage Location D7-8

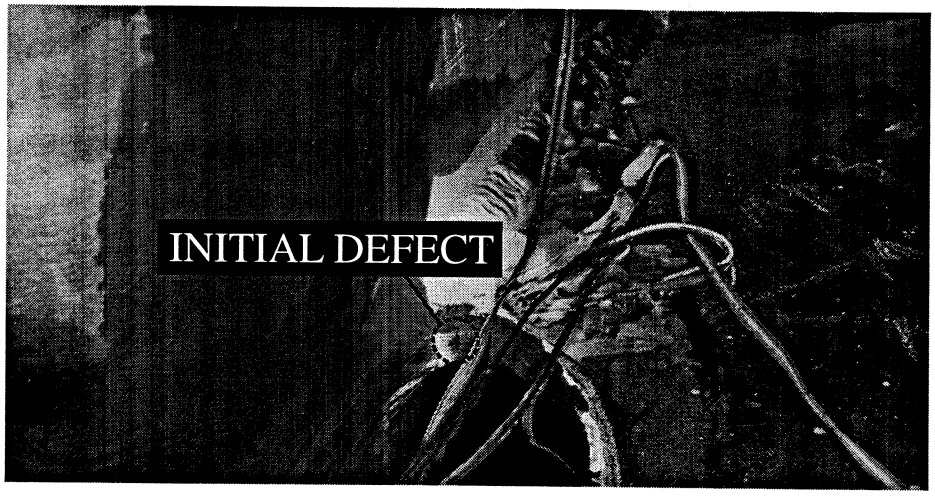

Figure 4.3 Initial Defect Leading to Crack on Inside Surface of Diaphragm Cutout on East Side of Rib 7

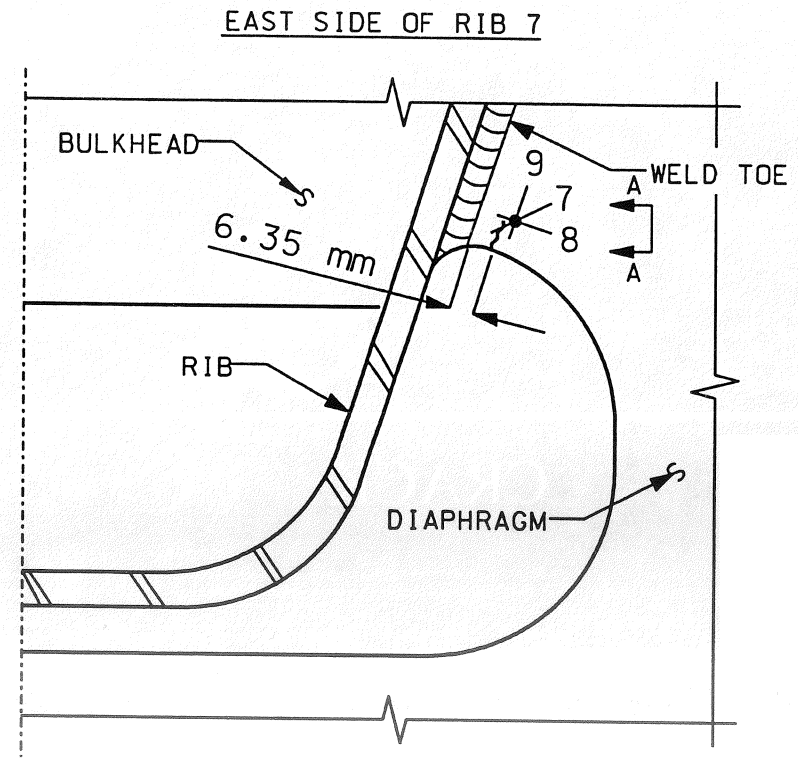

(a) Schematic showing south surface crack

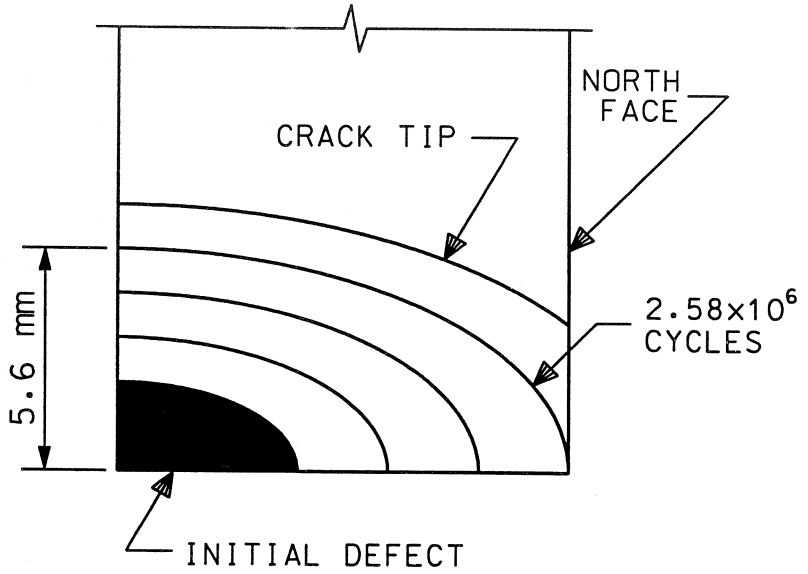

(b) SECTION A-A

Figure 4.4 Diaphragm Crack on East Side of Rib 7

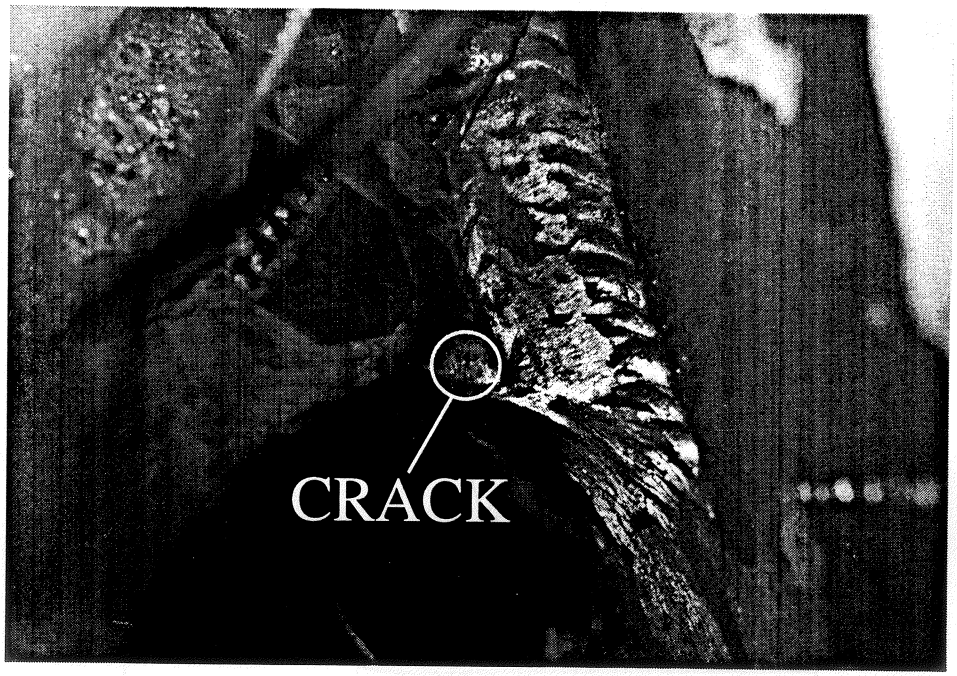

Figure 4.5 Crack on Northern Face of Diaphragm on East Side of Rib 7

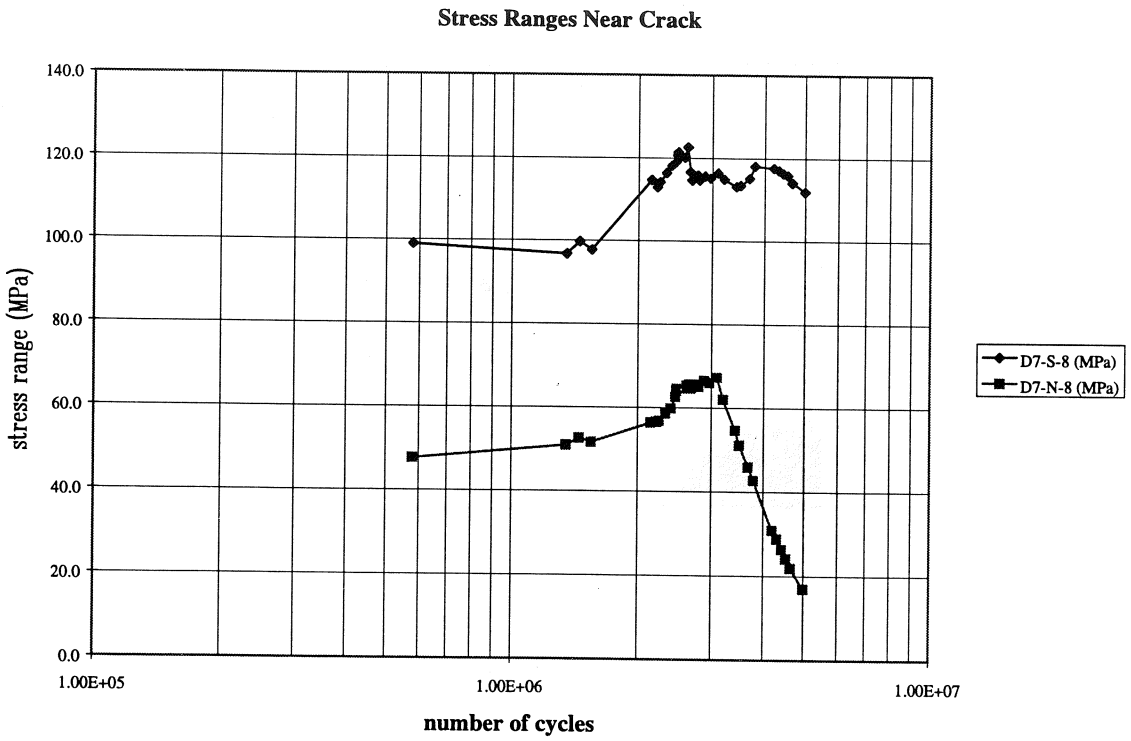

Figure 4.6 Variation of Stress Ranges Near Crack Location

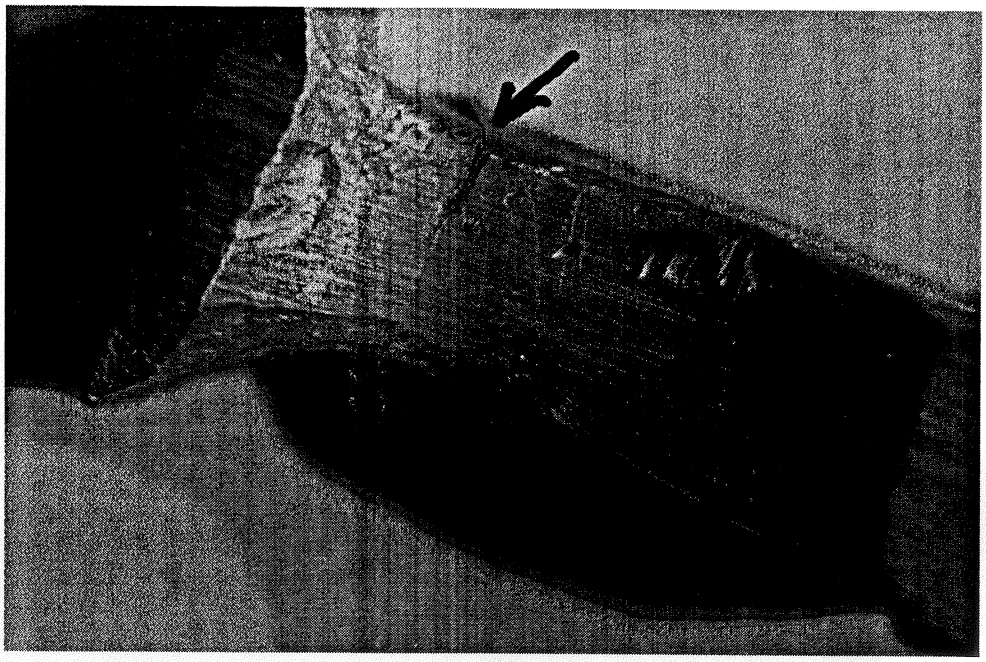

Figure 4.7 View of Ground Edge of Diaphragm Plate Showing Defects and Crack

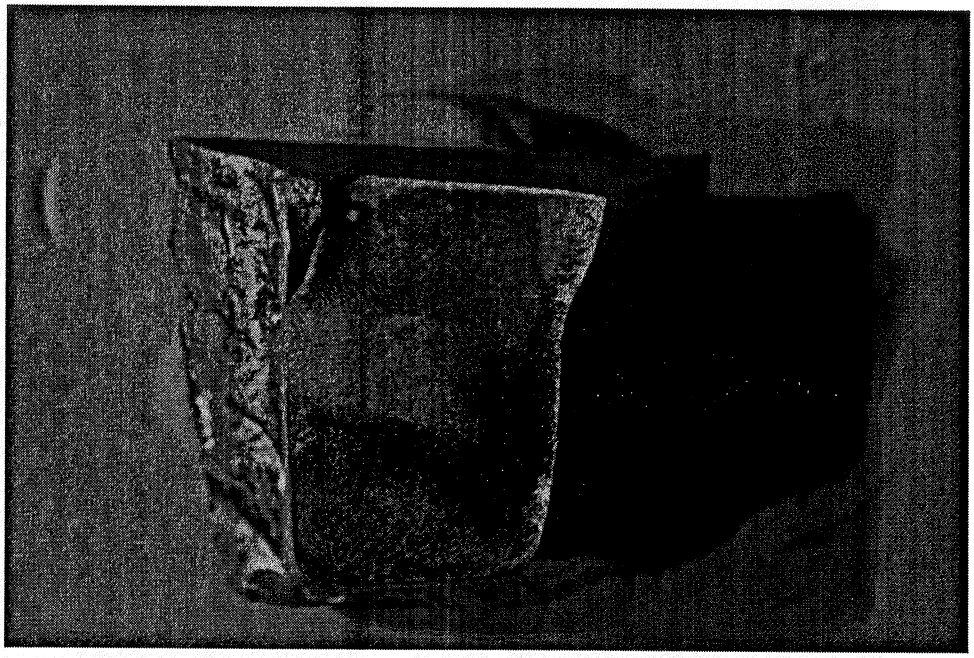

Figure 4.8 Cleaned Crack Surface Showing Beach Marks
and Semi-Elliptical Corner Crack

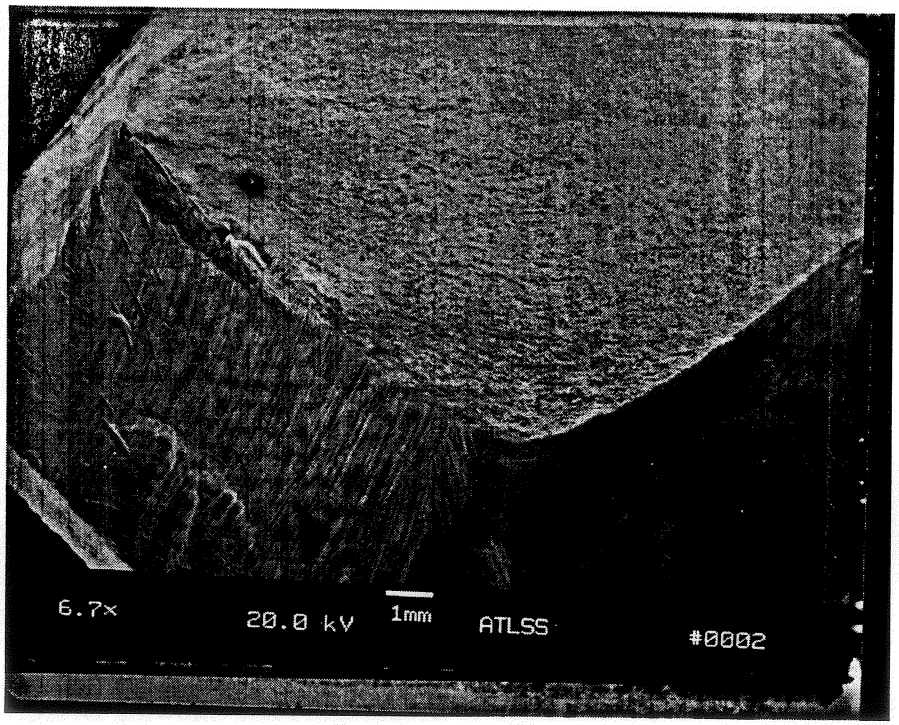

Figure 4.9 SEM View of the Crack Surface Showing Groove Along Plate Edge and Corner Crack Development @ 6.7X

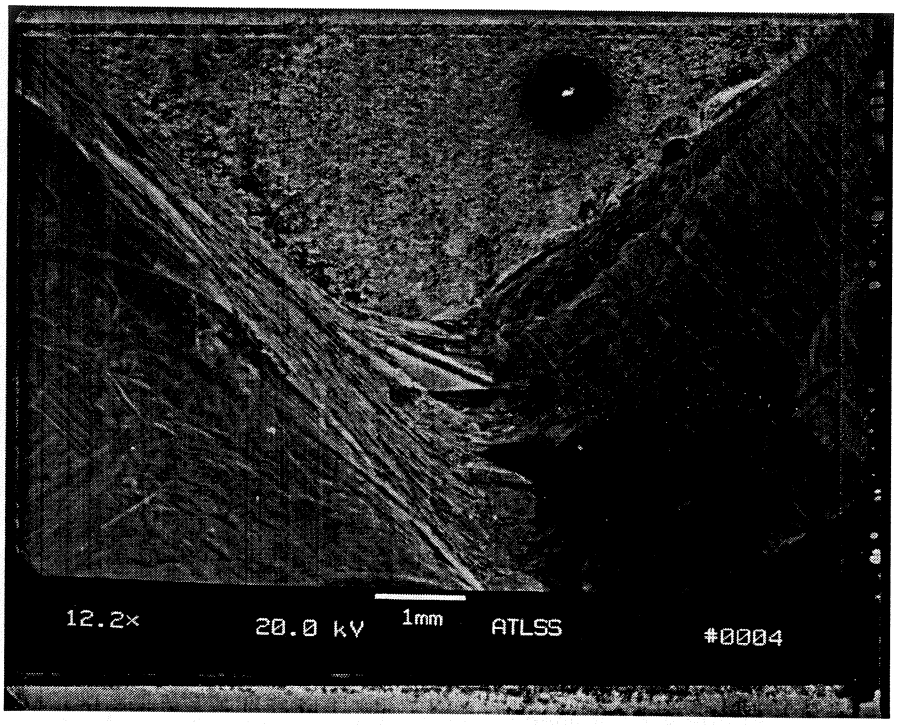

Figure 4.10 SEM View of the Initial Defect Along Plate Edge and Corner Notches @ 12.2X

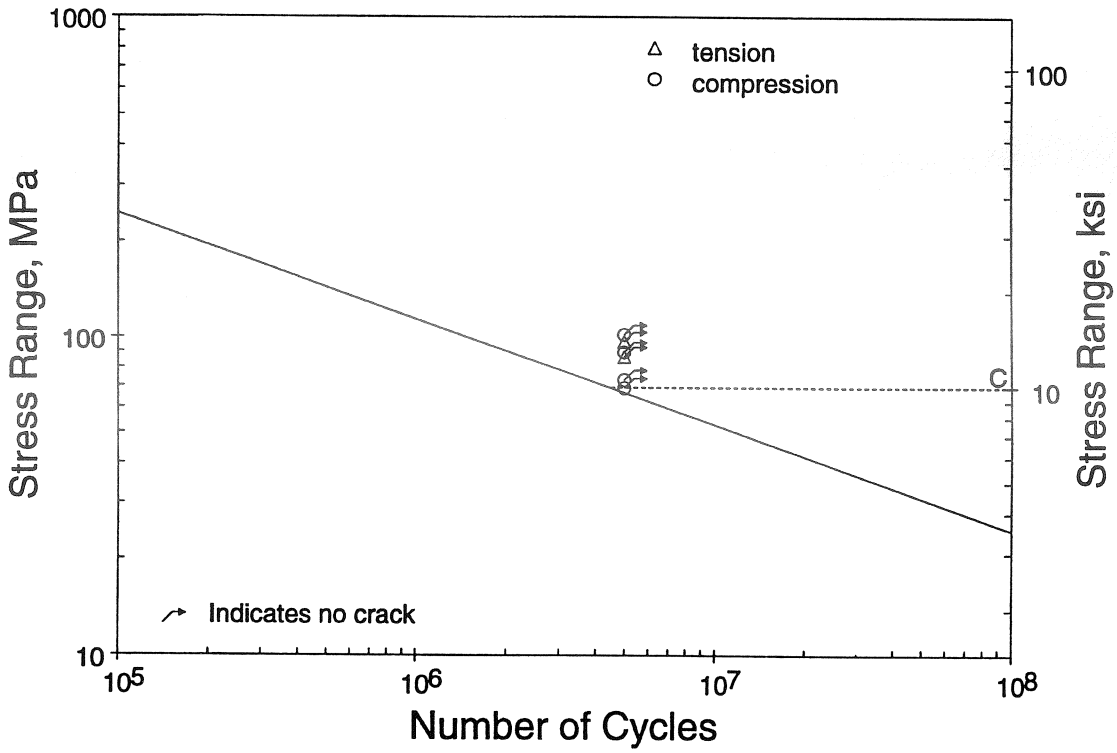

Figure 4.11 S-N Curve for Option A Rib to Diaphragm Weld

5.0 SUMMARY AND RECOMMENDATIONS

Both the static calibration and dynamic fatigue test demonstrated that the Phase I design recommendations incorporated into the actual replacement deck effectively improved its fatigue resistance. Comparison of static test data between Phase I and II showed that the increased diaphragm thickness and its associated geometric changes resulted in substantial reductions in the peak diaphragm cutout stresses. After the application of 5 million cycles of equivalent AASHTO LRFD extreme live loads, approximating 64 years of service for the cantilevered roadway, no detectable cracks had initiated at any Option A (combination full penetration - fillet weld) rib to diaphragm connections.

Static Tests

The static tests were conducted to study the global behavior of the entire deck system and the local behavior of the fatigue critical connection details on the new test panel. The highest stresses, which were produced during the in-plane load step, were measured on the diaphragm by gages located adjacent and perpendicular to the rib to diaphragm weld toe, directly above the diaphragm cutouts. The greatest compressive and tensile stress ranges, -107 MPa and 96 MPa, for the HS15 fatigue loading were recorded on the west and east sides of Rib 7, respectively. As in Phase I, data from back to back diaphragm gages provided evidence of a strain gradient through the thickness of the diaphragm. However, Phase II better characterized this gradient by showing that, during in-plane loading, the in-plane stress components measured by gages oriented

perpendicular to the rib to diaphragm weld toe were 2.8 to 5.6 times greater than the out-of-plane components. Furthermore, during out-of-plane loading increments, in-plane stresses still dominated by ratios from 1.5:1 to 2.1:1. The thicker diaphragm provided greater resistance and reduced both in-plane and out-of-plane stresses.

Overall, there was a significant reduction in peak diaphragm stresses from Phase I to Phase II. In ten of the twelve cases where direct comparisons were possible, the peak stresses decreased from 15% to 99%. Out-of-plane bending increased at two locations but these higher Phase II stresses did not exceed their Phase I counterparts over the two interior floorbeams.

As in Phase I, the stresses on the rib walls were low compared to those on the diaphragm. The greatest stress, measured transversely on the eastern, exterior wall of Rib 5 directly beneath the termination of the diaphragm, was only 26 MPa. The bulkhead plate demonstrated its effectiveness in eliminating distortion of the rib walls.

Fatigue Test

The dynamic fatigue test, run continuously for 5 million cycles by simulating AASHTO LRFD extreme live load conditions, did not cause any of the Option A, combination full penetration - fillet weld, rib to diaphragm connections to crack. Depending on the distribution of vehicles using the inner and outer roadways, the test approximated 64 years of service for the outer, cantilevered roadway.

Gages located adjacent and perpendicular to the uncracked rib to diaphragm welds of Ribs 4, 5, 6, and 7 recorded stress ranges greater than the CAFL for Category C details

and exceeded the life estimates provided by the S-N relationship. This reaffirms the conclusion from Phase I that the Option A rib to diaphragm weld is a Category C detail, and its current AASHTO LRFD Category D classification is inappropriate.

One crack formed in the diaphragm on the eastern side of Rib 7 near the rib to diaphragm weld toe. This crack, first detected at 2.46 million cycles, grew from an initial defect in the base metal of the diaphragm, not from the weld toe. After 5 million cycles, the crack was visible on both faces of the diaphragm, measuring 11 mm (0.43 in.) on its southern face and 18 mm (0.71 in.) on its northern face. The crack was removed from the structure and its cause assessed. It was found that a small crack-like defect remained on the cutout edge after grinding. Crack growth was predicted based on the observed stress range.

Future Work

After modifying the current actuator and spreader beam setup such that the loads are applied in the outside lane only, Phase IIB will be carried out. The objective is to create as much cracking as possible in the diaphragm at the various ribs within 2 million cycles of loading. The load cycle developed for Phase IIA will also be used for Phase IIB. Shifting these loads, which correspond to 2.3 times the fatigue truck, to the outside lane should sufficiently increase the stress ranges acting on the rib to diaphragm welds to promote fatigue cracking. This will enhance the data base and permit proper categorization of these connections. Since the measured stresses used for fatigue

classification purposes in Phases I and IIA contained some degree of stress concentration, Phase IIB will also attempt to define the nominal stress level acting on these welds.

A finite element model of the Phase II test setup will also be created. Loads from the Phase II load cycle will be applied, and the results will be correlated to the actual test data. A model is needed for design purposes, as the current AASHTO LRFD analytical model does not accurately predict the diaphragm stress range.

Upon their completion, the results of the Phase III field tests will be correlated with the Phase II laboratory test data and predicted stress range levels. Due to the inherent variability in the field loading conditions, the magnitudes of the stress ranges may differ between the two tests. However, general conclusions, such as the shape of the stress cycle and the dominance of in-plane loading, should be the same.

6.0 REFERENCES

1 Troitsky, M.S. Orthotropic Bridges, Theory and Design (2nd Edition), The James F. Lincoln Arc Welding Foundation, Cleveland, Ohio, 1987.

2 Merritt, F.S. (Ed.), M.K. Loftin (Ed.), J.T. Ricketts (Ed.). Standard Handbook for Civil Engineers, McGraw-Hill, New York, 1996.

3 Kaczinski, M.R., Stokes, F.E., Lugger, P., Fisher, J.W. Williamsburg Bridge Orthotropic Deck Fatigue Test, ATLSS Report No. 97-04, 1997.

4 Modjeski, R., Webster, G.S., Ball, L.A. The Bridge Over the Delaware River Connecting Philadelphia, P.A. and Camden, N.J. Final Report of the Board of Engineers to the Delaware River Bridge Joint Commission of the States of Pennsylvania and New Jersey, June 1, 1927.

5 Williamsburg Bridge Technical Advisory Committee. Summary Report to the Commissioners of Transportation of the City and State of New York, June 30, 1988.

6 Steinman Boynton Gronquist & Birdsall. CAD drawing.

7 American Association of State Highway and Transportation Officials. Standard Specifications for Highway Bridges - LRFD, 1st Edition, 1994.

8 Gajer, R.B., Patel, J., Khazem, D. "Orthotropic Steel Deck for the Williamsburg Bridge Reconstruction," Proceedings of ASCE Structures Congress, Chicago, IL, 1996.

9 DeLeuw Cather & Co., Williamsburg Bridge Truck Traffic Volumes, 1988 and May 1995.

10 Fisher, Jin, Wagner, Yen. Distortion-Induced Fatigue Cracking in Steel Bridges, NCHRP Report 336, December 1990.

7.0 ACKNOWLEDGEMENTS

The laboratory fatigue test of the as-built Williamsburg Bridge replacement orthotropic deck was supported by the Federal Highway Administration, the New York State Department of Transportation, and the New York City Department of Transportation. The study was performed in the multidirectional test facility of the ATLSS Center, Lehigh University.

Ruben Gajer, formerly of New York City DOT, and Jamey Barbas and Dyab Khazem of Steinman, Boynton, Gronquist & Birdsall provided assistance in planning the test program. The new orthotropic deck section was fabricated by Leonard Kunkin Associates. Installation was performed by the ATLSS Laboratory staff.

Thanks are due to the laboratory staff: Frank Stokes, John Hoffner, Roger Moyer, Todd Anthony, Steve Leonard, and Larry Heffner. Ed Tomlinson and Russ Longenbach provided assistance with instrumentation. The fractographic studies were carried out by Dr. Eric Kaufmann. Richard Sopko provided the photographic coverage.

Appendix A

Instrumentation Plan Drawings

Note: The scales on some drawings may be incorrect, as several drawings had to be shrunk for binding purposes

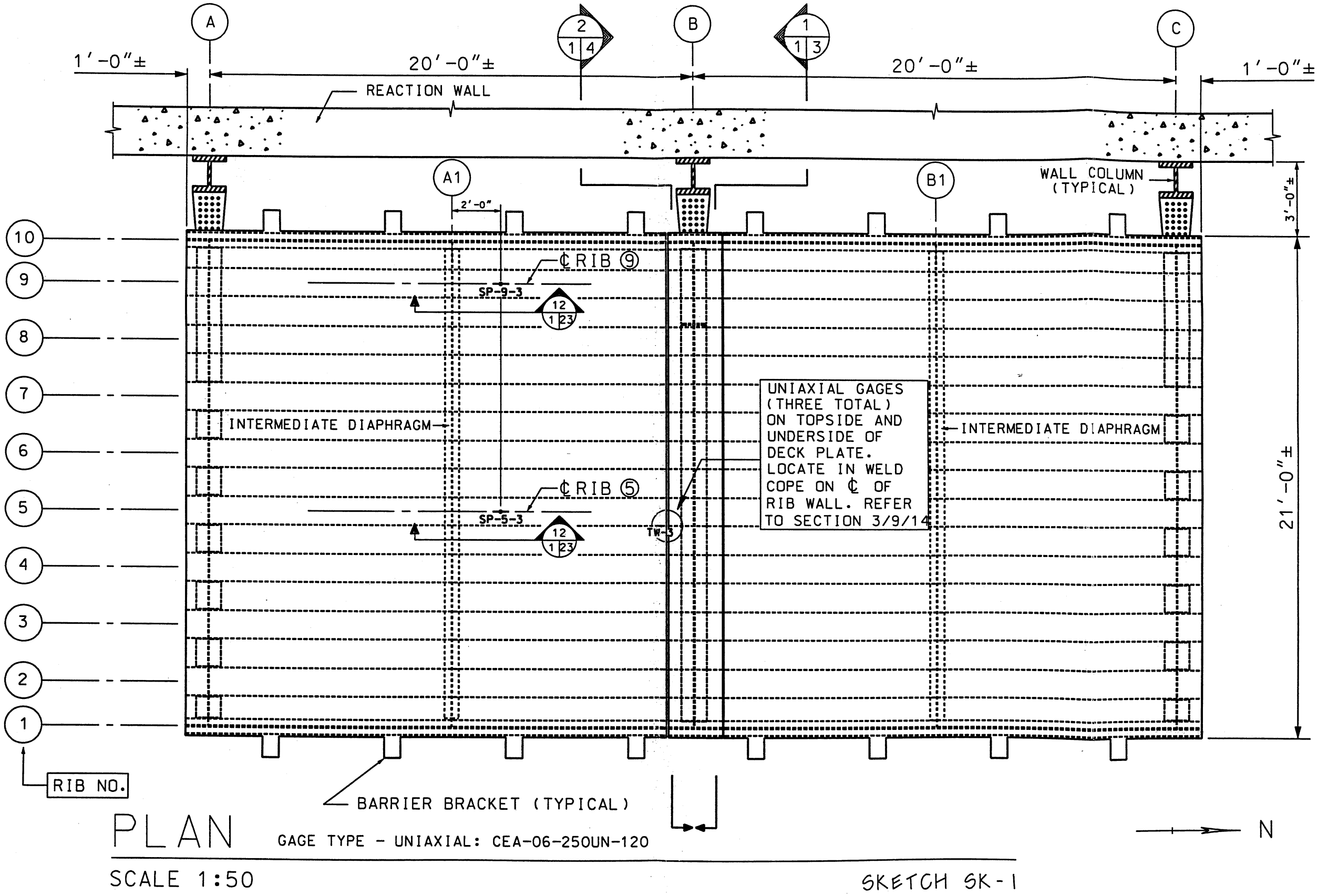

PLAN

GAGE TYPE - UNIAXIAL: CEA-06-250UN-120

SCALE 1:50

SKETCH SK-1

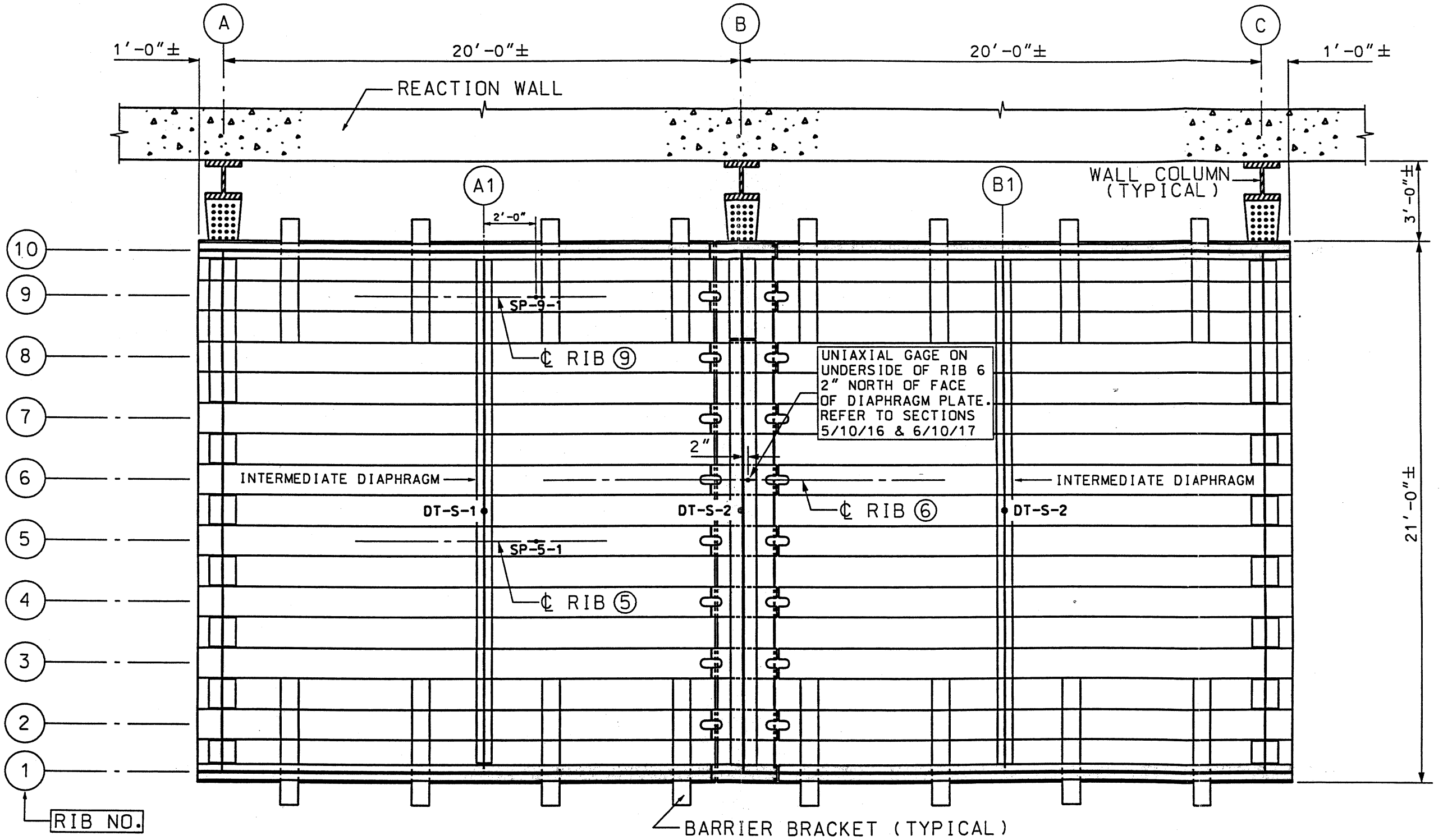

REFLECTED PLAN

GAGE TYPE - UNIAXIAL: CEA-06-250UN-120

N

SCALE 1:50

SKETCH SK-2

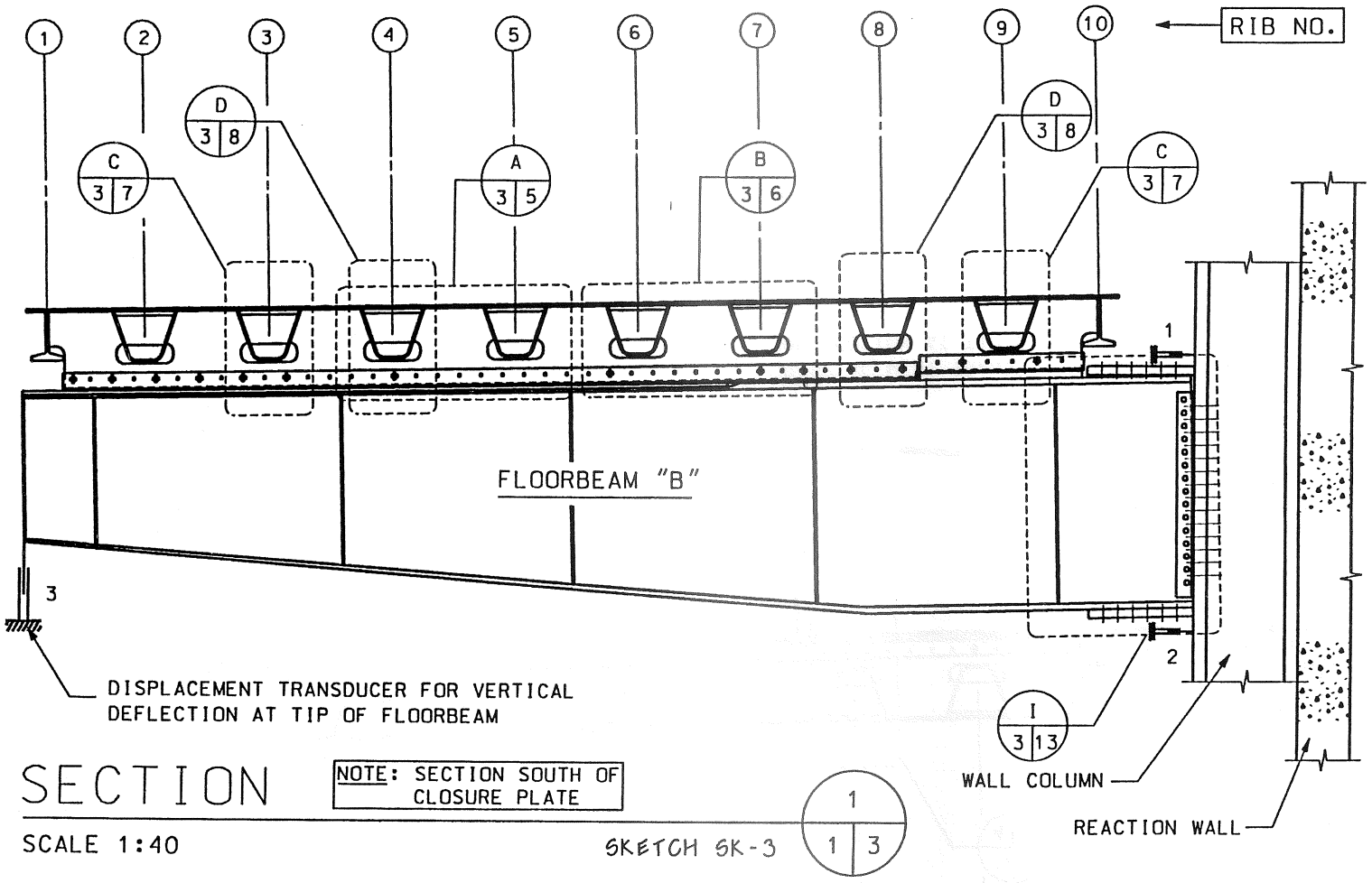

SECTION

NOTE: SECTION SOUTH OF CLOSURE PLATE

SCALE 1:40

SKETCH SK-3

1 | 1 3

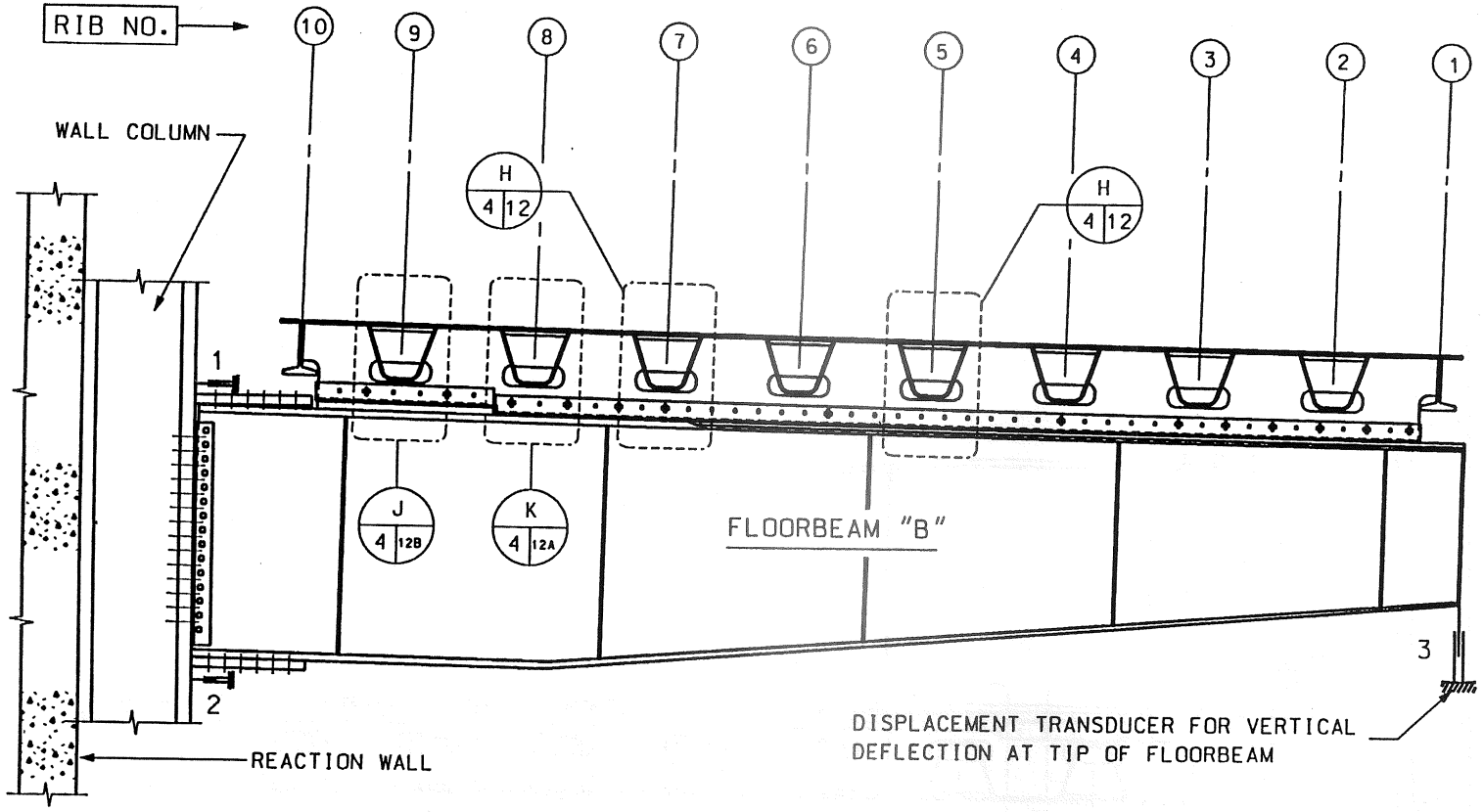

SECTION

SCALE 1:40

SKETCH SK-4

2
1 | 4

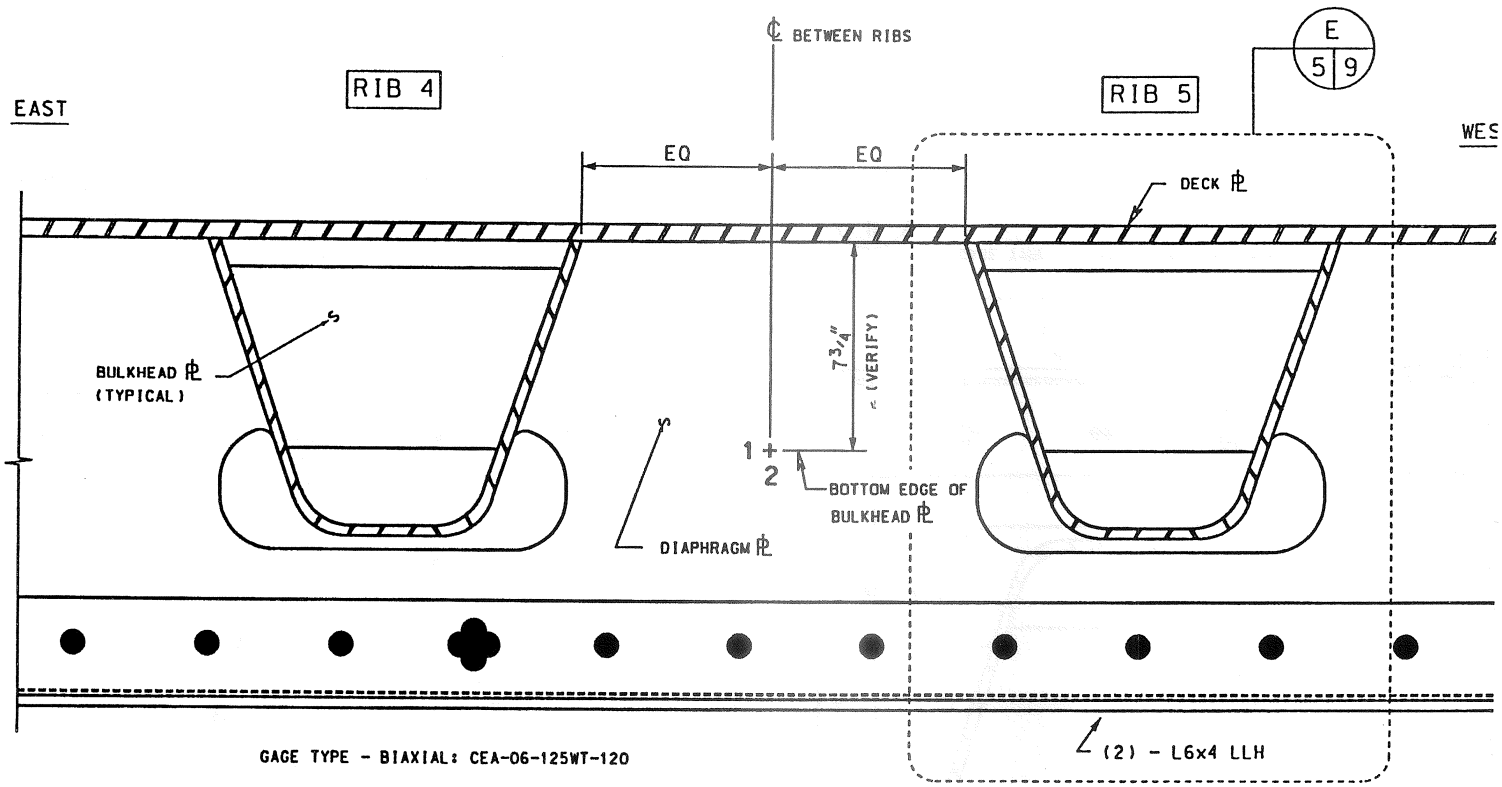

DETAIL- PARTIAL NORTH ELEVATION OF DIAPHRAGM OVER FLOORBEAM "B"

SCALE 1:6

SKETCH SK-5 A 3 5

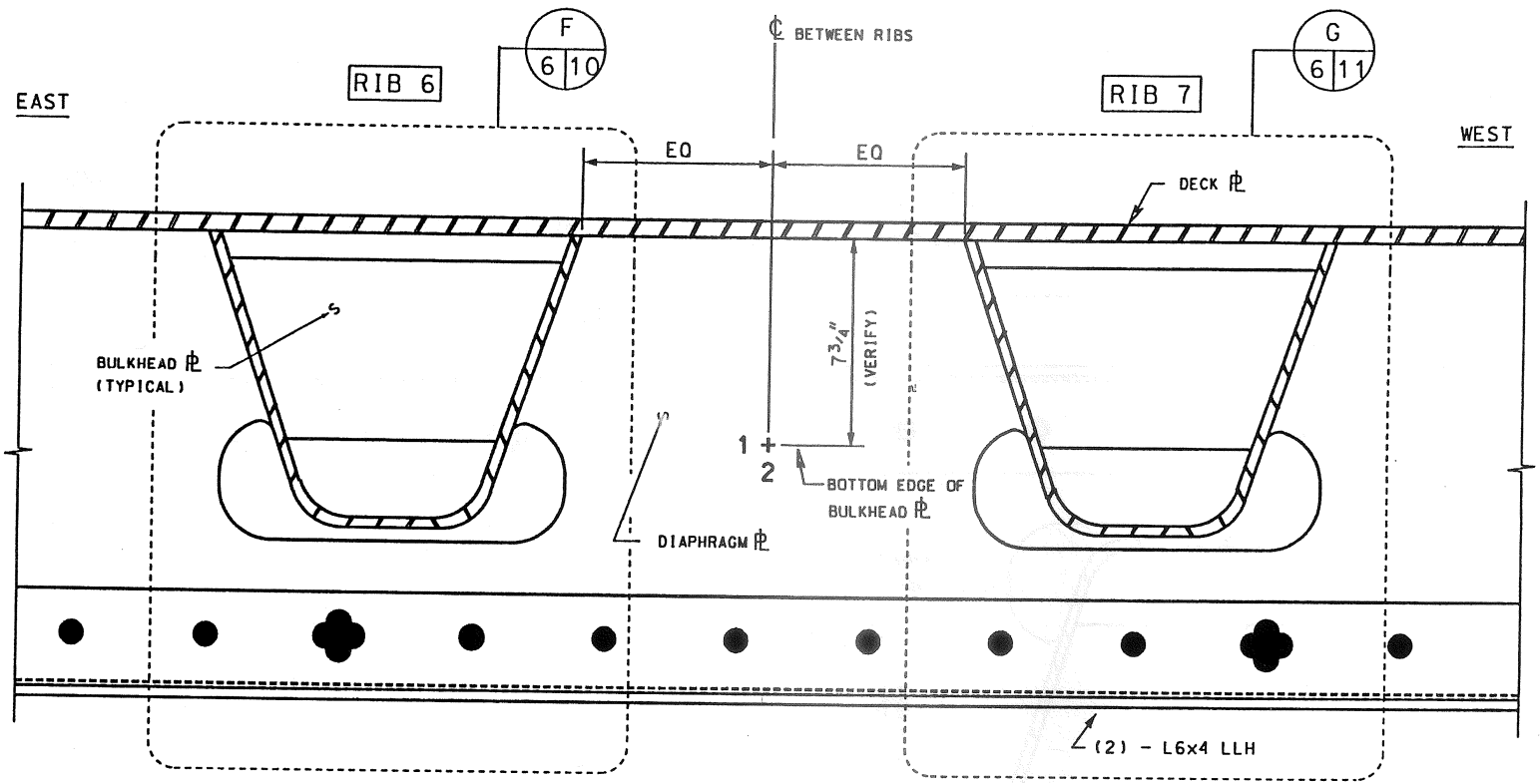

DETAIL - PARTIAL NORTH ELEVATION OF DIAPHRAGM OVER FLOORBEAM "B"

SCALE 1:6

SKETCH SK-6

B
3 | 6

GAGE TYPE - BIAXIAL: CEA-06-125WT-120

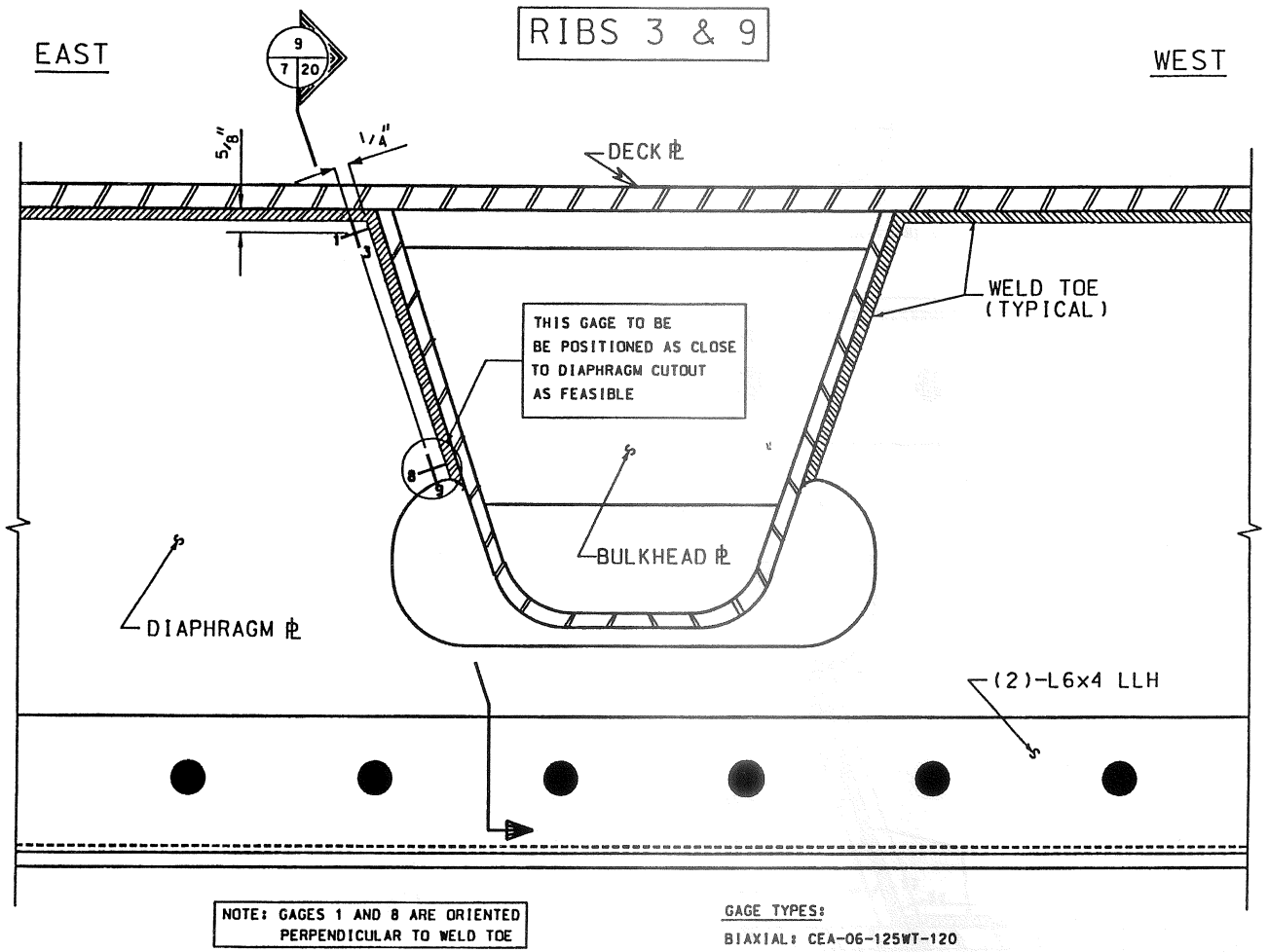

DETAIL - PARTIAL NORTH ELEVATION OF DIAPHRAGM OVER FLOORBEAM "B"

C
3 7

SCALE 1:5

SKETCH SK-7

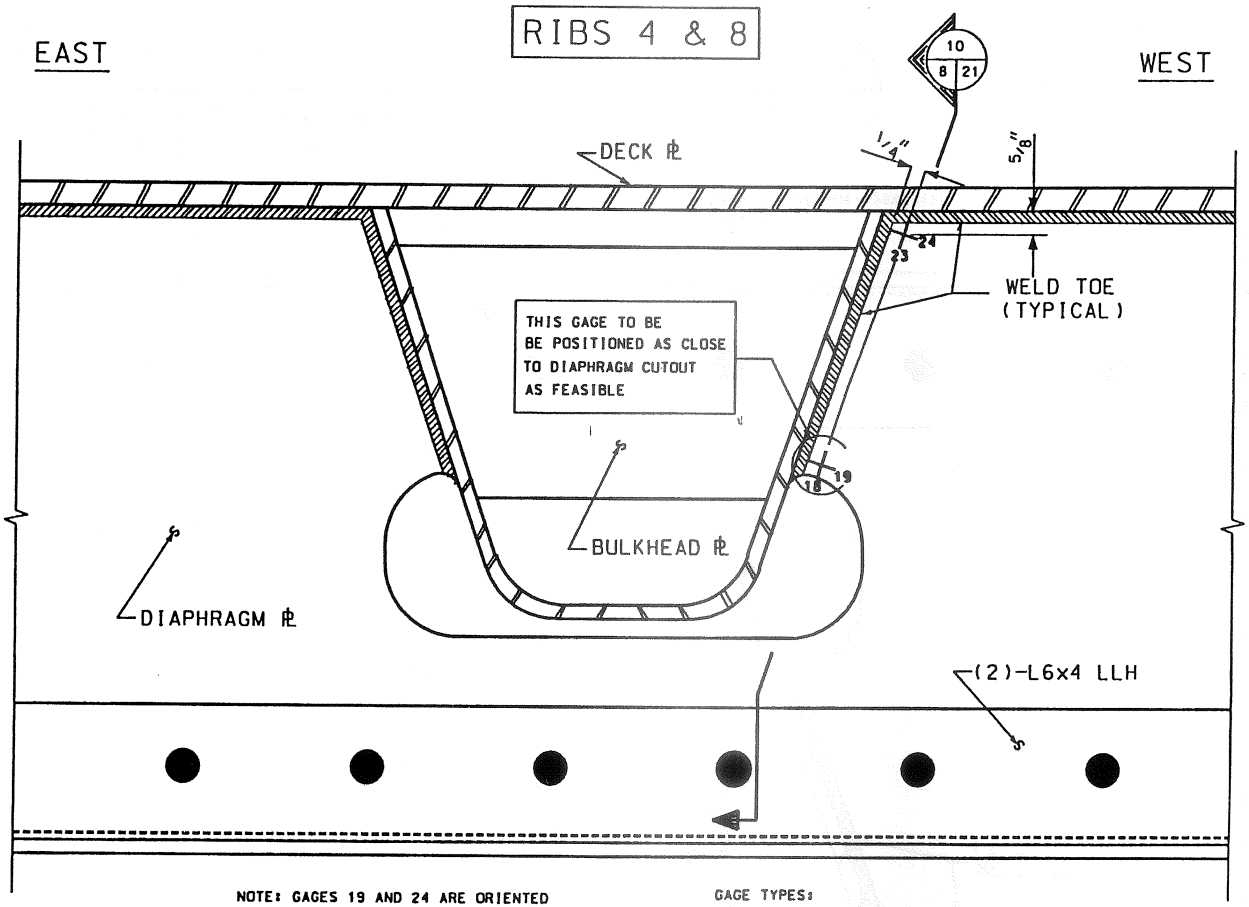

DETAIL - PARTIAL NORTH ELEVATION OF DIAPHRAGM OVER FLOORBEAM "B"

D
3 8

SCALE 1:5

SKETCH SK-8

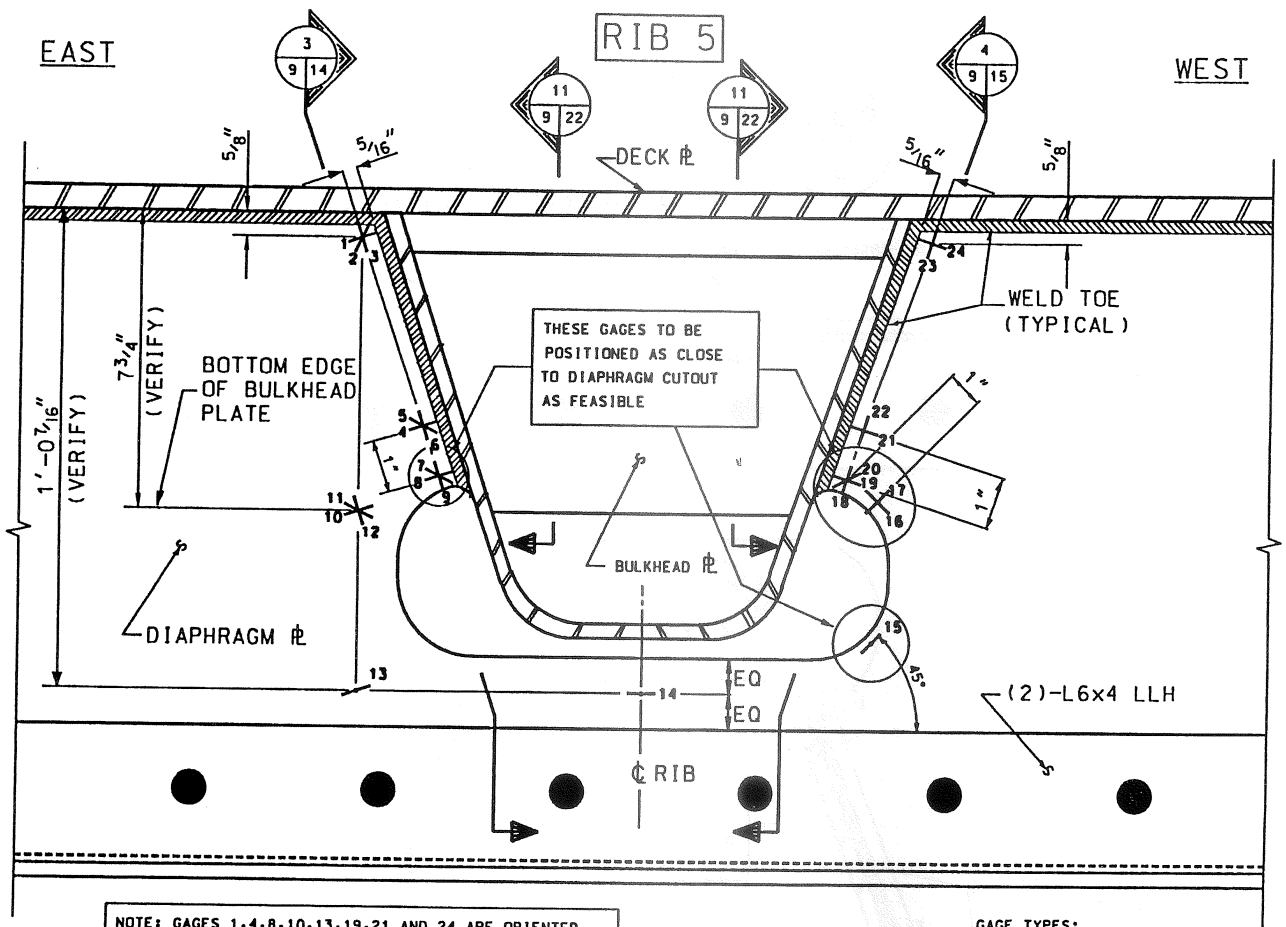

NOTE: GAGES 1.4.8.10.13.19.21 AND 24 ARE ORIENTED PERPENDICULAR TO WELD TOE

GAGE TYPES:

UNIAXIAL: CEA-06-250UN-120

BIAXIAL: CEA-06-125WT-120

ROSETTES: WA-06-250WR-120

DETAIL - PARTIAL NORTH ELEVATION OF DIAPHRAGM OVER FLOORBEAM "B"

SCALE 1:5

SKETCH SK-9

E 5 9

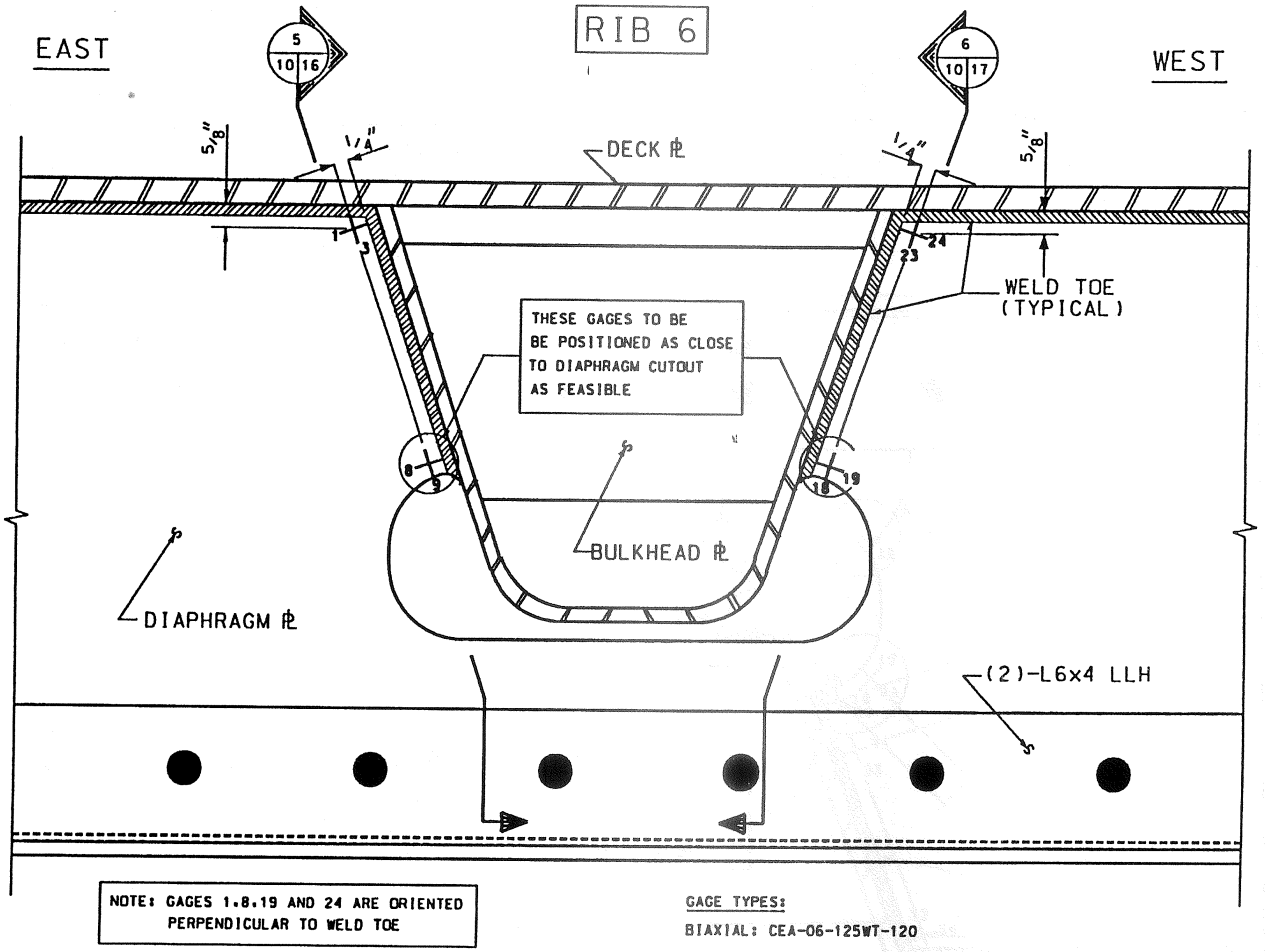

DETAIL - PARTIAL NORTH ELEVATION OF DIAPHRAGM OVER FLOORBEAM "B"

F
6 | 10

SCALE 1:5

SKETCH SK-10

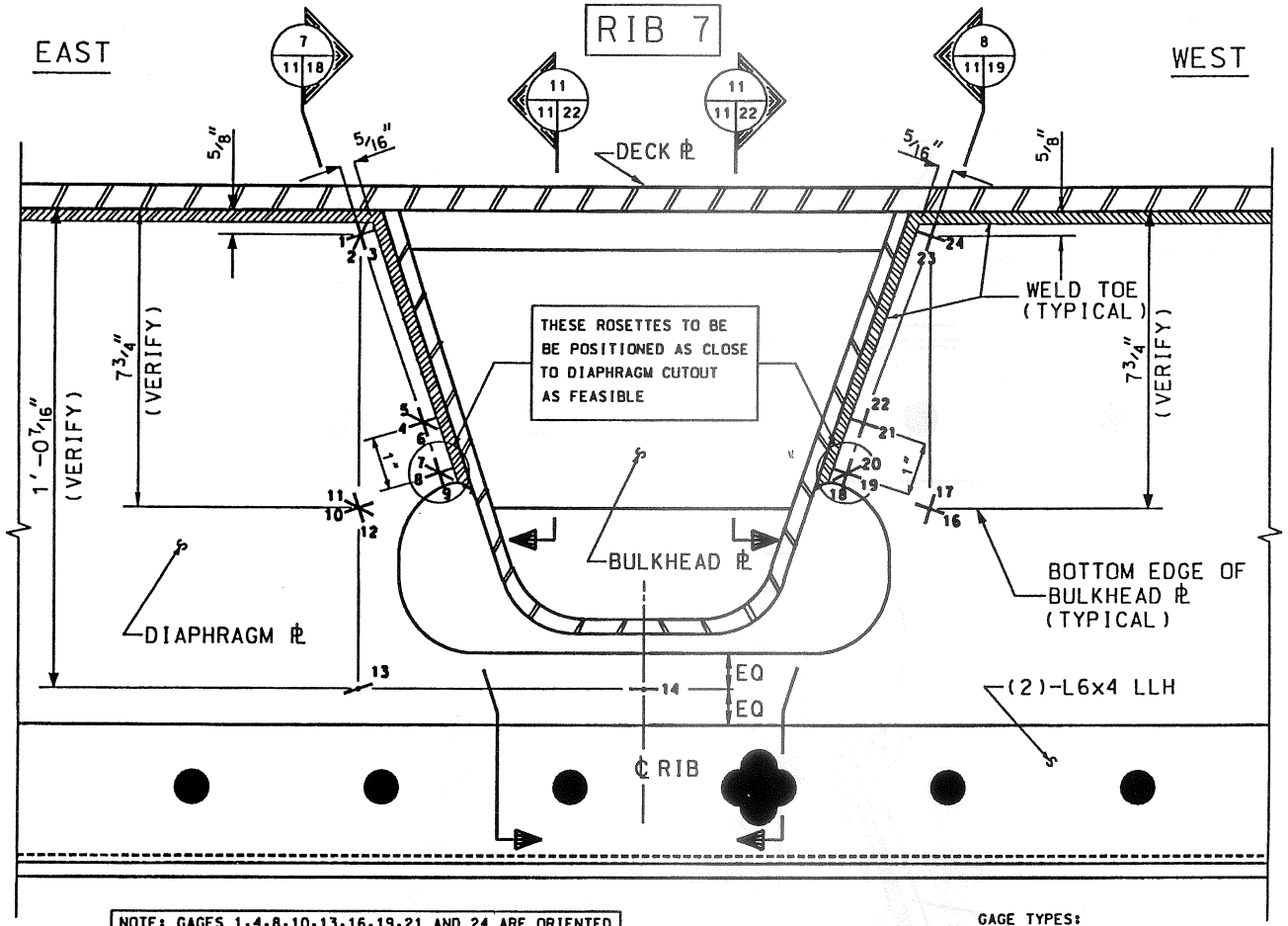

NOTE: GAGES 1.4.8.10.13.16.19.21 AND 24 ARE ORIENTED PERPENDICULAR TO WELD TOE

GAGE TYPES:
UNIAXIAL: CEA-06-250UN-120
BIAXIAL: CEA-06-125WT-120
ROSETTES: WA-06-250WR-120

DETAIL - PARTIAL NORTH ELEVATION OF DIAPHRAGM OVER FLOORBEAM "B"

G
6 | 11

SCALE 1:5

SKETCH SK-11

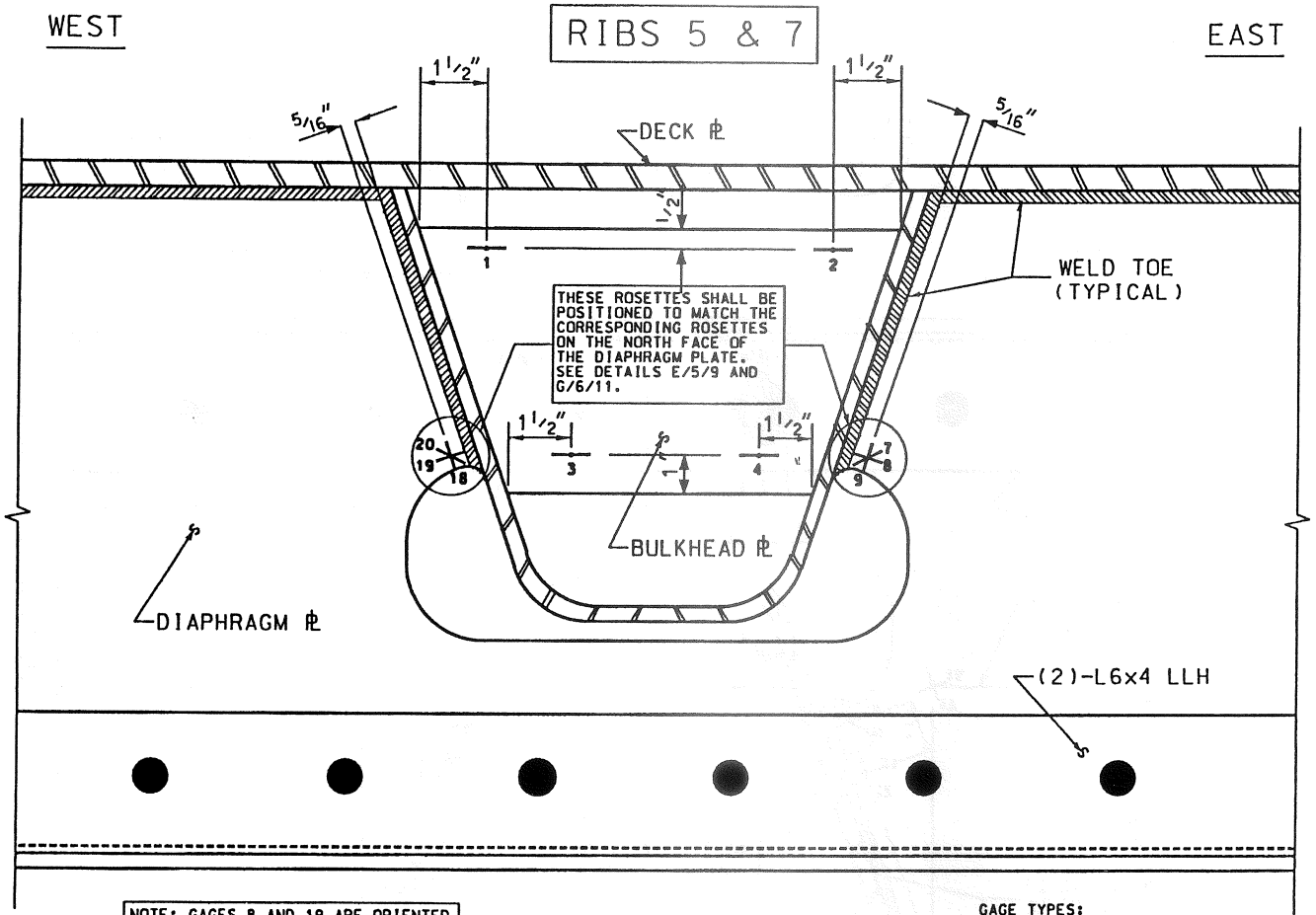

DETAIL – PARTIAL SOUTH ELEVATION OF DIAPHRAGM OVER FLOORBEAM "B"

SCALE 1:5

SKETCH SK-12

H
4 | 12

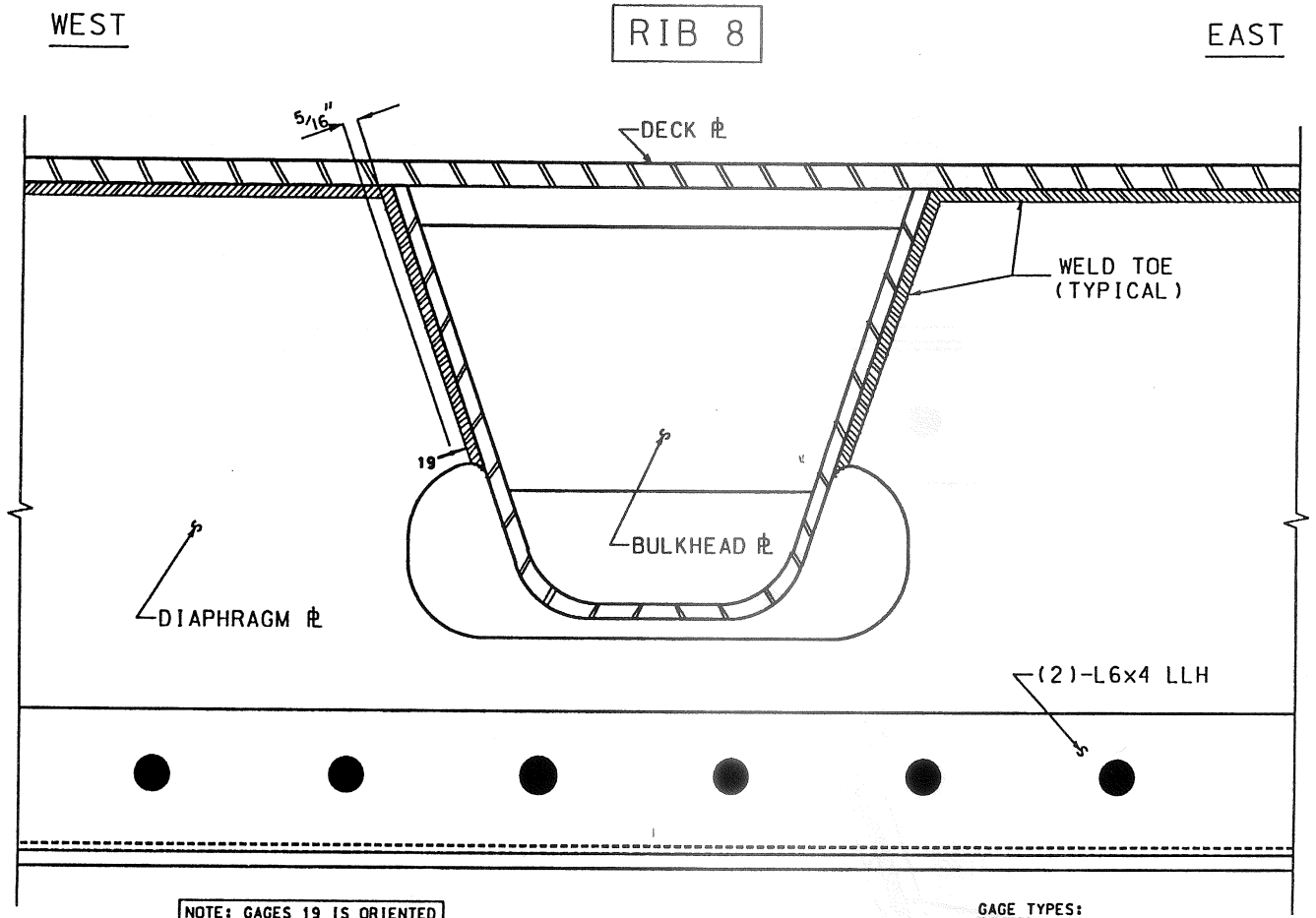

DETAIL - PARTIAL SOUTH ELEVATION OF DIAPHRAGM OVER FLOORBEAM "B"

SCALE 1:5

SKETCH SK-12A

H
4 | 12A

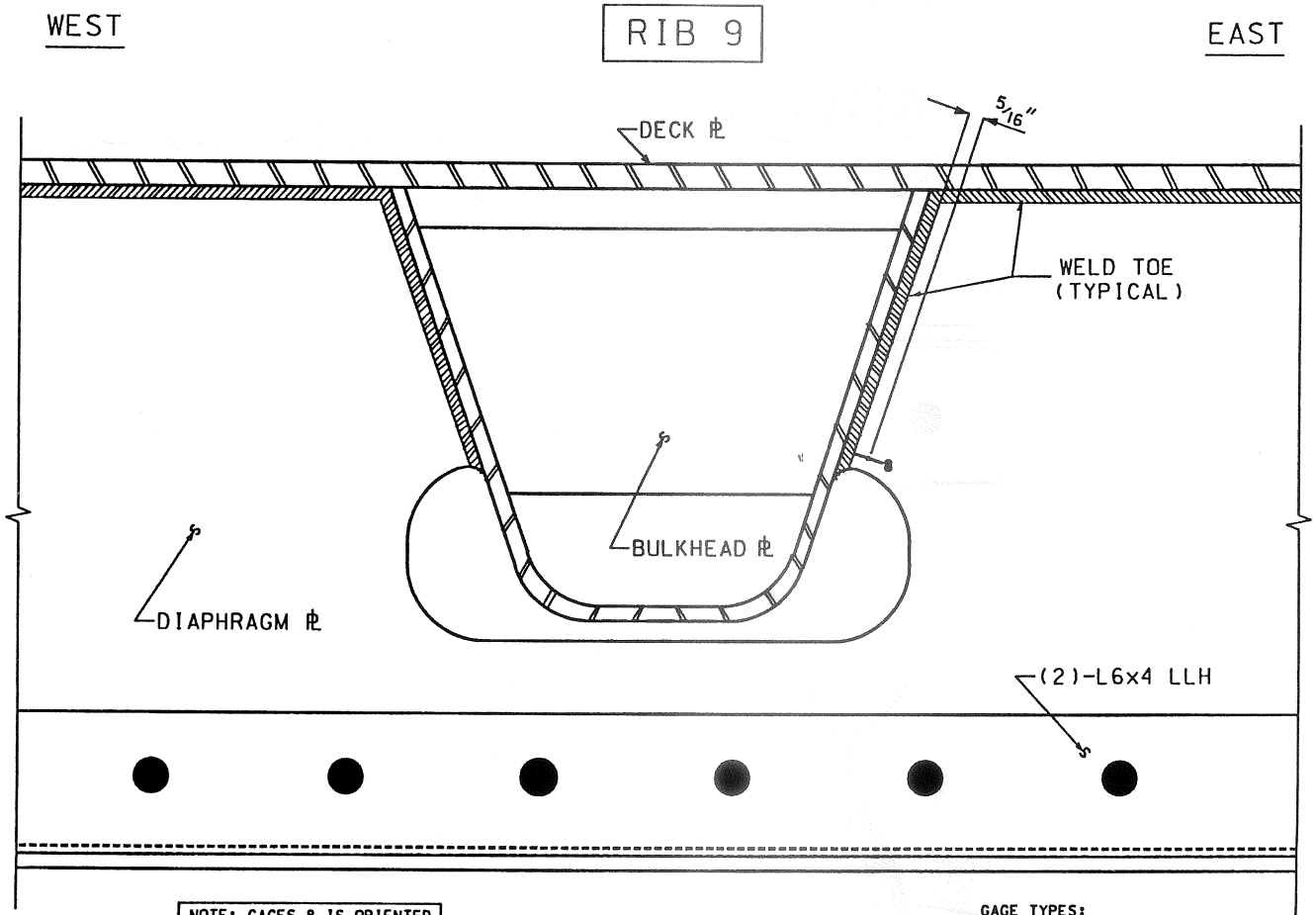

DETAIL - PARTIAL SOUTH ELEVATION OF DIAPHRAGM OVER FLOORBEAM "B"

SCALE 1:5

SKETCH SK-120

H
4 | 12B

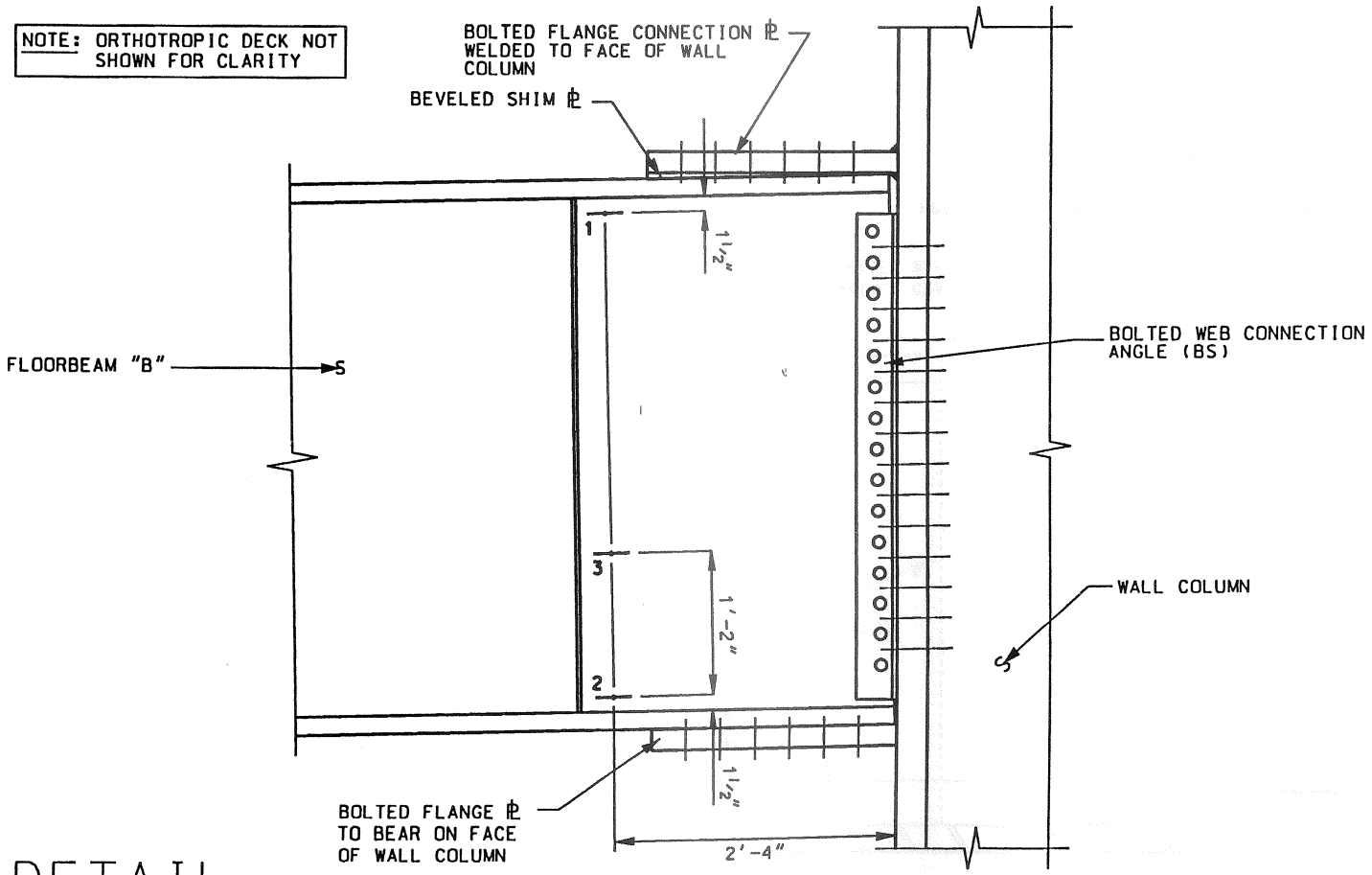

DETAIL GAGE TYPE - UNIAXIAL: CEA-06-250UN-120

SCALE 1:15 SKETCH SK-13

I
3 | 13

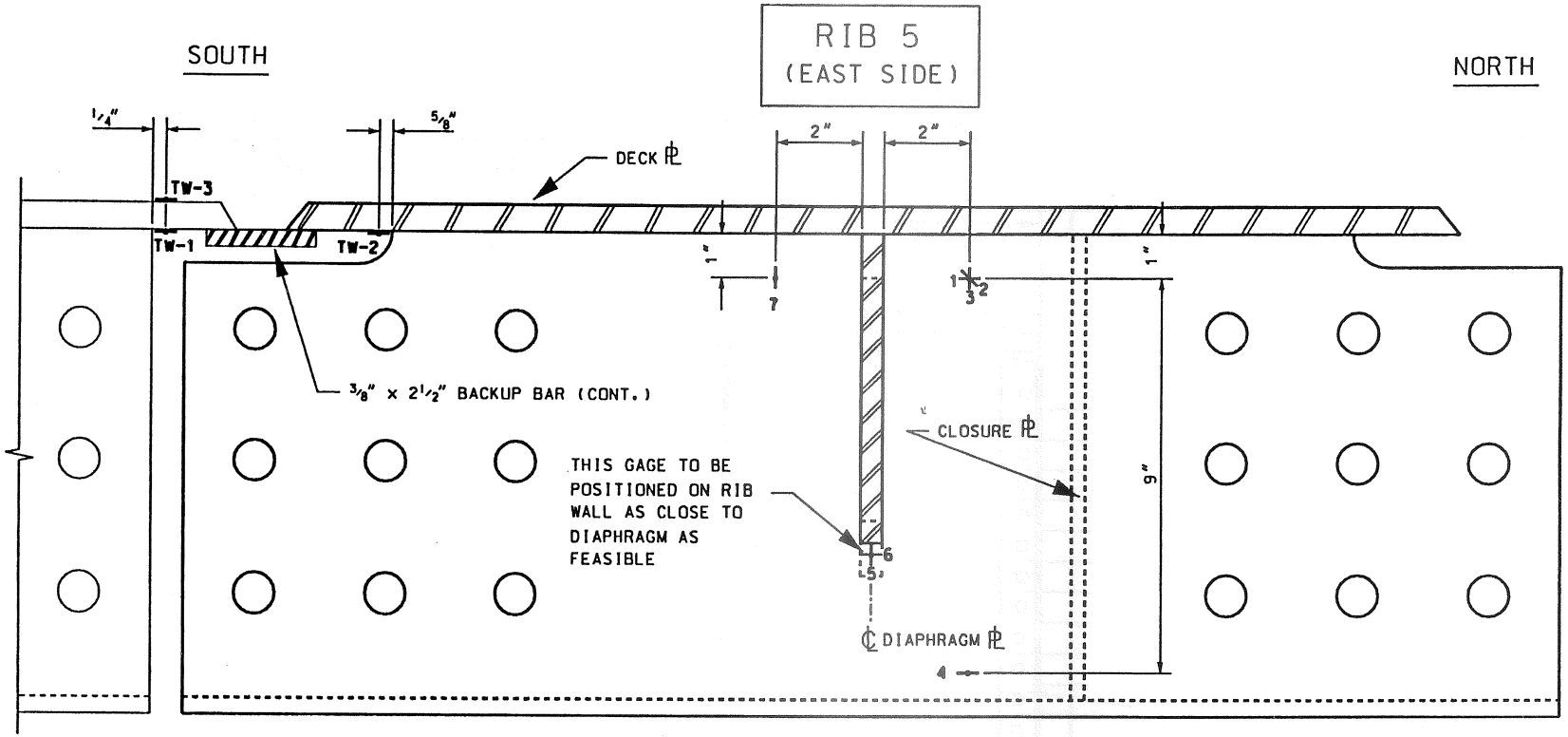

GAGE TYPES - UNIAXIAL: CEA-06-250UN-120 BIAXIAL: CEA-06-125WT-120
ROSETTE: WA-06-250WR-120

SECTION

SCALE 1:4 SKETCH SK-14

3
9 | 14

NOTES: 1. SPLICE PLATES, ADJACENT DECK SECTION AND (2)-L6x4's NOT SHOWN FOR CLARITY
2. DIMENSIONS SHOWN MEASURED ALONG FACE OF RIB WALL

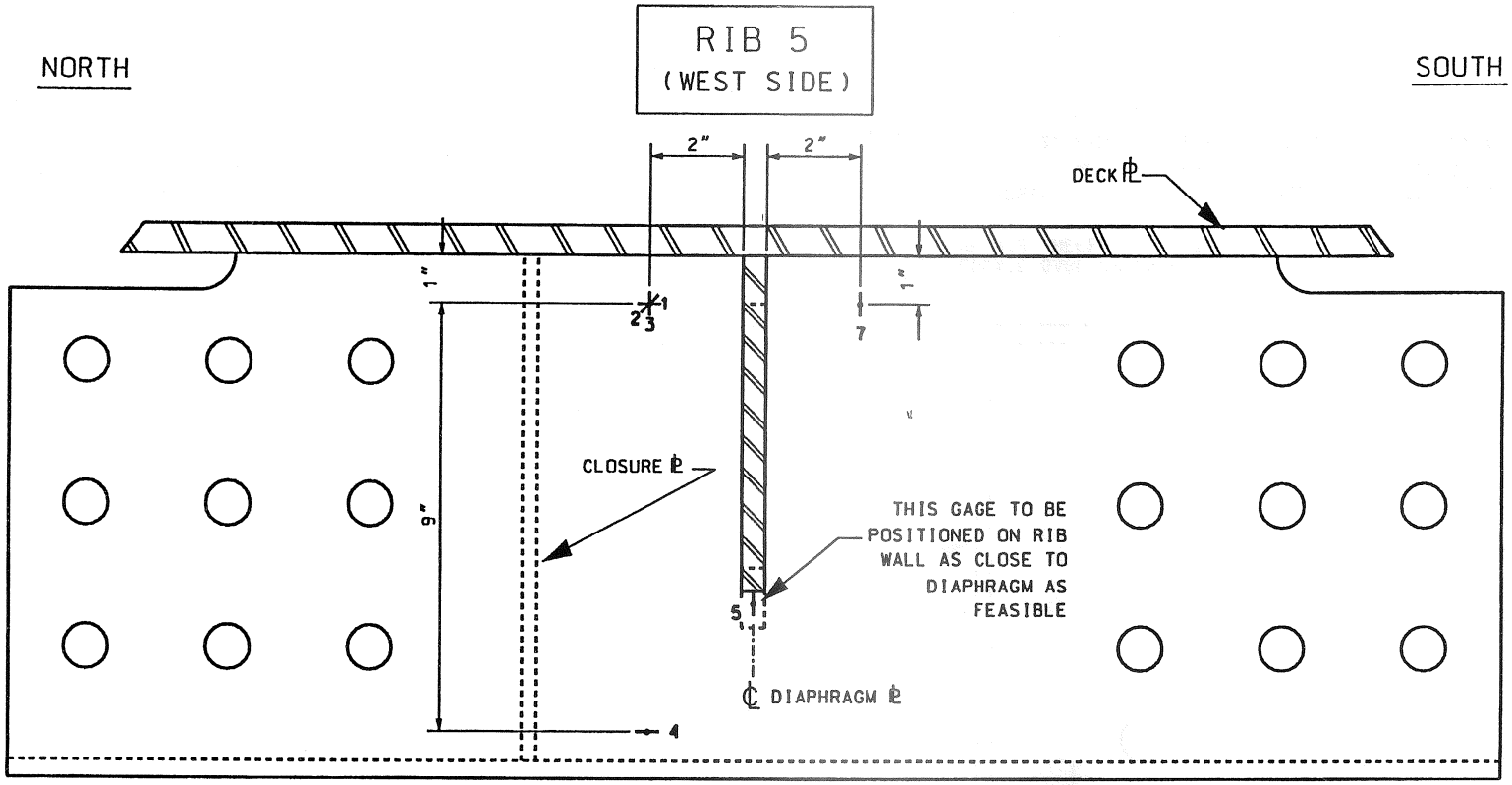

GAGE TYPES - UNIAXIAL: CEA-06-250UN-120 ROSETTE: WA-06-250WR-120

SECTION

SCALE 1:4

SKETCH SK-15

4
9 | 15

NOTES: 1. SPLICE PLATES, ADJACENT DECK SECTIONS AND (2)-L6x4's NOT SHOWN FOR CLARITY
2. DIMENSIONS SHOWN MEASURED ALONG FACE OF RIB WALL

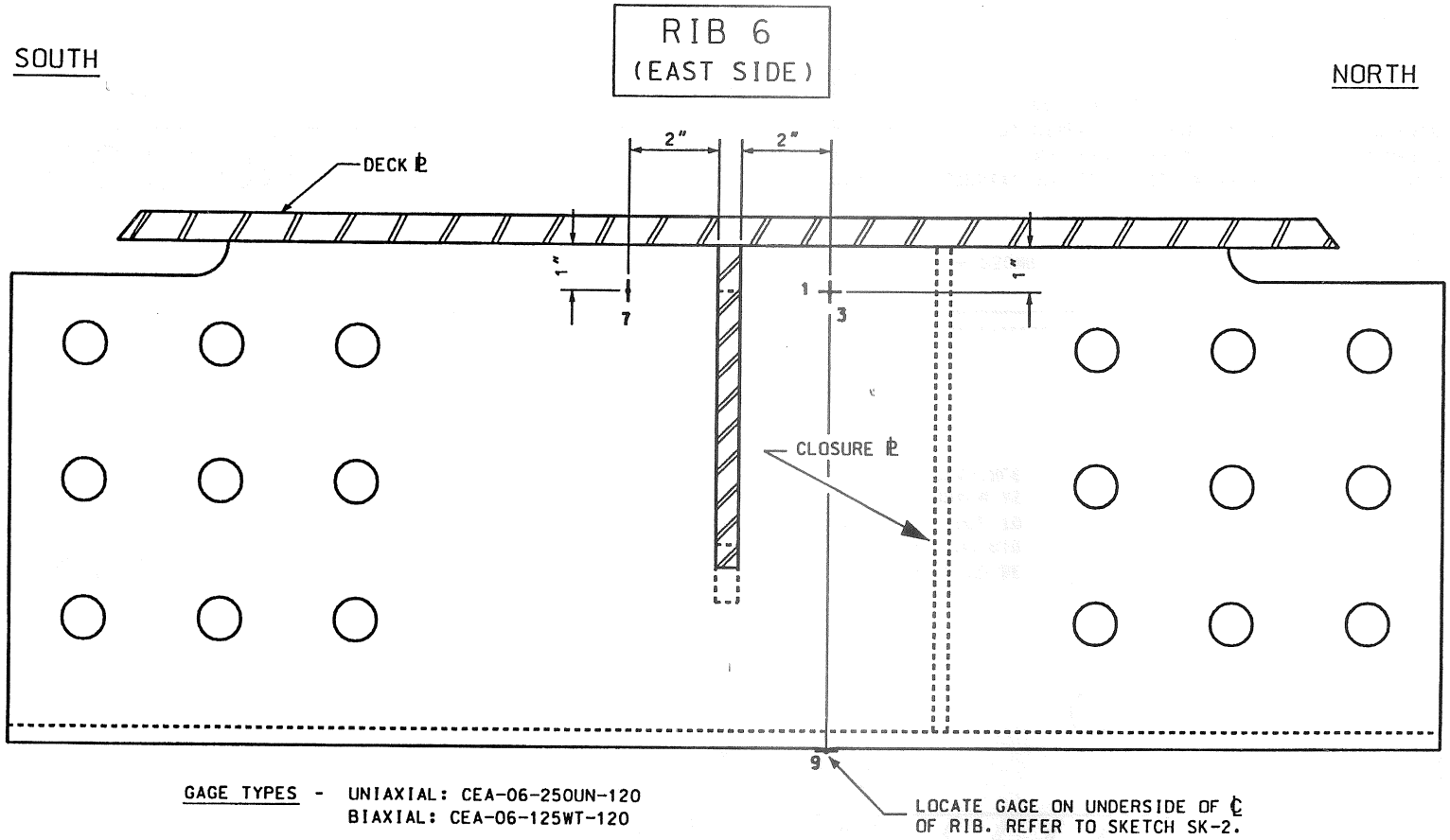

SECTION

SCALE 1:4

SKETCH SK-16

5
10 16

NOTES: 1. SPLICE PLATES, ADJACENT DECK SECTIONS AND (2)-L6x4's NOT SHOWN FOR CLARITY
2. DIMENSIONS SHOWN MEASURED ALONG FACE OF RIB WALL

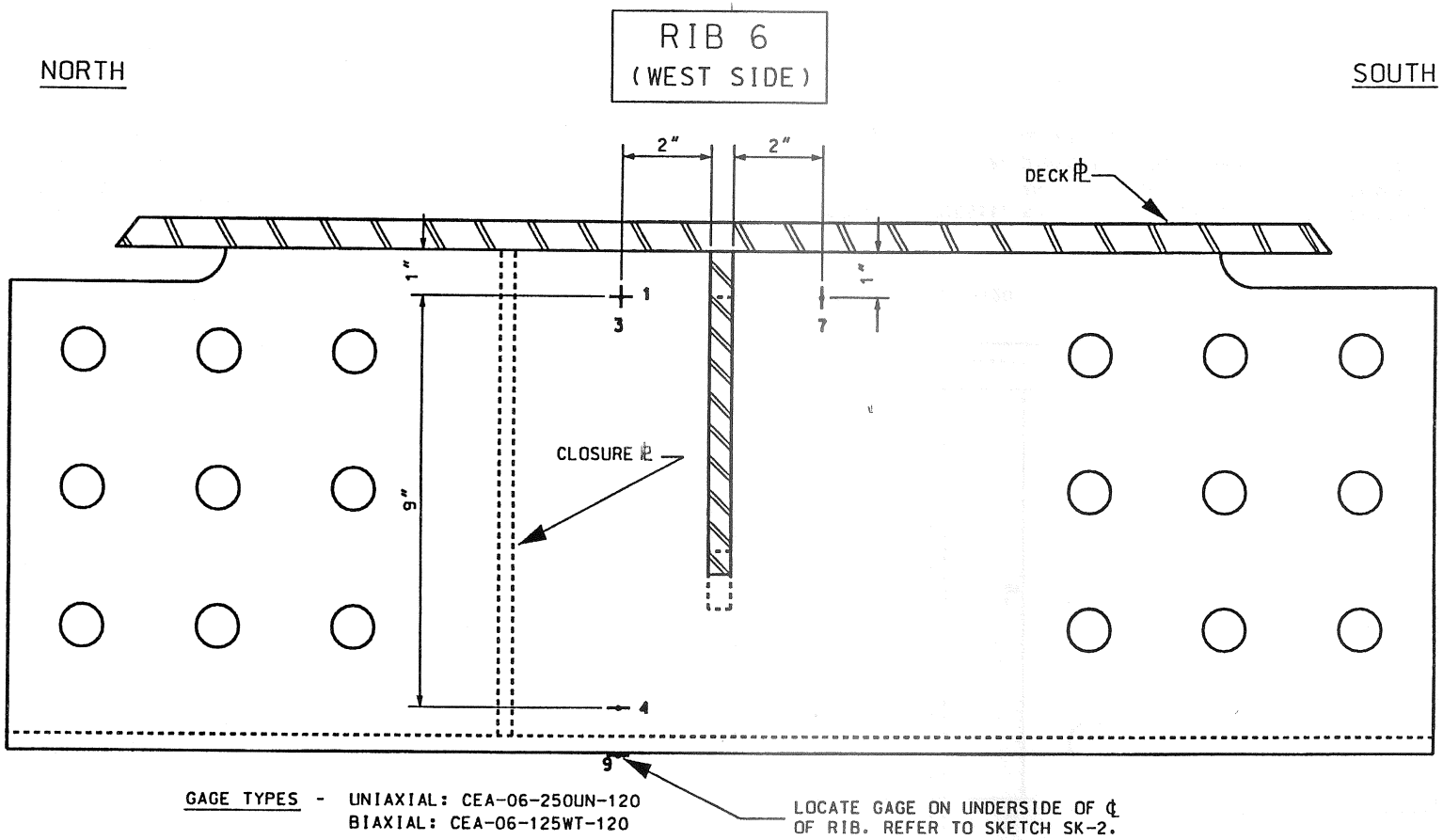

SECTION

SCALE 1:4

SKETCH SK-17

6
10 | 17

NOTES: 1. SPLICE PLATES, ADJACENT DECK SECTIONS AND (2)-L6x4's NOT SHOWN FOR CLARITY
2. DIMENSIONS SHOWN MEASURED ALONG FACE OF RIB WALL

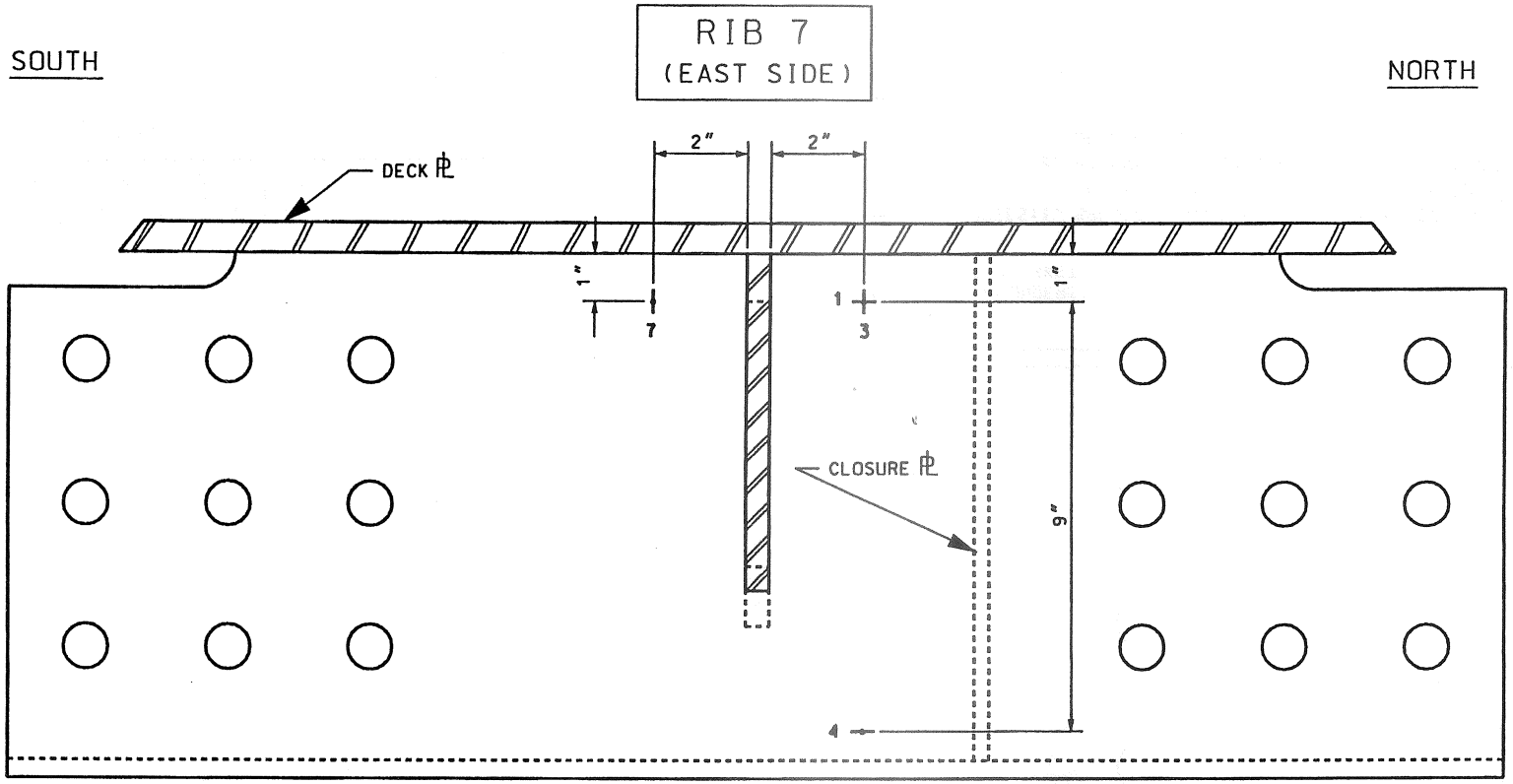

GAGE TYPES - UNIAXIAL: CEA-06-250UN-120 BIAXIAL: CEA-06-125WT-120

SECTION

SCALE 1:4

SKETCH SK-18

7
11 | 18

NOTES: 1. SPLICE PLATES, ADJACENT DECK SECTIONS AND (2)-L6x4's NOT SHOWN FOR CLARITY
2. DIMENSIONS SHOWN MEASURED ALONG FACE OF RIB WALL

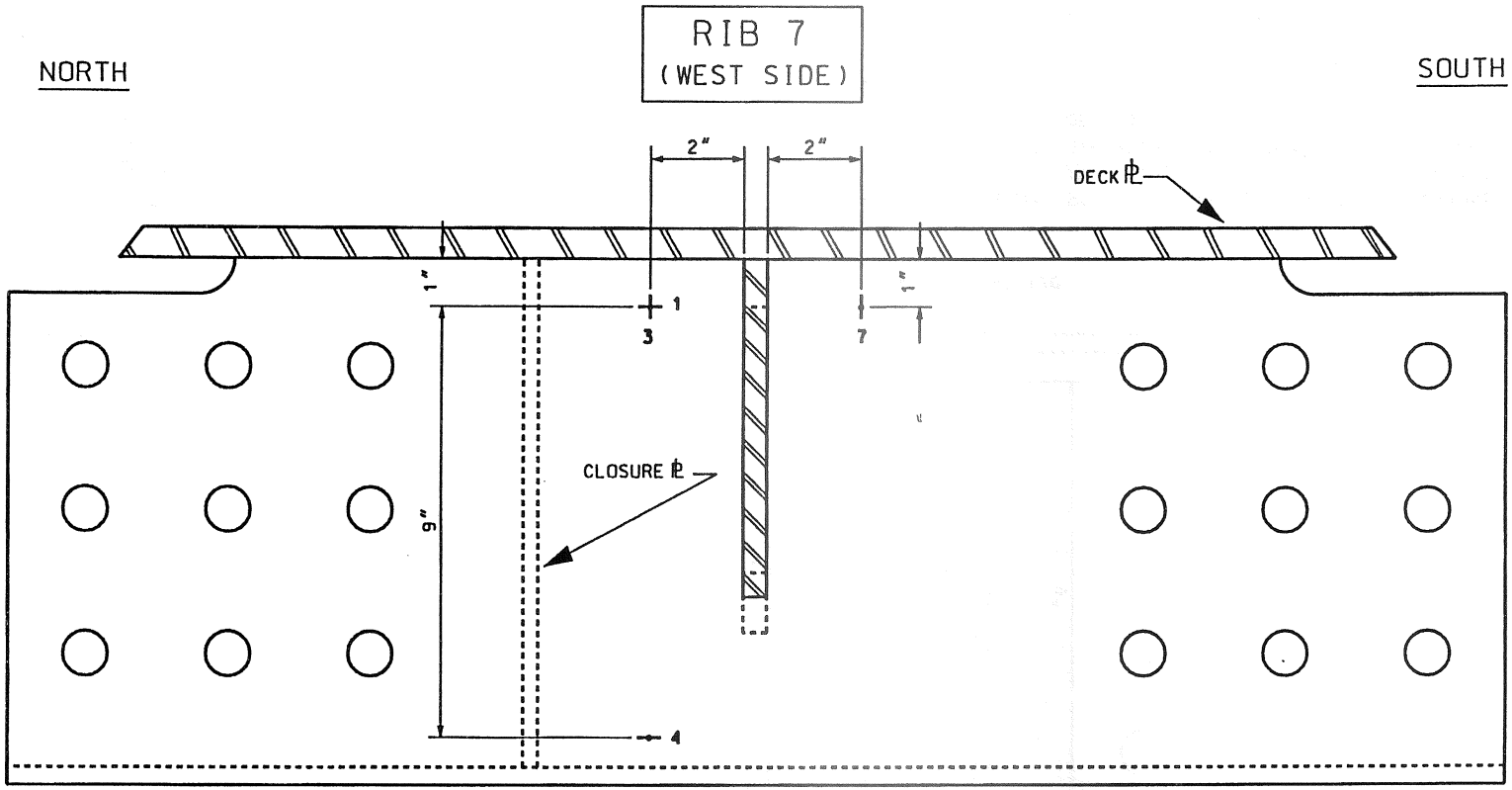

GAGE TYPES - UNIAXIAL: CEA-06-250UN-120 BIAXIAL: CEA-06-125WT-120

SECTION

SCALE 1:4

SKETCH SK-19

8
11 | 19

NOTES: 1. SPLICE PLATES, ADJACENT DECK SECTIONS AND (2)-L6x4's NOT SHOWN FOR CLARITY
2. DIMENSIONS SHOWN MEASURED ALONG FACE OF RIB WALL

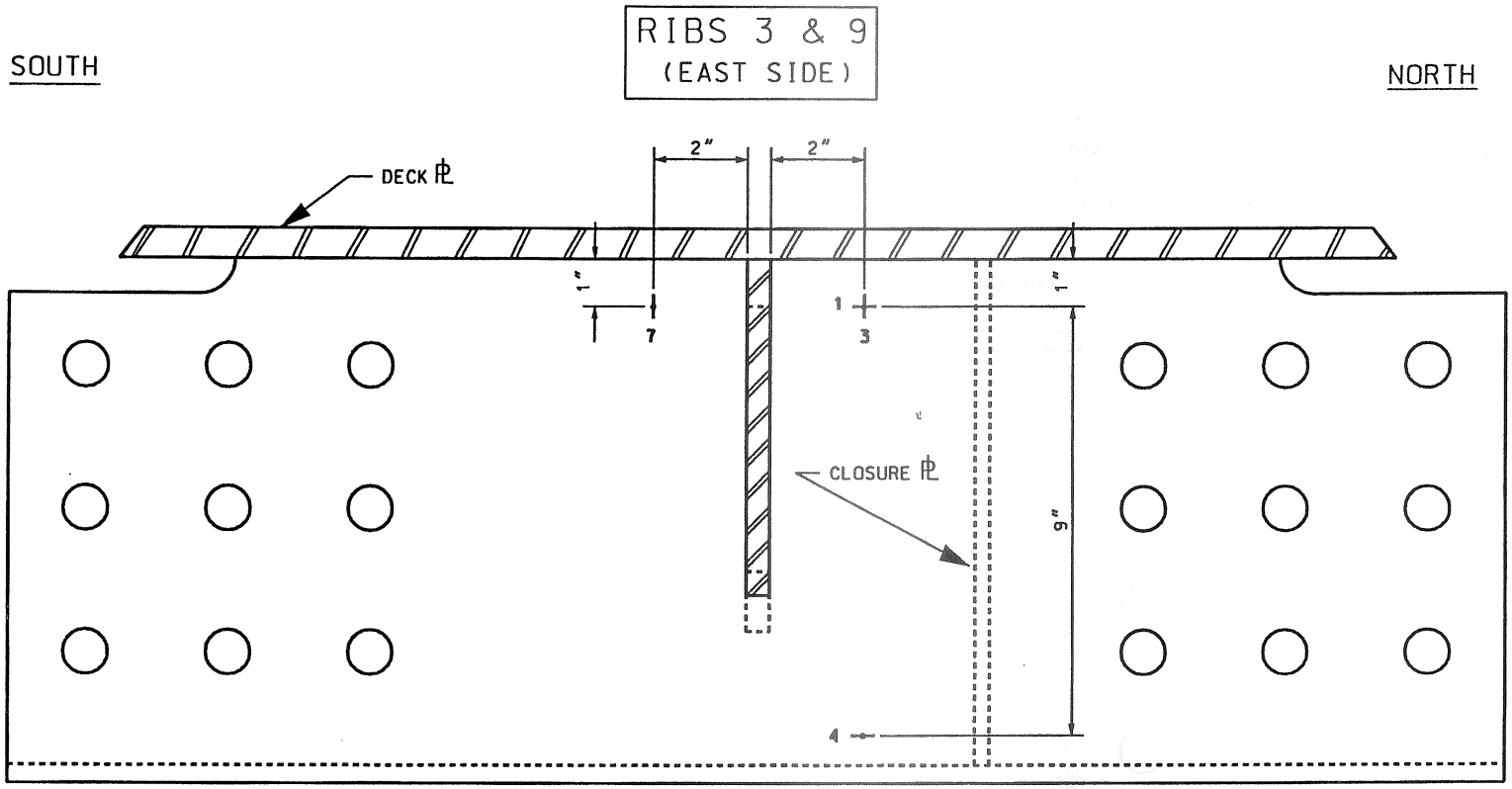

GAGE TYPES - UNIAXIAL: CEA-06-250UN-120 BIAXIAL: CEA-06-125WT-120

SECTION

SCALE 1:4

SKETCH SK-20

9
7 | 20

NOTES: 1. SPLICE PLATES, ADJACENT DECK SECTIONS AND (2)-L6x4's NOT SHOWN FOR CLARITY
2. DIMENSIONS SHOWN MEASURED ALONG FACE OF RIB WALL

RIBS 4 & 8
(WEST SIDE)

NORTH

SOUTH

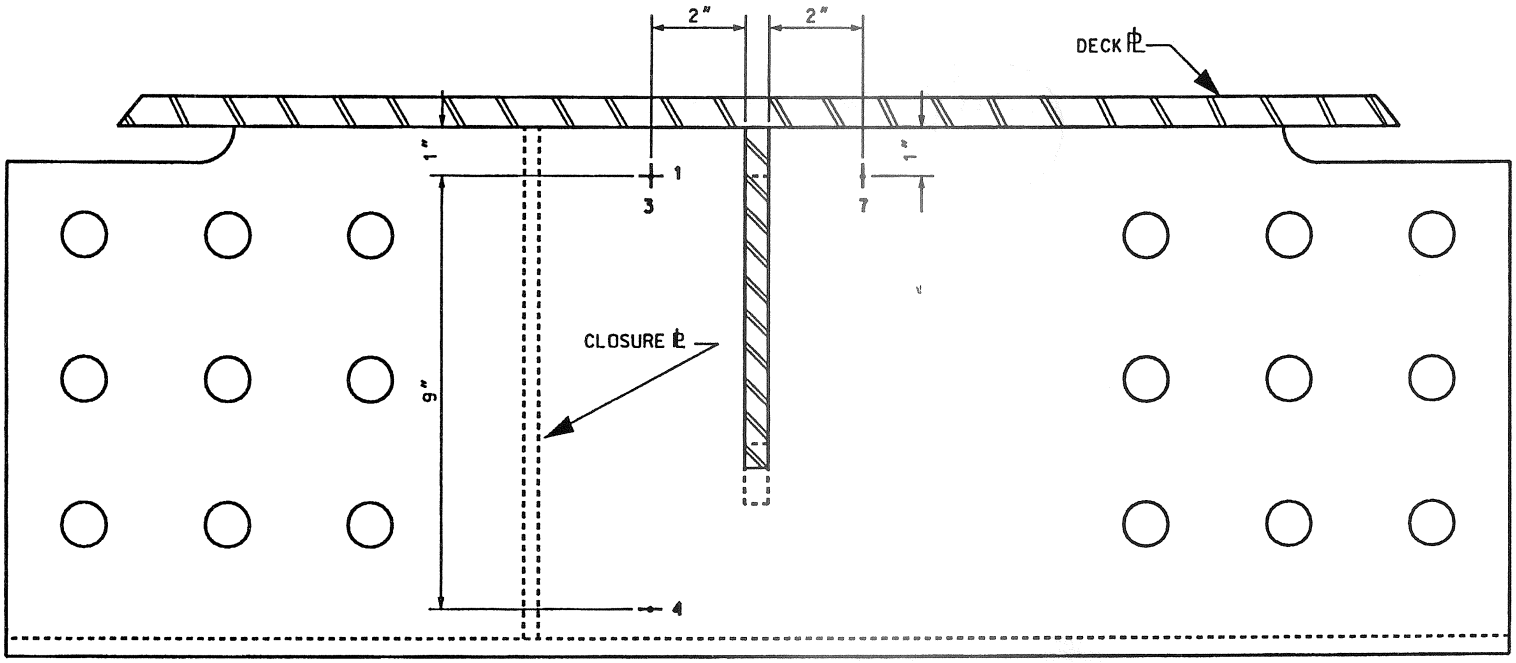

GAGE TYPES - UNIAXIAL: CEA-06-250UN-120 BIAXIAL: CEA-06-125WT-120

SECTION

SCALE 1:4

SKETCH SK-21

10
8 | 21

NOTES: 1. SPLICE PLATES, ADJACENT DECK SECTIONS AND (2)-L6x4's NOT SHOWN FOR CLARITY
2. DIMENSIONS SHOWN MEASURED ALONG FACE OF RIB WALL

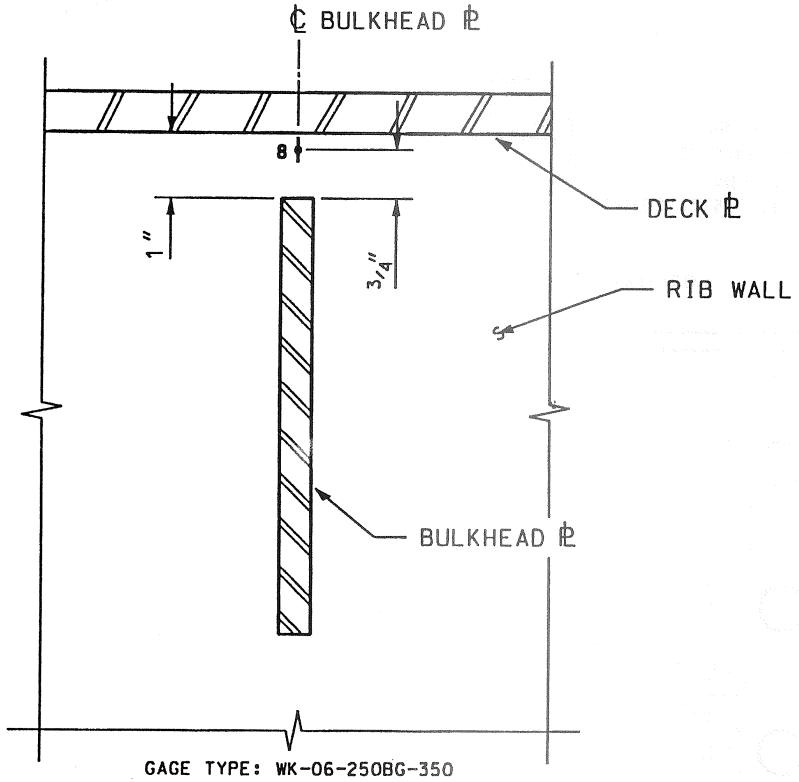

SECTION

SCALE 1:3

SKETCH SK-22

11

9 | 11 | 22

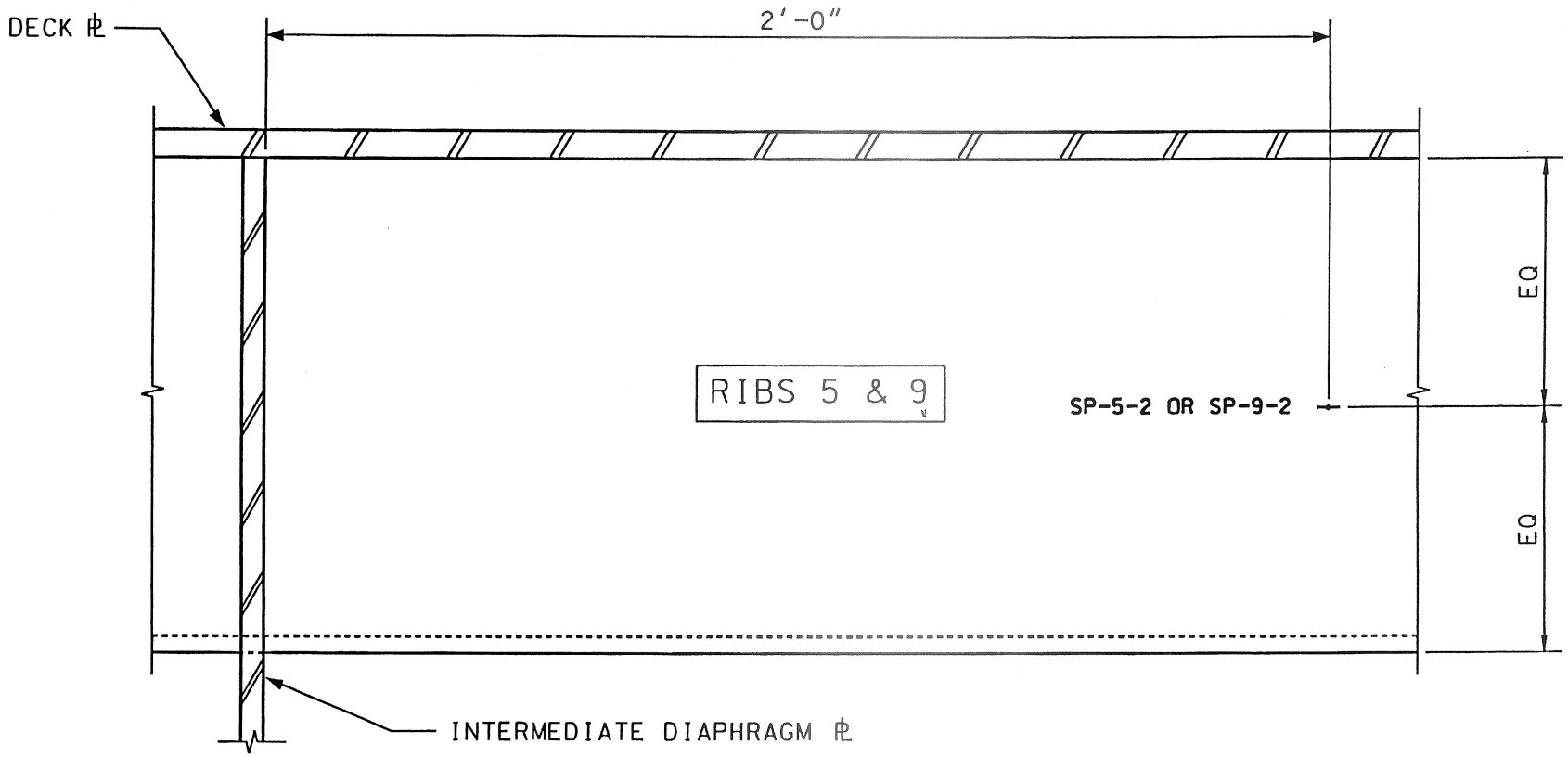

SECTION

GAGE TYPE - UNIAXIAL: CEA-06-250UN-120

SCALE 1:4

SKETCH SK-23

12
1 | 23

Appendix B

Static Calibration Test Data

Test 1	0 cycles
Test 2	1,090,000 cycles
Test 3	2,485,000 cycles
Test 4	5,000,000 cycles

All tests carried out at the HS20 load level with 30% impact in the outside lane

Williamsburg Bridge Static Calibration Test 1 27-Jan-98

Strain gages: MPa **Complete Equivalent HS20 Load Cycle**
LVDTs: mm **Current cycle count: 0**
Jacks: kN

At Step 0:
- **all jacks are at minimum load of approximately 44 kN**
- **all strain gages and LVDTs read zero**

Instrument	Step 1	Step 2	Step 3	
South Jack	379.1	326.6	43.9	Jacks
Center Jack	43.1	226.1	42.4	
North Jack	41.8	267.3	331.1	
B5-S-1	?	?	?	Bulkhead 5 - South Side
B5-S-2	-17.9	-42.5	-17.3	Refer to sketch SK-12
B5-S-3	-7.4	-18.1	-6.1	
B5-S-4	8.6	22.2	8.4	
B7-S-1	?	?	?	Bulkhead 7 - South Side
B7-S-2	?	?	?	Refer to sketch SK-12
B7-S-3	?	?	?	
B7-S-4	8.9	25.9	10.2	
D3-N-1	-2.5	-5.4	-2.7	Diaphragm 3 - North Side
D3-N-3	0.0	-2.7	-0.9	Refer to sketch SK-7
D3-N-8	27.5	36.4	-2.7	
D3-N-9	0.5	1.8	2.2	
D4-N-18	4.1	11.2	8.1	Diaphragm 4 - North Side
D4-N-19	-30.1	-92.9	-56.4	Refer to sketch SK-8
D4-N-23	4.4	2.4	2.8	
D4-N-24	-4.5	-7.3	-3.7	
D45-N-1	-0.6	1.2	1.7	North side of diaphragm between ribs 4 & 5
D45-N-2	1.5	-13.3	-11.0	Refer to sketch SK-5
D5-N-1	0.4	-6.5	0.4	Diaphragm 5 - North Side
D5-N-2	4.8	1.0	3.7	Refer to sketch SK-9
D5-N-3	-1.9	-5.3	-3.4	
D5-N-4	4.6	-1.4	-7.1	
D5-N-5	14.9	38.0	14.1	
D5-N-6	5.1	8.2	3.3	
D5-N-7	26.6	66.6	26.2	
D5-N-8	29.4	43.7	3.6	
D5-N-9	1.4	5.6	4.3	
D5-N-10	14.9	37.5	15.8	
D5-N-11	3.9	-14.0	-11.3	
D5-N-12	-14.6	-56.6	-28.2	

? instrument not working - instrument not hooked up

Strain gages: MPa **Complete Equivalent HS20 Load Cycle**
LVDTs: mm **Current cycle count: 0**
Jacks: kN

At Step 0:
- **all jacks are at minimum load of approximately 44 kN**
- **all strain gages and LVDTs read zero**

Instrument	Step 1	Step 2	Step 3	
D5-N-13	-4.2	-6.9	-2.6	Diaphragm 5 - North Side
D5-N-14	1.8	3.0	0.9	Refer to sketch SK-9
D5-N-15	35.7	66.0	19.8	
D5-N-16	-35.2	-100.6	-47.3	
D5-N-17	6.1	17.2	8.0	
D5-N-18	1.8	6.3	4.3	
D5-N-19	-39.1	-116.8	-56.3	
D5-N-20	-18.7	-44.7	-16.3	
D5-N-21	-16.2	-48.8	-24.4	
D5-N-22	-4.3	-13.3	-5.7	
D5-N-23	6.2	14.1	4.9	
D5-N-24	-5.6	-13.3	-2.8	
D5-S-7	33.0	76.9	28.9	Diaphragm 5 - South Side
D5-S-8	34.7	110.5	56.5	Refer to sketch SK-12
D5-S-9	?	?	?	
D5-S-18	0.9	-0.8	-1.3	
D5-S-19	-37.4	-61.1	-10.1	
D5-S-20	-15.5	-41.3	-15.8	
D6-N-1	1.3	-1.7	1.6	Diaphragm 6 - North Side
D6-N-3	-1.6	-2.9	-2.5	Refer to sketch SK-10
D6-N-8	21.5	30.1	-0.6	
D6-N-9	0.4	0.5	-0.2	
D6-N-18	4.9	17.3	11.2	
D6-N-19	-25.3	-92.3	-45.6	
D6-N-23	6.4	13.4	5.0	
D6-N-24	-6.2	-15.8	-6.1	
D67-N-1	0.1	2.9	2.0	North side of diaphragm between ribs 6 & 7
D67-N-2	-0.9	-16.0	-11.9	Refer to sketch SK-6
D7-N-1	-0.9	0.4	-1.1	Diaphragm 7 - North Side
D7-N-2	2.9	10.9	0.3	Refer to sketch SK-11
D7-N-3	-0.8	-7.7	-2.9	
D7-N-4	-0.5	-10.7	-11.4	
D7-N-5	15.8	32.2	15.0	
D7-N-6	7.9	16.6	8.3	
D7-N-7	29.2	69.7	32.8	

? instrument not working

- instrument not hooked up

Strain gages: MPa **Complete Equivalent HS20 Load Cycle**
LVDTs: mm **Current cycle count: 0**
Jacks: kN

At Step 0:
- **all jacks are at minimum load of approximately 44 kN**
- **all strain gages and LVDTs read zero**

Instrument	Step 1	Step 2	Step 3	
D7-N-8	22.4	35.1	2.9	Diaphragm 7 - North Side
D7-N-9	-0.2	-0.9	0.1	Refer to sketch SK-11
D7-N-10	16.9	43.8	16.4	
D7-N-11	-0.3	1.3	2.8	
D7-N-12	-19.6	-62.9	-30.7	
D7-N-13	-5.0	-9.8	-2.6	
D7-N-14	9.8	19.8	9.2	
D7-N-16	-8.5	-21.9	-7.5	
D7-N-17	-0.8	-0.9	0.5	
D7-N-18	3.6	11.1	5.3	
D7-N-19	-42.5	-129.9	-61.0	
D7-N-20	-36.9	-113.7	-53.4	
D7-N-21	-15.6	-49.5	-24.7	
D7-N-22	-4.2	-14.1	-6.5	
D7-N-23	4.8	16.6	10.1	
D7-N-24	-4.0	-13.0	-8.0	
D7-S-7	28.3	61.1	25.9	Diaphragm 7 - South Side
D7-S-8	38.2	120.9	57.6	Refer to sketch SK-12
D7-S-9	1.2	-3.4	-1.9	
D7-S-18	-0.4	-3.5	-2.3	
D7-S-19	-13.8	-12.5	8.3	
D7-S-20	-13.6	-38.2	-14.5	
D8-N-18	-23.0	-85.4	-39.2	Diaphragm 8 - North Side
D8-N-19	5.0	11.6	5.6	Refer to sketch SK-8
D8-N-23	0.9	2.3	0.2	
D8-N-24	-1.3	-5.3	-1.3	
D9-N-1	-3.0	-7.1	-2.1	Diaphragm 9 - North Side
D9-N-3	0.9	-2.0	-0.2	Refer to sketch SK-7
D9-N-8	-37.8	-94.7	-53.6	
D9-N-9	2.1	5.9	2.4	
FB1	13.1	27.9	13.2	Fixed End of Floorbeam B - North Side
FB2	-23.6	-50.6	-21.5	Refer to sketch SK-13
FB3	-9.8	-20.4	-8.8	

? instrument not working

- instrument not hooked up

Strain gages: MPa **Complete Equivalent HS20 Load Cycle**
LVDTs: mm **Current cycle count: 0**
Jacks: kN

At Step 0:
- **all jacks are at minimum load of approximately 44 kN**
- **all strain gages and LVDTs read zero**

Instrument	Step 1	Step 2	Step 3	
R3-E-1	4.7	6.1	3.9	Rib 3 - East Side
R3-E-3	-1.7	-3.2	-1.0	Refer to sketch SK-20
R3-E-4	-15.8	-19.7	-14.4	
R3-E-7	-1.9	-3.7	-1.6	
R4-W-1	7.0	10.2	5.2	Rib 4 - West Side
R4-W-3	2.2	3.3	2.5	Refer to sketch SK-21
R4-W-4	-20.9	-27.6	-17.1	
R4-W-7	1.4	1.2	1.5	
R5-E-1	3.6	8.1	2.0	Rib 5 - East Side
R5-E-2	3.0	13.8	11.9	Refer to sketch SK-14
R5-E-3	-1.1	-4.3	0.1	For gage 8, refer to sketch SK-22
R5-E-4	-17.9	-23.0	-15.7	
R5-E-5	17.0	32.9	16.8	
R5-E-6	-13.8	-12.8	-10.0	
R5-E-7	?	?	?	
R5-E-8	?	?	?	
R5-W-1	?	?	?	Rib 5 - West Side
R5-W-2	2.2	4.6	1.7	Refer to sketch SK-15
R5-W-3	1.0	4.7	1.6	For gage 8, refer to sketch SK-22
R5-W-4	-20.8	-28.3	-15.8	
R5-W-5	3.2	-0.9	-0.5	
R5-W-7	2.0	4.8	1.0	
R5-W-8	?	?	?	
R6-E/W-9	-18.3	-24.9	-15.2	Rib 6 - Bottom Centerline
				Refer to sketches SK-16 and SK-17
R6-E-1	2.6	4.2	1.6	Rib 6 - East Side
R6-E-3	?	?	?	Refer to sketch SK-16
R6-E-7	?	?	?	
R6-W-1	5.1	7.7	3.6	Rib 6 - West Side
R6-W-3	2.4	6.7	3.4	Refer to sketch SK-17
R6-W-4	-22.0	-32.6	-18.6	
R6-W-7	1.6	1.8	1.3	

? instrument not working

- instrument not hooked up

Strain gages: MPa **Complete Equivalent HS20 Load Cycle**
LVDTs: mm **Current cycle count: 0**
Jacks: kN

At Step 0:
- **all jacks are at minimum load of approximately 44 kN**
- **all strain gages and LVDTs read zero**

Instrument	Step 1	Step 2	Step 3	
R7-E-1	2.8	1.5	2.4	Rib 7 - East Side
R7-E-3	-0.6	-0.2	-0.2	Refer to sketch SK-18
R7-E-4	-18.7	-29.3	-19.4	For gage 8, refer to sketch SK-22
R7-E-7	-1.2	-10.8	0.0	
R7-E-8	0.2	1.7	0.9	
R7-W-1	2.5	3.0	1.4	Rib 7 - West Side
R7-W-3	2.7	7.5	3.1	Refer to sketch SK-19
R7-W-4	2.0	6.3	2.4	For gage 8, refer to sketch SK-22
R7-W-7	2.2	3.4	0.0	
R7-W-8	?	?	?	
R8-W-1	2.1	1.2	1.0	Rib 8 - West Side
R8-W-3	1.6	5.9	1.9	Refer to sketch SK-21
R8-W-4	-18.6	-28.8	-14.0	
R8-W-7	0.7	-1.6	-1.1	
R9-E-1	1.6	-2.0	1.2	Rib 9 - East Side
R9-E-3	2.2	8.5	2.5	Refer to sketch SK-20
R9-E-4	-15.8	-26.1	-14.8	
R9-E-7	-1.0	-17.5	0.0	
SP-5-1	45.1	32.6	-9.9	Midspan of Rib 5
SP-5-2	14.5	10.1	-3.0	Refer to sketches SK-1, SK-2, and SK-23
SP-5-3	-13.6	-9.0	3.0	
SP-9-1	24.9	14.7	-8.9	Midspan of Rib 9
SP-9-2	6.7	2.5	-3.3	Refer to sketches SK-1, SK-2, and SK-23
SP-9-3	-10.6	-9.5	2.1	
TW-1	11.8	13.1	6.0	Adjacent to Transverse Deck Weld
TW-2	1.2	5.5	7.4	Refer to sketch SK-14
TW-3	1.5	2.8	4.2	

? instrument not working

- instrument not hooked up

Strain gages: MPa **Complete Equivalent HS20 Load Cycle**
LVDTs: mm **Current cycle count: 0**
Jacks: kN

At Step 0:
- **all jacks are at minimum load of approximately 44 kN**
- **all strain gages and LVDTs read zero**

Instrument	Step 1	Step 2	Step 3	
DT-A1	-0.1	-0.1	0.0	LVDTs at Floorbeam A
DT-A2	0.0	0.0	0.0	Refer to sketch SK-3
DT-A3	-5.8	-7.4	-0.3	
DT-B1	0.0	-0.2	-0.1	LVDTs at Floorbeam B
DT-B2	0.0	0.0	0.0	Refer to sketch SK-3
DT-B3	-5.5	-11.9	-5.0	
DT-C1	0.0	0.0	0.0	LVDTs at Floorbeam C
DT-C2	0.6	0.5	-0.2	Refer to sketch SK-3
DT-C3	-0.5	-6.7	-5.4	
DT-S1	-6.8	-7.6	-0.5	LVDTs measuring deck displacement under jacks
DT-S2	-3.0	-6.2	-2.6	Refer to sketch SK-2
DT-S3	-0.5	-6.6	-6.2	

? instrument not working

- instrument not hooked up

Williamsburg Bridge Static Calibration Test 2 20-Feb-98

Strain gages: MPa **Complete Equivalent HS20 Load Cycle**
LVDTs: mm **Current cycle count: 1090000**
Jacks: kN

At Step 0:
- **all jacks are at minimum load of approximately 44 kN**
- **all strain gages and LVDTs read zero**

Instrument	Step 1	Step 2	Step 3	
JACK 1	371.1	318.6	37.2	Jacks
JACK 2	44.2	228.4	44.1	
JACK 3	44.2	270.3	334.2	
B5-S-1	?	?	?	Bulkhead 5 - South Side
B5-S-2	-19.6	-50.1	-19.3	Refer to sketch SK-12
B5-S-3	-10.1	-23.3	-7.4	
B5-S-4	8.2	24.3	8.9	
B7-S-1	?	?	?	Bulkhead 7 - South Side
B7-S-2	?	?	?	Refer to sketch SK-12
B7-S-3	?	?	?	
B7-S-4	12.1	30.5	10.7	
D3-N-1	-2.1	-4.6	-2.6	Diaphragm 3 - North Side
D3-N-3	?	?	?	Refer to sketch SK-7
D3-N-8	33.9	48.3	3.3	
D3-N-9	0.0	1.1	1.9	
D4-N-18	4.0	10.4	7.6	Diaphragm 4 - North Side
D4-N-19	-25.9	-90.8	-53.3	Refer to sketch SK-8
D4-N-23	4.7	3.2	4.4	
D4-N-24	-5.0	-8.6	-6.5	
D45-N-1	-0.6	0.9	1.3	North side of diaphragm between ribs 4 & 5
D45-N-2	2.8	-10.0	-9.8	Refer to sketch SK-5
D5-N-1	0.6	-5.4	0.8	Diaphragm 5 - North Side
D5-N-2	6.2	4.9	5.4	Refer to sketch SK-9
D5-N-3	-2.7	-7.5	-3.7	
D5-N-4	6.9	3.8	-4.4	
D5-N-5	15.3	40.3	14.4	
D5-N-6	5.9	10.1	4.4	
D5-N-7	28.2	71.9	27.2	
D5-N-8	35.9	60.0	10.4	
D5-N-9	1.0	5.0	3.9	
D5-N-10	15.8	41.2	16.3	
D5-N-11	6.5	-7.7	-8.9	
D5-N-12	-12.7	-55.2	-26.3	

Strain gages: MPa **Complete Equivalent HS20 Load Cycle**
LVDTs: mm **Current cycle count: 1090000**
Jacks: kN

At Step 0:
- **all jacks are at minimum load of approximately 44 kN**
- **all strain gages and LVDTs read zero**

Instrument	Step 1	Step 2	Step 3	
D5-N-13	-5.7	-9.8	-4.0	Diaphragm 5 - North Side
D5-N-14	1.1	0.8	-0.4	Refer to sketch SK-9
D5-N-15	41.4	81.1	25.3	
D5-N-16	-36.2	-104.4	-48.1	
D5-N-17	6.2	17.7	7.9	
D5-N-18	1.7	5.4	3.8	
D5-N-19	-40.6	-121.5	-57.1	
D5-N-20	-21.8	-54.9	-20.2	
D5-N-21	-16.1	-49.4	-24.3	
D5-N-22	-5.1	-14.5	-6.0	
D5-N-23	7.1	16.1	5.7	
D5-N-24	-6.9	-16.0	-5.6	
D5-S-7	35.4	85.1	30.5	Diaphragm 5 - South Side
D5-S-8	35.0	115.2	55.3	Refer to sketch SK-12
D5-S-9	?	?	?	
D5-S-18	0.9	-0.4	-1.2	
D5-S-19	-45.9	-84.5	-20.0	
D5-S-20	-18.8	-50.4	-19.5	
D6-N-1	1.6	0.8	2.0	Diaphragm 6 - North Side
D6-N-3	-2.1	-5.4	-2.8	Refer to sketch SK-10
D6-N-8	30.2	52.5	9.1	
D6-N-9	0.4	0.6	-0.2	
D6-N-18	4.5	15.1	10.3	
D6-N-19	-28.6	-100.7	-50.7	
D6-N-23	7.9	17.3	6.0	
D6-N-24	-7.6	-19.3	-8.5	
D67-N-1	-0.7	1.1	0.9	North side of diaphragm between ribs 6 & 7
D67-N-2	0.7	-12.0	-9.9	Refer to sketch SK-6
D7-N-1	0.7	3.4	0.2	Diaphragm 7 - North Side
D7-N-2	7.8	24.9	6.1	Refer to sketch SK-11
D7-N-3	-2.0	-10.6	-4.7	
D7-N-4	4.7	2.5	-6.0	
D7-N-5	18.0	36.7	16.5	
D7-N-6	9.1	18.7	9.6	
D7-N-7	33.0	78.4	36.3	

? instrument not working

- instrument not hooked up

Strain gages: MPa **Complete Equivalent HS20 Load Cycle**
LVDTs: mm **Current cycle count: 1090000**
Jacks: kN

At Step 0:
- **all jacks are at minimum load of approximately 44 kN**
- **all strain gages and LVDTs read zero**

Instrument	Step 1	Step 2	Step 3	
D7-N-8	36.8	69.8	18.3	Diaphragm 7 - North Side
D7-N-9	-0.3	-0.4	0.0	Refer to sketch SK-11
D7-N-10	19.5	51.2	19.5	
D7-N-11	-1.2	0.3	1.5	
D7-N-12	-19.2	-59.9	-30.4	
D7-N-13	-7.2	-16.2	-5.5	
D7-N-14	6.2	11.8	4.3	
D7-N-16	-16.3	-39.3	-15.8	
D7-N-17	7.8	7.0	-4.2	
D7-N-18	3.7	11.0	5.3	
D7-N-19	-49.0	-142.0	-68.1	
D7-N-20	-18.4	-44.6	-17.3	
D7-N-21	-15.5	-48.0	-24.9	
D7-N-22	-5.4	-16.0	-7.4	
D7-N-23	6.8	17.2	6.7	
D7-N-24	-7.2	-18.0	-7.3	
D7-S-7	34.5	75.0	32.3	Diaphragm 7 - South Side
D7-S-8	41.8	128.4	62.6	Refer to sketch SK-12
D7-S-9	1.3	-3.5	-2.4	
D7-S-18	0.7	-1.2	-1.6	
D7-S-19	-37.1	-67.2	-16.7	
D7-S-20	-21.9	-58.1	-24.9	
D8-N-18	-30.4	-100.4	-51.5	Diaphragm 8 - North Side
D8-N-19	2.9	5.3	3.5	Refer to sketch SK-8
D8-N-23	4.7	10.7	4.3	
D8-N-24	-4.2	-12.0	-4.5	
D8-S-19	-9.7	-1.8	8.7	Diaphragm 8 - South Side
				Refer to sketch SK-12A
D9-N-1	-0.8	-1.1	0.3	Diaphragm 9 - North Side
D9-N-3	-0.5	-6.3	-2.5	Refer to sketch SK-7
D9-N-8	-1.6	-6.1	-15.2	
D9-N-9	1.8	3.9	1.9	
D9-S-8	20.4	77.2	35.1	Diaphragm 9 - South Side
				Refer to sketch SK-12B

? instrument not working

- instrument not hooked up

Strain gages: MPa **Complete Equivalent HS20 Load Cycle**
LVDTs: mm **Current cycle count: 1090000**
Jacks: kN

At Step 0:
- **all jacks are at minimum load of approximately 44 kN**
- **all strain gages and LVDTs read zero**

Instrument	Step 1	Step 2	Step 3	
FB1	8.3	14.4	5.9	Fixed End of Floorbeam B - North Side
FB2	-22.1	-48.6	-17.5	Refer to sketch SK-13
FB3	-10.3	-19.7	-8.8	
R3-E-1	3.7	4.5	3.0	Rib 3 - East Side
R3-E-3	-1.9	-3.5	-1.0	Refer to sketch SK-20
R3-E-4	-16.0	-20.7	-14.9	
R3-E-7	-1.3	-3.1	-1.5	
R4-W-1	6.9	9.9	5.2	Rib 4 - West Side
R4-W-3	2.7	3.8	2.9	Refer to sketch SK-21
R4-W-4	-22.2	-29.6	-17.8	
R4-W-7	1.7	2.1	1.7	
R5-E-1	3.9	8.5	2.1	Rib 5 - East Side
R5-E-2	3.1	14.5	11.3	Refer to sketch SK-14
R5-E-3	-1.3	-5.8	-0.1	For gage 8, refer to sketch SK-22
R5-E-4	-18.5	-23.5	-16.1	
R5-E-5	17.8	35.6	17.1	
R5-E-6	-14.0	-12.3	-9.9	
R5-E-7	?	?	?	
R5-E-8	?	?	?	
R5-W-1	0.0	0.0	0.0	Rib 5 - West Side
R5-W-2	1.9	3.9	1.5	Refer to sketch SK-15
R5-W-3	1.4	4.9	1.5	For gage 8, refer to sketch SK-22
R5-W-4	-21.4	-29.0	-16.4	
R5-W-5	2.1	-3.1	-1.5	
R5-W-7	2.1	5.6	1.3	
R5-W-8	?	?	?	
R6-E/W-9	-19.1	-26.2	-15.9	Rib 6 - Bottom Centerline
				Refer to sketches SK-16 and SK-17
R6-E-1	2.2	3.3	1.4	Rib 6 - East Side
R6-E-3	-2.1	-3.7	-2.0	Refer to sketch SK-16
R6-E-7	?	?	?	
R6-W-1	5.8	8.9	4.6	Rib 6 - West Side
R6-W-3	2.7	7.2	4.0	Refer to sketch SK-17
R6-W-4	-22.8	-33.6	-19.5	
R6-W-7	2.1	2.1	2.0	

? instrument not working

- instrument not hooked up

Strain gages: MPa **Complete Equivalent HS20 Load Cycle**
LVDTs: mm **Current cycle count: 1090000**
Jacks: kN

At Step 0:
- **all jacks are at minimum load of approximately 44 kN**
- **all strain gages and LVDTs read zero**

Instrument	Step 1	Step 2	Step 3	
R7-E-1	2.8	1.7	2.4	Rib 7 - East Side
R7-E-3	-1.5	-2.6	-1.1	Refer to sketch SK-18
R7-E-4	-18.4	-28.1	-18.6	For gage 8, refer to sketch SK-22
R7-E-7	-2.0	-11.4	-1.2	
R7-E-8	2.0	1.4	1.1	
R7-W-1	3.3	4.8	2.8	Rib 7 - West Side
R7-W-3	3.3	9.5	4.0	Refer to sketch SK-19
R7-W-4	-19.2	-28.9	-14.9	For gage 8, refer to sketch SK-22
R7-W-7	3.7	7.4	2.1	
R7-W-8	?	?	?	
R8-W-1	4.3	5.3	3.4	Rib 8 - West Side
R8-W-3	3.1	7.8	3.3	Refer to sketch SK-21
R8-W-4	-18.9	-30.1	-14.6	
R8-W-7	2.0	2.0	0.5	
R9-E-1	2.6	0.0	1.6	Rib 9 - East Side
R9-E-3	0.3	3.0	0.4	Refer to sketch SK-20
R9-E-4	-15.7	-24.8	-14.0	
R9-E-7	-1.4	-17.9	-1.3	
SP-5-1	43.6	30.0	-10.5	Midspan of Rib 5
SP-5-2	13.7	10.3	-3.0	Refer to sketches SK-1, SK-2, and SK-23
SP-5-3	-12.5	-7.7	3.3	
SP-9-1	24.8	12.7	-9.4	Midspan of Rib 9
SP-9-2	6.0	1.8	-3.5	Refer to sketches SK-1, SK-2, and SK-23
SP-9-3	-9.8	-5.5	3.2	
TW-1	11.3	12.9	5.7	Adjacent to Transverse Deck Weld
TW-2	0.4	5.0	7.2	Refer to sketch SK-14
TW-3	1.4	3.6	3.9	

? instrument not working

- instrument not hooked up

Strain gages: MPa **Complete Equivalent HS20 Load Cycle**
LVDTs: mm **Current cycle count: 1090000**
Jacks: kN

At Step 0:
- **all jacks are at minimum load of approximately 44 kN**
- **all strain gages and LVDTs read zero**

Instrument	Step 1	Step 2	Step 3	
DT-A1	0.0	0.0	0.0	LVDTs at Floorbeam A
DT-A2	-	-	-	Refer to sketch SK-3
DT-A3	-4.6	-4.8	0.1	
DT-B1	0.1	0.0	0.0	LVDTs at Floorbeam B
DT-B2	-	-	-	Refer to sketch SK-3
DT-B3	-4.0	-8.5	-3.1	
DT-C1	0.0	0.0	0.0	LVDTs at Floorbeam C
DT-C2	-	-	-	Refer to sketch SK-3
DT-C3	0.7	-1.3	-3.0	
DT-S1	-4.7	-6.0	0.1	LVDTs measuring deck displacement under jacks
DT-S2	-2.1	-4.4	-1.5	Refer to sketch SK-2
DT-S3	0.1	-4.6	-4.7	

? instrument not working

- instrument not hooked up

Williamsburg Bridge Static Calibration Test 3 17-Mar-98

Strain gages: MPa **Complete Equivalent HS20 Load Cycle**
LVDTs: mm **Current cycle count: 2485000**
Jacks: kN

At Step 0:
- **all jacks are at minimum load of approximately 44 kN**
- **all strain gages and LVDTs read zero**

Instrument	Step 1	Step 2	Step 3	
JACK 1	375.2	322.5	40.4	Jacks
JACK 2	37.7	221.6	37.9	
JACK 3	41.5	267.5	331.6	
B5-N-1A	1.0	2.4	1.0	Bulkhead 5 - North Side
B5-N-1B	0.0	0.0	0.1	Refer to sketch SK-9
B5-N-1C	-1.2	-2.8	-1.5	
B5-N-2A	-4.3	-9.4	-3.4	
B5-N-2B	-18.5	-43.0	-15.0	
B5-N-2C	-10.5	-25.3	-9.0	
B5-N-3A	?	?	?	
B5-N-3B	-3.8	-9.1	-3.8	
B5-N-3C	1.0	2.7	1.5	
B5-N-4A	7.5	17.0	5.3	
B5-N-4B	8.7	20.4	5.8	
B5-N-4C	-0.4	-1.4	-0.3	
B5-N-5A	?	?	?	
B5-N-5B	?	?	?	
B5-N-5C	0.2	0.8	0.5	
B5-N-6A	10.6	25.1	9.5	
B5-N-6B	-3.0	-7.4	-2.8	
B5-N-6C	-10.3	-25.9	-9.3	
B5-S-1	?	?	?	Bulkhead 5 - South Side
B5-S-2	-20.7	-50.3	-19.4	Refer to sketch SK-12
B5-S-3	-9.7	-21.8	-8.3	
B5-S-4	9.1	24.3	8.8	
B7-N-1A	-0.3	-0.6	-0.3	Bulkhead 7 - North Side
B7-N-1B	?	?	?	Refer to sketch SK-11
B7-N-1C	-0.2	-0.2	-0.5	
B7-N-2A	-5.6	-11.9	-4.1	
B7-N-2B	-11.7	-28.6	-10.9	
B7-N-2C	-24.0	-55.7	-21.1	
B7-N-3A	-7.9	-21.4	-9.4	
B7-N-3B	-5.8	-15.7	-6.8	

? instrument not working - instrument not hooked up

Strain gages: MPa **Complete Equivalent HS20 Load Cycle**
LVDTs: mm **Current cycle count: 2485000**
Jacks: kN

At Step 0:
- **all jacks are at minimum load of approximately 44 kN**
- **all strain gages and LVDTs read zero**

Instrument	Step 1	Step 2	Step 3	
B7-N-3C	0.9	1.7	0.2	Bulkhead 7 - North Side
B7-N-4A	5.3	11.0	3.5	Refer to sketch SK-11
B7-N-4B	11.7	25.7	9.4	
B7-N-4C	2.0	3.4	1.7	
B7-N-5A	-3.7	-9.2	-4.3	
B7-N-5B	0.3	0.6	-0.4	
B7-N-5C	?	?	?	
B7-N-6A	9.2	21.7	8.6	
B7-N-6B	-3.2	-7.0	-2.9	
B7-N-6C	-9.8	-24.7	-9.5	
B7-S-1	?	?	?	Bulkhead 7 - South Side
B7-S-2	?	?	?	Refer to sketch SK-12
B7-S-3	?	?	?	
B7-S-4	12.9	31.1	13.0	
D3-N-1	-1.9	-4.5	-2.5	Diaphragm 3 - North Side
D3-N-3	?	?	?	Refer to sketch SK-7
D3-N-8	32.1	46.6	3.6	
D3-N-9	-0.1	1.2	1.7	
D4-N-18	4.1	10.6	7.7	Diaphragm 4 - North Side
D4-N-19	-26.2	-90.4	-52.9	Refer to sketch SK-8
D4-N-23	4.2	5.1	2.7	
D4-N-24	-5.5	-10.1	-4.5	
D45-N-1	-0.6	1.2	1.3	North side of diaphragm between ribs 4 & 5
D45-N-2	2.8	-9.7	-9.4	Refer to sketch SK-5
D5-N-1	0.8	-5.4	0.5	Diaphragm 5 - North Side
D5-N-2	6.4	5.5	5.5	Refer to sketch SK-9
D5-N-3	-2.6	-6.9	-3.8	
D5-N-4	6.0	2.6	-4.4	
D5-N-5	14.9	39.0	14.6	
D5-N-6	5.4	9.5	4.9	
D5-N-7	27.6	70.4	27.3	
D5-N-8	34.9	58.0	10.2	
D5-N-9	0.7	4.5	4.1	
D5-N-10	15.1	40.6	16.6	
D5-N-11	5.8	-7.6	-8.7	

? instrument not working

- instrument not hooked up

Strain gages: MPa **Complete Equivalent HS20 Load Cycle**
LVDTs: mm **Current cycle count: 2485000**
Jacks: kN

At Step 0:
- **all jacks are at minimum load of approximately 44 kN**
- **all strain gages and LVDTs read zero**

Instrument	Step 1	Step 2	Step 3	
D5-N-12	-13.6	-54.6	-25.8	Diaphragm 5 - North Side
D5-N-13	-6.1	-9.9	-3.7	Refer to sketch SK-9
D5-N-14	-0.5	-0.4	-0.4	
D5-N-15	40.6	79.8	25.5	
D5-N-16	-35.7	-103.4	-47.8	
D5-N-17	6.5	18.6	9.1	
D5-N-18	1.1	5.2	3.5	
D5-N-19	-40.0	-119.5	-57.1	
D5-N-20	-22.0	-54.3	-20.2	
D5-N-21	-15.7	-48.8	-24.1	
D5-N-22	-4.8	-13.9	-5.8	
D5-N-23	7.3	17.4	6.1	
D5-N-24	-7.1	-17.5	-5.9	
D5-S-7	34.2	83.0	30.7	Diaphragm 5 - South Side
D5-S-8	34.5	113.2	55.2	Refer to sketch SK-12
D5-S-9	?	?	?	
D5-S-18	0.7	-0.6	-0.9	
D5-S-19	-47.1	-86.4	-20.8	
D5-S-20	-19.3	-49.7	-19.4	
D6-N-1	1.3	0.7	2.0	Diaphragm 6 - North Side
D6-N-3	-2.8	-5.9	-2.9	Refer to sketch SK-10
D6-N-8	30.1	52.7	9.8	
D6-N-9	0.9	0.7	-0.1	
D6-N-18	3.8	14.7	10.3	
D6-N-19	-27.7	-98.9	-49.9	
D6-N-23	7.2	17.1	5.9	
D6-N-24	-7.3	-19.5	-7.7	
D67-N-1	-1.4	0.4	0.6	North side of diaphragm between ribs 6 & 7
D67-N-2	1.3	-11.3	-9.2	Refer to sketch SK-6
D7-N-1	1.2	3.6	0.5	Diaphragm 7 - North Side
D7-N-2	8.1	24.4	6.3	Refer to sketch SK-11
D7-N-3	-2.5	-10.6	-4.5	
D7-N-4	3.1	-0.7	-6.6	
D7-N-5	19.8	41.0	19.2	
D7-N-6	10.5	22.5	12.0	

? instrument not working

- instrument not hooked up

Strain gages: MPa **Complete Equivalent HS20 Load Cycle**
LVDTs: mm **Current cycle count: 2485000**
Jacks: kN

At Step 0:
- **all jacks are at minimum load of approximately 44 kN**
- **all strain gages and LVDTs read zero**

Instrument	Step 1	Step 2	Step 3	
D7-N-7	35.8	81.3	35.3	Diaphragm 7 - North Side
D7-N-8	44.2	95.1	34.2	Refer to sketch SK-11
D7-N-9	-5.6	-20.3	-9.3	
D7-N-10	18.8	48.4	18.1	
D7-N-11	-1.8	-1.4	0.9	
D7-N-12	-17.9	-57.8	-29.7	
D7-N-13	-7.7	-15.9	-5.4	
D7-N-14	6.8	11.6	4.1	
D7-N-16	-16.4	-39.6	-15.8	
D7-N-17	8.7	8.3	-3.6	
D7-N-18	3.7	10.6	5.3	
D7-N-19	-48.7	-141.4	-69.2	
D7-N-20	-19.0	-46.7	-18.7	
D7-N-21	-14.6	-46.0	-24.3	
D7-N-22	-4.5	-14.6	-7.2	
D7-N-23	7.1	16.8	6.6	
D7-N-24	-8.4	-20.4	-8.5	
D7-S-7	13.5	15.3	8.2	Diaphragm 7 - South Side
D7-S-8	58.8	167.4	79.6	Refer to sketch SK-12
D7-S-9	-16.9	-39.8	-18.0	
D7-S-18	0.5	-1.2	-1.4	
D7-S-19	-38.2	-70.0	-18.5	
D7-S-20	-22.8	-60.2	-26.1	
D8-N-18	-30.2	-98.7	-51.4	Diaphragm 8 - North Side
D8-N-19	2.6	5.6	3.1	Refer to sketch SK-8
D8-N-23	4.5	10.7	4.2	
D8-N-24	-4.2	-11.9	-4.7	
D8-S-19	-10.5	-3.7	7.4	Diaphragm 8 - South Side
				Refer to sketch SK-12A
D9-N-1	-0.4	-1.1	0.3	Diaphragm 9 - North Side
D9-N-3	-0.8	-6.9	-2.7	Refer to sketch SK-7
D9-N-8	-0.6	-4.5	-14.8	
D9-N-9	1.4	4.0	1.8	

? instrument not working - instrument not hooked up

Strain gages: MPa **Complete Equivalent HS20 Load Cycle**
LVDTs: mm **Current cycle count: 2485000**
Jacks: kN

At Step 0:
- **all jacks are at minimum load of approximately 44 kN**
- **all strain gages and LVDTs read zero**

Instrument	Step 1	Step 2	Step 3	
D9-S-8	19.2	75.0	34.3	Diaphragm 9 - South Side
				Refer to sketch SK-12B
FB1	5.8	14.5	5.9	Fixed End of Floorbeam B - North Side
FB2	-20.6	-46.9	-17.5	Refer to sketch SK-13
FB3	-7.7	-18.9	-7.9	
R3-E-1	3.2	3.8	2.7	Rib 3 - East Side
R3-E-3	-1.9	-3.4	-0.8	Refer to sketch SK-20
R3-E-4	-15.7	-20.4	-14.9	
R3-E-7	-1.4	-3.3	-1.4	
R4-W-1	6.4	9.7	4.8	Rib 4 - West Side
R4-W-3	2.6	4.7	2.7	Refer to sketch SK-21
R4-W-4	-22.3	-30.0	-18.2	
R4-W-7	1.2	2.0	1.5	
R5-E-1	4.0	8.7	2.2	Rib 5 - East Side
R5-E-2	3.1	16.0	12.7	Refer to sketch SK-14
R5-E-3	-1.3	-5.0	-0.2	For gage 8, refer to sketch SK-22
R5-E-4	-19.1	-24.2	-16.1	
R5-E-5	16.8	34.7	17.5	
R5-E-6	-14.2	-12.9	-10.0	
R5-E-7	?	?	?	
R5-E-8	?	?	?	
R5-W-1	?	?	?	Rib 5 - West Side
R5-W-2	2.0	4.4	1.6	Refer to sketch SK-15
R5-W-3	1.2	5.6	1.8	For gage 8, refer to sketch SK-22
R5-W-4	-21.3	-28.9	-16.3	
R5-W-5	1.4	-3.8	-1.2	
R5-W-7	2.0	5.6	1.9	
R5-W-8	?	?	?	
R6-E/W-9	-19.5	-26.5	-16.0	Rib 6 - Bottom Centerline
				Refer to sketches SK-16 and SK-17
R6-E-1	2.5	3.8	2.0	Rib 6 - East Side
R6-E-3	-1.8	-3.6	-1.7	Refer to sketch SK-16
R6-E-7	?	?	?	

? instrument not working

- instrument not hooked up

Strain gages: MPa **Complete Equivalent HS20 Load Cycle**
LVDTs: mm **Current cycle count: 2485000**
Jacks: kN

At Step 0:
- **all jacks are at minimum load of approximately 44 kN**
- **all strain gages and LVDTs read zero**

Instrument	Step 1	Step 2	Step 3	
R6-W-1	5.5	9.2	5.0	Rib 6 - West Side
R6-W-3	2.7	7.4	4.2	Refer to sketch SK-17
R6-W-4	-23.3	-34.4	-20.1	
R6-W-7	2.0	1.7	1.8	
R7-E-1	2.4	1.4	2.7	Rib 7 - East Side
R7-E-3	-0.6	-1.4	-0.2	Refer to sketch SK-18
R7-E-4	-18.3	-27.7	-18.6	For gage 8, refer to sketch SK-22
R7-E-7	-1.9	-11.7	-1.0	
R7-E-8	-0.6	-1.0	0.4	
R7-W-1	2.2	2.1	1.5	Rib 7 - West Side
R7-W-3	3.9	10.8	4.5	Refer to sketch SK-19
R7-W-4	-19.0	-29.1	-15.2	For gage 8, refer to sketch SK-22
R7-W-7	4.3	8.7	2.2	
R7-W-8	?	?	?	
R8-W-1	3.9	5.1	2.9	Rib 8 - West Side
R8-W-3	2.3	7.5	2.9	Refer to sketch SK-21
R8-W-4	-19.5	-29.9	-14.7	
R8-W-7	1.9	1.7	0.1	
R9-E-1	2.6	-1.0	1.4	Rib 9 - East Side
R9-E-3	-0.2	2.8	0.5	Refer to sketch SK-20
R9-E-4	-15.1	-23.4	-13.7	
R9-E-7	-1.4	-18.6	-1.3	
SP-5-1	26.9	26.9	-14.9	Midspan of Rib 5
SP-5-2	14.7	10.7	-3.6	Refer to sketches SK-1, SK-2, and SK-23
SP-5-3	-12.8	-9.1	3.3	
SP-9-1	24.0	12.8	-8.8	Midspan of Rib 9
SP-9-2	6.3	2.5	-3.1	Refer to sketches SK-1, SK-2, and SK-23
SP-9-3	-8.8	-6.7	2.2	
TW-1	11.5	13.1	6.1	Adjacent to Transverse Deck Weld
TW-2	1.2	5.8	7.3	Refer to sketch SK-14
TW-3	1.9	3.2	4.0	

? instrument not working

- instrument not hooked up

Strain gages: MPa **Complete Equivalent HS20 Load Cycle**
LVDTs: mm **Current cycle count: 2485000**
Jacks: kN

At Step 0:
- **all jacks are at minimum load of approximately 44 kN**
- **all strain gages and LVDTs read zero**

Instrument	Step 1	Step 2	Step 3	
DT-A1	0.0	0.0	0.0	LVDTs at Floorbeam A
DT-A2	-	-	-	Refer to sketch SK-3
DT-A3	-4.6	-4.7	0.2	
DT-B1	0.0	0.0	0.0	LVDTs at Floorbeam B
DT-B2	-	-	-	Refer to sketch SK-3
DT-B3	-3.4	-7.0	-2.7	
DT-C1	0.0	0.0	0.0	LVDTs at Floorbeam C
DT-C2	-	-	-	Refer to sketch SK-3
DT-C3	0.7	-2.2	-3.0	
DT-S1	-5.9	-6.0	0.1	LVDTs measuring deck displacement under jacks
DT-S2	-2.0	-4.1	-1.4	Refer to sketch SK-2
DT-S3	0.1	-4.7	-4.3	

? instrument not working

- instrument not hooked up

Williamsburg Bridge Static Calibration Test 4 20-Apr-98

Strain gages: MPa **Complete Equivalent HS20 Load Cycle**
LVDTs: mm **Current cycle count: 5000000**
Jacks: kN

At Step 0:
- **all jacks are at minimum load of approximately 44 kN**
- **all strain gages and LVDTs read zero**

Instrument	Step 1	Step 2	Step 3	
JACK 1	372.9	322.3	39.0	Jacks
JACK 2	43.5	227.5	43.3	
JACK 3	41.8	268.2	331.6	
B5-N-1A	0.4	1.5	0.3	Bulkhead 5 - North Side
B5-N-1B	-0.8	-0.5	-0.7	Refer to sketch SK-9
B5-N-1C	-1.5	-2.9	-2.0	
B5-N-2A	-4.2	-10.0	-3.3	
B5-N-2B	?	?	?	
B5-N-2C	-10.1	-25.9	-8.5	
B5-N-3A	?	?	?	
B5-N-3B	-4.2	-10.1	-4.2	
B5-N-3C	0.5	2.4	0.9	
B5-N-4A	7.1	18.4	5.2	
B5-N-4B	8.8	22.4	6.0	
B5-N-4C	-0.5	-1.7	-0.5	
B5-N-5A	?	?	?	
B5-N-5B	?	?	?	
B5-N-5C	-0.2	0.0	-0.1	
B5-N-6A	10.3	25.8	9.1	
B5-N-6B	-3.1	-8.1	-2.9	
B5-N-6C	-10.5	-27.3	-9.2	
B5-S-1	?	?	?	Bulkhead 5 - South Side
B5-S-2	-20.3	-52.3	-19.5	Refer to sketch SK-12
B5-S-3	-9.4	-23.2	-7.2	
B5-S-4	8.7	26.0	8.7	
B7-N-1A	-0.4	-0.4	-0.4	Bulkhead 7 - North Side
B7-N-1B	?	?	?	Refer to sketch SK-11
B7-N-1C	-0.5	-0.8	-0.6	
B7-N-2A	-6.4	-13.3	-5.0	
B7-N-2B	-12.6	-30.8	-11.7	
B7-N-2C	-25.8	-60.4	-23.0	
B7-N-3A	-8.2	-22.4	-9.5	
B7-N-3B	-6.3	-16.4	-7.1	

? instrument not working - instrument not hooked up

Strain gages: MPa **Complete Equivalent HS20 Load Cycle**
LVDTs: mm **Current cycle count: 5000000**
Jacks: kN

At Step 0:
- **all jacks are at minimum load of approximately 44 kN**
- **all strain gages and LVDTs read zero**

Instrument	Step 1	Step 2	Step 3	
B7-N-3C	0.7	2.2	0.5	Bulkhead 7 - North Side
B7-N-4A	1.8	2.5	0.5	Refer to sketch SK-11
B7-N-4B	8.5	18.1	6.9	
B7-N-4C	2.0	4.8	2.0	
B7-N-5A	-3.5	-8.4	-4.1	
B7-N-5B	0.3	0.7	-0.5	
B7-N-5C	?	?	?	
B7-N-6A	8.6	22.2	8.6	
B7-N-6B	-3.2	-6.3	-3.1	
B7-N-6C	-10.2	-25.7	-9.9	
B7-S-1	?	?	?	Bulkhead 7 - South Side
B7-S-2	?	?	?	Refer to sketch SK-12
B7-S-3	?	?	?	
B7-S-4	11.1	25.9	10.2	
D3-N-1	-2.1	-4.6	-2.4	Diaphragm 3 - North Side
D3-N-3	?	?	?	Refer to sketch SK-7
D3-N-8	31.3	46.6	4.2	
D3-N-9	0.2	1.5	1.8	
D4-N-18	4.2	10.3	7.7	Diaphragm 4 - North Side
D4-N-19	-26.7	-91.9	-52.0	Refer to sketch SK-8
D4-N-23	4.7	8.5	3.0	
D4-N-24	-5.6	-11.2	-4.8	
D45-N-1	-0.6	0.7	1.2	North side of diaphragm between ribs 4 & 5
D45-N-2	2.8	-9.0	-9.2	Refer to sketch SK-5
D5-N-1	0.8	-5.5	1.0	Diaphragm 5 - North Side
D5-N-2	6.5	0.2	5.5	Refer to sketch SK-9
D5-N-3	-3.0	-11.3	-3.9	
D5-N-4	6.6	3.1	-4.4	
D5-N-5	15.5	44.5	14.5	
D5-N-6	6.2	10.4	4.5	
D5-N-7	28.0	77.4	27.4	
D5-N-8	35.5	62.2	10.3	
D5-N-9	1.0	5.5	3.6	
D5-N-10	16.1	42.5	16.3	
D5-N-11	6.5	-10.5	-8.6	

? instrument not working - instrument not hooked up

Strain gages: MPa **Complete Equivalent HS20 Load Cycle**
LVDTs: mm **Current cycle count: 5000000**
Jacks: kN

At Step 0:
- **all jacks are at minimum load of approximately 44 kN**
- **all strain gages and LVDTs read zero**

Instrument	Step 1	Step 2	Step 3	
D5-N-12	-12.9	-58.4	-26.1	Diaphragm 5 - North Side
D5-N-13	-5.1	-9.2	-4.0	Refer to sketch SK-9
D5-N-14	0.7	0.9	-0.2	
D5-N-15	41.0	82.3	25.1	
D5-N-16	-35.8	-106.0	-48.2	
D5-N-17	6.2	18.2	8.1	
D5-N-18	1.0	4.8	3.4	
D5-N-19	-40.0	-124.3	-56.7	
D5-N-20	-22.2	-58.4	-20.6	
D5-N-21	-15.5	-49.9	-23.9	
D5-N-22	-4.6	-14.1	-5.6	
D5-N-23	7.7	16.6	6.4	
D5-N-24	-7.4	-16.1	-6.1	
D5-S-7	35.2	91.3	30.2	Diaphragm 5 - South Side
D5-S-8	35.5	118.9	54.9	Refer to sketch SK-12
D5-S-9	?	?	?	
D5-S-18	1.1	-0.4	-0.9	
D5-S-19	-46.3	-90.2	-21.1	
D5-S-20	-18.5	-52.8	-19.0	
D6-N-1	2.0	1.9	1.7	Diaphragm 6 - North Side
D6-N-3	-2.3	-6.4	-2.9	Refer to sketch SK-10
D6-N-8	30.0	51.3	9.8	
D6-N-9	1.1	1.4	0.3	
D6-N-18	3.6	14.4	9.1	
D6-N-19	-27.8	-97.9	-50.4	
D6-N-23	7.8	17.5	6.2	
D6-N-24	-7.4	-20.1	-7.5	
D67-N-1	-2.1	-1.4	-0.3	North side of diaphragm between ribs 6 & 7
D67-N-2	1.0	-11.2	-9.4	Refer to sketch SK-6
D7-N-1	0.6	3.3	0.1	Diaphragm 7 - North Side
D7-N-2	8.8	26.3	6.9	Refer to sketch SK-11
D7-N-3	-2.7	-11.8	-5.0	
D7-N-4	9.3	11.3	-2.2	
D7-N-5	24.6	55.5	23.3	
D7-N-6	9.5	20.6	8.7	

? instrument not working - instrument not hooked up

Strain gages: MPa **Complete Equivalent HS20 Load Cycle**
LVDTs: mm **Current cycle count: 5000000**
Jacks: kN

At Step 0:
- **all jacks are at minimum load of approximately 44 kN**
- **all strain gages and LVDTs read zero**

Instrument	Step 1	Step 2	Step 3	
D7-N-7	-8.4	-12.9	-1.7	Diaphragm 7 - North Side
D7-N-8	11.2	22.2	2.5	Refer to sketch SK-11
D7-N-9	-6.7	-19.2	-11.4	
D7-N-10	14.8	40.3	15.3	
D7-N-11	-3.4	-6.6	-0.8	
D7-N-12	-18.7	-58.0	-29.8	
D7-N-13	-7.7	-16.7	-6.3	
D7-N-14	6.9	12.5	4.8	
D7-N-16	-16.6	-39.9	-16.2	
D7-N-17	9.0	10.1	-3.4	
D7-N-18	3.4	10.8	5.0	
D7-N-19	-49.2	-144.8	-70.0	
D7-N-20	-20.7	-51.4	-20.2	
D7-N-21	-13.3	-43.7	-23.3	
D7-N-22	-4.6	-15.0	-6.9	
D7-N-23	6.5	15.6	6.3	
D7-N-24	-8.2	-20.0	-8.3	
D7-S-7	38.1	27.3	32.0	Diaphragm 7 - South Side
D7-S-8	76.5	122.0	87.6	Refer to sketch SK-12
D7-S-9	-12.6	-12.1	-9.6	
D7-S-18	0.4	-1.5	-1.6	
D7-S-19	-39.2	-74.3	-19.7	
D7-S-20	-24.5	-65.8	-28.5	
D8-N-18	-30.3	-100.4	-52.0	Diaphragm 8 - North Side
D8-N-19	2.6	5.4	3.1	Refer to sketch SK-8
D8-N-23	4.5	10.9	4.4	
D8-N-24	-4.4	-12.3	-4.7	
D8-S-19	-11.2	-5.6	6.5	Diaphragm 8 - South Side
				Refer to sketch SK-12A
D9-N-1	-0.4	-0.6	0.3	Diaphragm 9 - North Side
D9-N-3	-1.0	-6.9	-3.1	Refer to sketch SK-7
D9-N-8	-0.2	-3.4	-13.5	
D9-N-9	1.6	4.4	1.9	

? instrument not working - instrument not hooked up

Strain gages: MPa **Complete Equivalent HS20 Load Cycle**
LVDTs: mm **Current cycle count: 5000000**
Jacks: kN

At Step 0:
- **all jacks are at minimum load of approximately 44 kN**
- **all strain gages and LVDTs read zero**

Instrument	Step 1	Step 2	Step 3	
D9-S-8	19.1	75.5	34.5	Diaphragm 9 - South Side
				Refer to sketch SK-12B
FB1	6.9	12.5	4.1	Fixed End of Floorbeam B - North Side
FB2	-21.0	-47.1	-17.9	Refer to sketch SK-13
FB3	-8.4	-17.5	-6.6	
R3-E-1	3.5	4.1	2.9	Rib 3 - East Side
R3-E-3	-1.9	-3.4	-1.1	Refer to sketch SK-20
R3-E-4	-15.9	-20.4	-14.9	
R3-E-7	-1.2	-3.0	-1.2	
R4-W-1	6.5	9.4	4.9	Rib 4 - West Side
R4-W-3	-	-	-	Refer to sketch SK-21
R4-W-4	-21.8	-30.0	-17.9	
R4-W-7	1.3	2.0	1.4	
R5-E-1	3.8	10.2	2.1	Rib 5 - East Side
R5-E-2	3.1	15.6	11.7	Refer to sketch SK-14
R5-E-3	-1.4	-9.5	-0.2	For gage 8, refer to sketch SK-22
R5-E-4	-18.0	-23.3	-16.4	
R5-E-5	17.9	37.9	17.7	
R5-E-6	-13.0	-10.9	-9.8	
R5-E-7	?	?	?	
R5-E-8	?	?	?	
R5-W-1	?	?	?	Rib 5 - West Side
R5-W-2	1.9	3.5	1.9	Refer to sketch SK-15
R5-W-3	1.4	5.8	2.0	For gage 8, refer to sketch SK-22
R5-W-4	-21.2	-29.2	-16.4	
R5-W-5	2.4	-3.3	-0.9	
R5-W-7	2.9	5.4	1.8	
R5-W-8	?	?	?	
R6-E/W-9	-18.9	-26.6	-15.7	Rib 6 - Bottom Centerline
R6-E/W-9	-18.7	-26.3	-15.8	Refer to sketches SK-16 and SK-17
R6-E-1	2.3	3.4	1.8	Rib 6 - East Side
R6-E-3	-2.0	-3.8	-2.1	Refer to sketch SK-16
R6-E-7	?	?	?	

? instrument not working

- instrument not hooked up

Strain gages: MPa **Complete Equivalent HS20 Load Cycle**
LVDTs: mm **Current cycle count: 5000000**
Jacks: kN

At Step 0:
- **all jacks are at minimum load of approximately 44 kN**
- **all strain gages and LVDTs read zero**

Instrument	Step 1	Step 2	Step 3	
R6-W-1	6.1	8.8	4.5	Rib 6 - West Side
R6-W-3	2.5	7.1	3.6	Refer to sketch SK-17
R6-W-4	-22.5	-33.8	-19.8	
R6-W-7	2.3	1.4	2.9	
R7-E-1	2.0	0.8	1.6	Rib 7 - East Side
R7-E-3	-1.1	-1.8	-1.0	Refer to sketch SK-18
R7-E-4	-18.8	-28.5	-19.1	For gage 8, refer to sketch SK-22
R7-E-7	-1.7	-9.8	-1.0	
R7-E-8	0.1	1.1	0.5	
R7-W-1	2.0	2.2	1.1	Rib 7 - West Side
R7-W-3	3.4	9.7	3.8	Refer to sketch SK-19
R7-W-4	-19.4	-29.7	-15.5	For gage 8, refer to sketch SK-22
R7-W-7	4.5	8.8	2.6	
R7-W-8	?	?	?	
R8-W-1	3.8	5.2	2.9	Rib 8 - West Side
R8-W-3	2.3	7.5	2.9	Refer to sketch SK-21
R8-W-4	-19.2	-30.1	-14.5	
R8-W-7	2.8	3.0	1.4	
R9-E-1	2.6	-0.3	1.3	Rib 9 - East Side
R9-E-3	-0.3	2.4	0.0	Refer to sketch SK-20
R9-E-4	-15.4	-23.9	-13.3	
R9-E-7	-1.3	-18.2	-1.7	
SP-5-1	43.4	30.7	-10.5	Midspan of Rib 5
SP-5-2	14.5	10.9	-2.6	Refer to sketches SK-1, SK-2, and SK-23
SP-5-3	-12.7	-8.3	3.1	
SP-9-1	24.8	14.3	-8.9	Midspan of Rib 9
SP-9-2	6.4	2.6	-3.0	Refer to sketches SK-1, SK-2, and SK-23
SP-9-3	-8.8	-6.7	2.5	
TW-1	11.8	13.7	6.6	Adjacent to Transverse Deck Weld
TW-2	1.4	6.1	7.9	Refer to sketch SK-14
TW-3	1.7	3.1	4.0	

? instrument not working

- instrument not hooked up

Strain gages: MPa **Complete Equivalent HS20 Load Cycle**
LVDTs: mm **Current cycle count: 5000000**
Jacks: kN

At Step 0:
- **all jacks are at minimum load of approximately 44 kN**
- **all strain gages and LVDTs read zero**

Instrument	Step 1	Step 2	Step 3	
DT-A1	0.0	0.0	0.0	LVDTs at Floorbeam A
DT-A2	-	-	-	Refer to sketch SK-3
DT-A3	-3.4	-4.8	0.1	
DT-B1	0.0	0.1	0.0	LVDTs at Floorbeam B
DT-B2	-	-	-	Refer to sketch SK-3
DT-B3	-3.5	-7.1	-2.8	
DT-C1	0.0	0.0	0.0	LVDTs at Floorbeam C
DT-C2	-	-	-	Refer to sketch SK-3
DT-C3	0.8	-2.1	-2.9	
DT-S1	-5.9	-6.1	0.1	LVDTs measuring deck displacement under jacks
DT-S2	-0.9	-2.6	-0.8	Refer to sketch SK-2
DT-S3	0.1	-4.7	-4.8	

? instrument not working

- instrument not hooked up